

University of Naples “Federico II”

**PhD Program
Molecular Pathology and Physiopathology**



**School of Molecular Medicine
XXVIII Cycle**

**NCOA4 Deficiency
Impairs Systemic Iron Homeostasis**

Supervisor
Prof. Carlomagno Francesca

Candidate
Giorgia Federico

PhD Coordinator
Prof. Vittorio Enrico Avvedimento

Academic Year 2015-2016

**“NCOA4 Deficiency
Impairs Systemic Iron
Homeostasis”**

Sommario

LIST OF PUBLICATIONS	3
LIST OF ABBREVIATIONS	4
ABSTRACT.....	6
1 BACKGROUND	7
1.1 Iron: the essential ion for life	7
1.2 Systemic iron homeostasis (absorption, utilization, recycling)	7
1.3 Systemic Iron overload and iron deficiency	10
1.4 Cellular iron homeostasis: from uptake to storage.....	11
1.5 Iron levels and cell cycle: evidence of a an iron-dependent check-point.....	13
1.6 NCOA4 protein: a multifunctional protein involved in iron metabolism and DNA replication.....	15
2 AIMS OF THE STUDY	18
3 MATERIALS AND METHODS.....	19
3.1 Cell Culture	19
3.2 Cell fractionation	19
3.3 Chromatin Immunoprecipitation (ChIP).....	20
3.4 Histology Analysis.....	21
3.5 RNA Extraction and RT-PCR.....	21
3.6 Retrovirus-mediated MEFs transduction	22
3.7 Tissue and Serum Iron Determination	22
3.8 Flow Cytometric Analysis of Mouse Bone Marrow erythroblast precursors.	22
4 RESULTS	23
4.1 Impaired ferritinophagy in NCOA4 deficient mice promotes tissue ferritin accumulation.....	23
4.2 The Hepcidin-ferroportin axis limits iron absorption in NCOA4 null mice	25
4.3 NCOA4 null mice were unable to mobilize iron reserve under iron deprivation	27
4.4 NCOA4 null mice display ineffective erythropoiesis and an impaired terminal erythroid differentiation under iron poor diet	29
4.5 NCOA4 ^{-/-} mice develop fatal liver damage under hyperferric diet.....	32

4.6 NCOA4 protein controls ferritinophagy through its C-terminal portion	34
4.8 Iron bioavailability affects intracellular NCOA4 levels and cell cycle progression.....	36
4.9 NCOA4 is enriched at DNA replication origins in response to iron depletion..	40
4.10 NCOA4 mediates DNA replication arrest during iron depletion.....	41
5 DISCUSSION	43
6 CONCLUSIONS.....	45
REFERENCES	46

LIST OF PUBLICATIONS

“NCOA4 Deficiency Impairs Systemic Iron Homeostasis”

Bellelli Roberto, Federico Giorgia, Matte' Alessandro, Colecchia David, Iolascon Achille, Chiariello Mario, Santoro Massimo, De Franceschi Lucia, Carlomagno Francesca.
Cell Rep. 2016 Jan 26;14(3):411-21.

“Identification of novel small molecules inhibitors of oncogenic RET kinase”

Moccia Marialuisa, Liu Qingsong, Guida Teresa, Federico Giorgia, Brescia Annalisa, Zhao Zheng, Geun Choi Hwan, Deng Xianming, Tan Li, Wang Jinhua, Billaud Marc, Gray Nathanael S., Carlomagno Francesca, Santoro Massimo
PLoS One. 2015 Jun 5;10(6):e0128364

“Fragment-based discovery of a dual pan-RET/VEGFR2 kinase inhibitor optimized for single-agent polypharmacology.”

Frett Brendan, Carlomagno Francesca, Moccia Maria Luisa, Brescia Annalisa, Federico Giorgia, De Falco Valentina, Admire Brittany, Chen Zhongzhu, Qi Wenqing, Santoro Massimo, Li Hong-Yu.
Angew Chem Int Ed Engl. 2015 Jul 20;54(30):8717-21.

LIST OF ABBREVIATIONS

ACD	Anemia of Chronic Disease
ACTRIIA	Activin type IIA receptor
ALAS-2	5'Aminolevulinate Synthase 2
Alk2	Activin receptor-like kinase-2
Alk3	Activin receptor-like kinase-3
AR	Androgen receptor
ARA70	Androgen receptor-associated protein 70
ATG8	Autophagy-related protein 8
BMP6	Bone Morphogenetic protein 6
Cdc25	Cell division cycle 25
CDC6	Cell division cycle 6
Cdc7	Cell Cycle Division 7
CDK	Cyclin Dependent Kinase
CDT1	CDC10-dependent transcript 1
Chk1	Checkpoint kinase 1
CMG	Cdc45-MCM2-7-GINS complex
DcytB	Duodenal Cytochrome B
DDK	DbF4 and Drf1 dependent kinase
DDR	DNA damage response
DFO	Deferoxamine
DMT1	Divalent metal transporter 1
dNTPs	Deoxyribonucleotides
E2F	E2 transcription Factor
EPO	Erythropoietin
ER	Estrogen receptor
ERFE	Erythroferrone
ERK	Extracellular-signal-regulated kinases
FANCI	Fanconi anemia group J protein
FBxL5	Fbox and leucin rich repeat protein 5
FPN1	Ferroportin1
FTH	Ferritin Heavy Chain
FTL	Ferritin Light Chain
GABARAP	GABA (A) Receptor-Associated Protein
GINS	Go, Ichi, Nii, and San
HAMP	Hepcidin Antimicrobial Peptide
HERC2	HECT and RLD Domain Containing E3 Ubiquitin Protein Ligase
HFE	Human hemochromatosis protein
HH	Hereditary Hemocromatosis
HIF2 α	Hipoxia Inducible Factor 2 alfa
Hjv	Hemojuvelin
IL-6	Interleukine 6
IRIDA	Iron refractory iron deficiency anemia
IRP1	Iron Binding Protein1

IRP2	Iron Binding Protein2
ISC	Iron-Sulfur cluster
JAK	Janus kinase
KO	Knock-out
LIC	Liver Iron Concentration
LIP	Labile Iron Pool
MAPK	Mitogen-activated protein kinases
MCM	Mini-chromosome maintenance
MDM-2	Mouse double minute 2 homolog
MEF	Mouse Embryo Fibroblast
Mfrn	Mitoferrin
NCOA4	Nuclear Receptor Coactivator 4
NTBI	Non-Transferrin Bound Iron
NTRK1	Neurotrophic receptor-tyrosine kinase 1
ORC	Origin Recognition Complex
PCBP1	Poly-(rC)-binding protein
PCNA	Proliferating cell nuclear antigen
PPAR γ	Peroxisome Proliferator-activated receptor gamma
PRIM2	Primase 2
Psf1-3	Partner of sld five 1
PTC	Papillary Thyroid Carcinoma
Rb	Retinoblastoma
RET	Rearranged During Transfection
RET/PTC	RET/papillary thyroid carcinoma
RFG,	Ret Fused Gene
RNR	Ribonucleotide Reductases
ROS	Reactive Oxygen Species
SLC11A2	Solute Carrier Family 11 Member 2
SLC25A37	Solute carrier Family 25 (mitochondrial inner membrane)
SLC46A1	Solute Carrier Family 46 (Folate Transporter), Member 1
Sld5	Synthetic Lethality with DPB11-1 5
SMAD	Small mother against decapentaplegic
STAT3	Signal transducer and activator of transcription 3
STEAP	Six-transmembrane epithelial antigen of the prostate
Tf	Transferrin
TfR1	Transferrin Receptor 1
TfR2	Transferrin receptor 2
TMPRSS6	Transmembrane Protease, Serine 6
TWSG1	Twisted Gastrulation BMP Signaling Modulator 1
UTR	Untranslated region
WT	Wilde type
XPD	Xeroderma pigmentosum group D
ZIP 14	Zinc transporter 14

ABSTRACT

NCOA4 protein is involved in iron metabolism. Indeed, under low iron conditions, NCOA4 accumulates and promotes, as cargo receptor, the autophagic degradation of the iron-storage macromolecule ferritin. This process, called ferritinophagy, is critical to restore the appropriate cellular iron levels and could impair systemic iron homeostasis. Consistently, we have demonstrated that mice carrying genetic ablation of NCOA4 were unable to mobilize iron from deposits, featuring tissue iron overload as well as mild anemia. Because of impaired ferritinophagy, NCOA4 null mice displayed a severe microcytic hypochromic anemia and ineffective erythropoiesis when fed with an iron low diet. Conversely, they poorly tolerated an iron rich diet, dying prematurely for iron toxicity. Since in previous studies we discovered that nuclear NCOA4 is a chromatin binding protein that acts as a negative regulator of DNA replication origin activation, inhibiting the MCM2-7 DNA helicase, we also investigated whether NCOA4 could regulate DNA replication as a function of iron bioavailability. Treatment with iron chelators promoted a G1-arrest, blocking DNA replication origins activation. In cell fractionation experiments, we observed that iron depletion induced nuclear translocation of NCOA4, and by ChIP and co-immunoprecipitation assays we demonstrated that NCOA4 increased its binding to DNA replication origins and to MCM2-7 complex, respectively. Silencing of NCOA4 induced an unscheduled activation of DNA replication under iron-depleted conditions that promotes replication stress and reduction of cell viability. In conclusion, our data indicate NCOA4 as a novel inter player coupling DNA replication origin activation to cellular iron levels.

1 BACKGROUND

1.1 Iron: the essential ion for life

Iron is a vital element for almost all organisms because of its ability to assume multiple oxidation states. Indeed, it can transiently cycle between divalent ferrous (Fe^{2+}) and trivalent ferric (Fe^{3+}) iron functioning as a cofactor for several hemoproteins (hemoglobins, catalases, peroxidases and cytochromes) and non-heme iron containing proteins (ribonucleotide reductase) (Pantopoulus et al, 2012). This property may also render the metal toxic to biological systems (as ferrous iron Fe^{2+}): in presence of H_2O_2 , normally produced during cellular respiration, it generates highly reactive hydroxyl radicals-Fenton reaction- that readily attack and damage organic macromolecules. However, in nature iron often adopts the oxidized state (Fe^{3+}) which is insoluble at physiological pH. Because of this low solubility and high toxicity cells and organism have evolved a tight control over the uptake and the distribution of iron in order to avoid its excess but also its deficiency.

1.2 Systemic iron homeostasis (absorption, utilization, recycling)

In mammals the absorption of inorganic iron involves firstly its reduction ($\text{Fe}^{3+} \rightarrow \text{Fe}^{2+}$) by ascorbate or by membrane associated ferrireductases (the best known is duodenal cytochrome b, DcytB) at the brush border of duodenal enterocytes. As there is little or no paracellular iron transport under normal circumstances, Fe^{2+} crosses the apical membrane of enterocytes through the divalent metal transporter 1 DMT1/SLC11A2 (Gunshin et al, 1997).

Iron contained in the prosthetic group of hemoglobin (Hb) is absorbed in a not well-defined way and the only carrier proposed is SLC46A1, mostly involved in folate absorption (McKie et al, 2008). However, after the disassembly of the macromolecule by heme oxygenase, free iron follows the same destiny taken by inorganic iron (Andrews et al, 2007).

Depending on body's requirements, then iron can be stored in ferritin macromolecule within cells and lost along the old enterocytes or it can be exported into the blood circulation by the only known basolateral carrier present in mammals called ferroportin (Slc40A1) (Mckie et al, 2000). There, it is first oxidized ($\text{Fe}^{2+} \rightarrow \text{Fe}^{3+}$) by hephaestin, a multicopper oxidase associated to Slc40A1, and then delivered to all tissue by the glycoprotein transferrin (Tf).

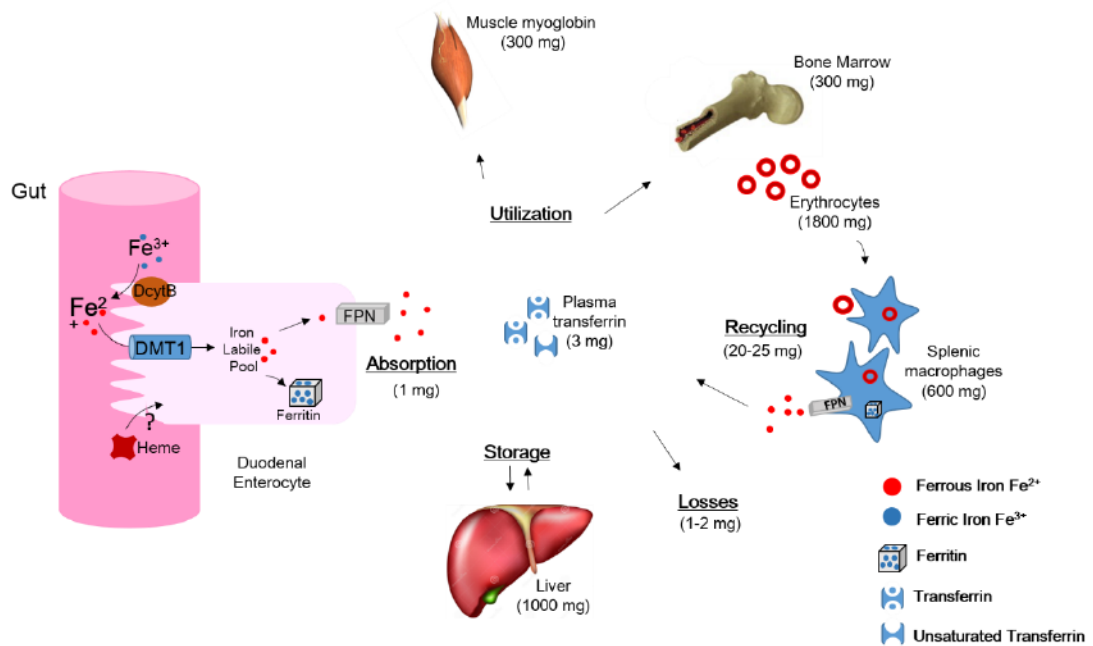


Figure 1. Systemic Iron Homeostasis and Main Iron Flows

Iron flows through a closed system with no active excretion mechanism. Iron can be absorbed only in Ferrous state (Fe^{2+} - red bullet). Every day only 1-2 mg of iron can be absorbed, balancing iron losses and tissue needs. The majority of iron is recovered by splenic macrophages.

Transferrin has two high-affinity binding sites for Fe^{3+} and its holo form, holo-transferrin, can bind two different membrane receptors: a highly affinity receptor TfR1, which is ubiquitously expressed and is involved in iron release to cells and a specific liver and bone marrow receptor, TfR2, that binds to Tf with low affinity and appears to be regulatory (Nia et al, 2015).

Under physiological conditions, transferrin is partially saturated (in humans 30%, in mice 50%) and the percentage of saturation reflects body iron level: when it exceed 60%, non-transferrin-bound iron accumulates in circulation and damages parenchymal cells since there is no active mechanism ensuring iron excretion (Hentze et al, 2010). Thus, iron levels can be controlled only through a fine regulation of its enteric absorption and its splenic/hepatic recycling.

Every day, 1-2 mg of iron are absorbed to offset iron loss due to desquamation of epithelial or enteric cells or bleeding but the majority of it (20-25 mg) is recovered from splenic and hepatic macrophages. These cells phagocitate senescent and damaged erythrocytes and catabolize hemoglobin to release iron in blood through ferroportin carrier (Fig. 1)

The key mechanism that mammals have evolved to control systemic iron level affects mainly ferroportin stability and is related to the hepatic hormone hepcidin.

Hepcidin protein is a liver peptide of 25 amino acid encoded by HAMP gene. HAMP gene was soon linked to iron metabolism, being overexpressed in mice

livers subjected to iron overload (Pigeon et al, 2001). Indeed, hepcidin acts as a “ferroportin ligand” able to induce ferroportin internalization and degradation (Nemeth et al., 2004) in order to limit iron availability, blocking iron uptake from enterocytes as well as iron release from macrophages.

Hepcidin production is basically regulated by the Bone Morphogenetic Protein 6 (BMP6), a member of transforming growth factor-beta superfamily (Figure 2). This factor, in complex with Hemojuvenile coreceptor (Hjv), joins the liver BMP receptors type I (Alk2 or Alk3) and the type II (ACTRIIA) to activate HAMP transcription *via* SMAD transcriptional complexes (Wang et al. 2005). Hepatocytes can “sense” iron overload and release BMP6, that in an autocrine manner potentiate the SMAD axis, as mentioned before. However, additional levels of control are exerted on hepcidin expression (Enns et al, 2013). When circulating iron levels increase, transferrin buffers this excess and the resulting Tf-Fe complexes bind not only to Tf-receptor 1, but also to the lower affinity receptor TfR2. On the hepatocytes membranes, TfR1 changes its conformation and allows the detachment of HFE protein, an atypical major histocompatibility complex class I molecule, that in turn stabilizes TfR2—Tf complex and promotes ERK-MAP kinase-dependent hepcidin expression. In this way, both serum iron and tissue iron act as a positive stimulus on HAMP gene in order to reduce iron absorption and recycling.

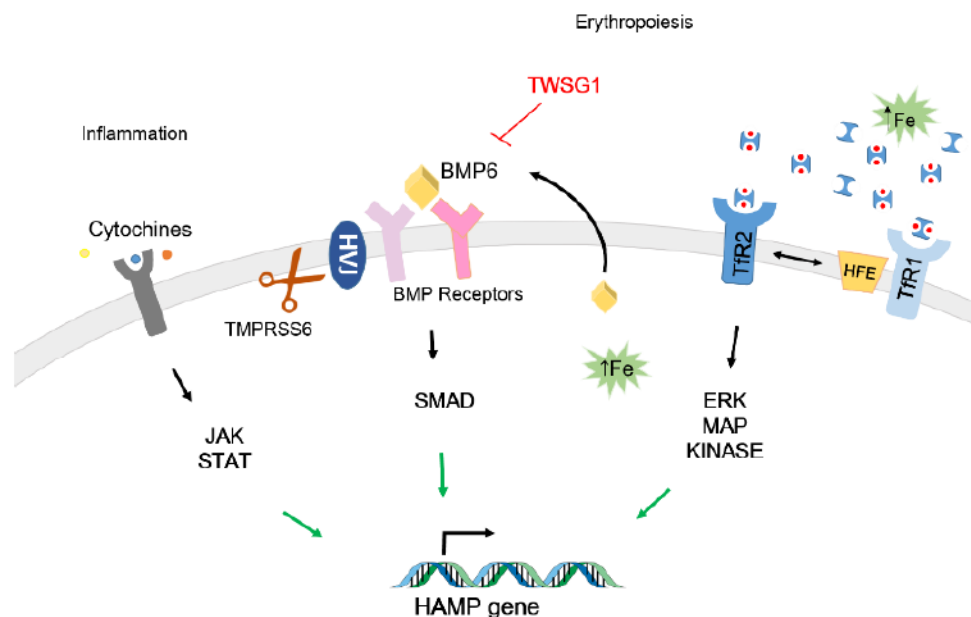


Figure 2. Main signaling affecting HAMP transcription

High tissue iron or serum iron and inflammation represent the major positive stimuli known to increase hepatic hepcidin transcription whereas erythropeiosis process, which require a constant supply of iron, act as negative stimulus.

The increase in hepcidin levels is also achieved in response to infections via cytokines such as IL-6 and the subsequent activation of JAK-STAT3 pathway. The latter has evolved as a defense mechanism to restrict serum iron availability to pathogens (Rishi et al, 2015).

Otherwise, erythropoietic signals sent from bone marrow such as the BMP antagonist TWSG1 (Tanno et al, 2009) or the novel erythroid regulator, erithroferrone (ERFE) (Kauts et al, 2014) can override the regulation by iron stores and strongly suppress HAMP gene in order to keep up with the erythropoietic iron demand. In condition of anemia, tissue hypoxia blocks hepcidin expression firstly stimulating proliferation and differentiation of erythroid precursor through erythropoietin (EPO) and secondly, the stabilization of HIF transcription factors induces the expression of a specific liver protease (matriptase-2 or TMPRSS6) able to cleave Hvj and to interfere with BMP6/SMAD signaling (Silvestri et al, 2008 and Lakhali et al, 2011).

1.3 Systemic Iron overload and iron deficiency

Either iron deficiency or iron excess could have deleterious effects on health leading to anemia or iron overload and hemochromatosis.

Inadequate absorption of iron from diet can cause microcytic anemia especially during growth or pregnancy. Likewise, also abnormal high levels of hepcidin lower iron and cause anemia (Gozzelino et al, 2016). For example, patients with chronic inflammation (malignancies, infections, etc.) have higher amounts of inflammatory cytokines, which stimulates hepcidin and lead to ACD, Anemia of Chronic Disease. Furthermore, mutations in TMPRSS6 (matriptase-2) impair one of the negative control on BMP6/SMAD/hepcidin axis, leading to a hereditary form of iron deficiency called IRIDA (Iron refractory iron deficiency anemia).

All the genetic alterations affecting proteins involved in hepcidin-ferroportin signaling lead to a form of primary iron overload belonging to Hereditary Hemochromatosis (HH), the most frequent recessive inherited disorder of the western world. A common mutation found in HH affects HFE gene (C282Y substitution) and abolish HFE localization on cell surface (Feder et al, 1997). Other mutations have been found in TFR2 or in HVJ gene leading to a more severe or a juvenile form of the disease, respectively, whereas in rare case hepcidin-encoding gene itself can be mutated.

Studies in mice carrying HFE, TFR2 or HJV genetic inactivation have clarified the role of the main signaling pathways involved in iron homeostasis and have demonstrated how alterations in these axes lead to inappropriately low expression of hepcidin which fails to be modulated in spite of liver iron overload and related increased BMP6 expression.

Moreover, a peculiar form of HH presents gain-of-function mutations on ferroportin gene (FPN1). In this condition, hepcidin levels reflects iron deposits but the carrier ferroportin results insensitive to hepcidin down-downregulation.

Iron overload could also be associated to certain congenital disorders, such as Beta-thalassemia, characterized by ineffective erythropoiesis, accumulation of erythroid precursors, hypoxia and the release of antagonist factors of BMP6 signaling (i.e. ERFE), that completely block hepcidin function despite high iron levels.

Whatever the cause of HH, when iron exceeds body needs, it saturates all transferrin molecules and circulates in a toxic form as non-transferrin bound iron (NTBI) loosely chelated by albumin or by small organic molecules such as citrate (Brissot et al, 2012). Membrane transporter such as DMT1 or ZIP 14 have been proposed as possible candidate for NTBI uptake (Liuzzi et al, 2006 and Gunshin et al, 2005). Thus, iron can accumulate in several organs: firstly in liver, a primary site of storage, but also in heart, impairing cardiomyocytes contractility or in pancreas and in all ductless gland. Interestingly, in HH the key organ in iron recycling, the spleen represents the only site “free of iron” because of FPN stabilization in splenic macrophages secondary to low hepcidin production.

In all cells, the excess of ferrous iron (Fe^{2+}) can donate electrons beginning cycles of redox reactions that readily attack and break lipids, nucleotides and proteins leading to cell death.

Although the inappropriate amounts of free iron in HH, method to determine plasma free iron are not well defined. On the contrary, the evaluation of serum iron, transferrin saturation and the determination of liver iron concentration (LIC) from liver biopsy, represent the main standard to monitor iron overload. Moreover, when tissue iron levels increased, a glycosylated isoform of L-ferritin circulates in bloodstream. This form contains very low amounts of iron, probably derived from damaged tissue or splenic macrophages that can easily be detected as an indirect marker of iron burden (Taher et al, 2009).

1.4 Cellular iron homeostasis: from uptake to storage

Besides the complex systemic iron metabolism, also cells coordinately regulate iron uptake, storage, utilization and final export. The circulating complex Fe^{3+} -Tf bound to the TfR, is internalized into cells by clathrin-dependent endocytosis (Hentze et al. 2010). There, low pH of vesicles allows the release of Fe^{3+} from the complex Tf-TfR and its reduction by STEAP metalloredutases, prior its export to cytosol via DMT1 transporter. Then Apo-Tf can be recycled and secreted into the bloodstream because of the low affinity to transferrin receptor. All cells that rapidly divide, such as erythroid progenitor, intestinal epithelial cells or also neoplastic cells, show increased needs for iron and express high TfR1 levels and are particularly addicted to Tf/TfT1 cycle (Gkouvatsos et al, 2012).

Newly acquired iron immediately associates with several low molecular-weight chelates, such as citrate, ATP, AMP, pyrophosphate or peptides in a transient pool called Labile Iron Pool (LIP). From LIP, iron can enter the mitochondria, the major site of its utilization via mitoferrin transporter (Mfrn or SLC25A37)

to synthesize heme or iron sulfur clusters whereas all the excess can be stored in a redox inactive form (Fe^{3+}) into ferritin.

Mammalian ferritin is a heteropolymer made of 24 subunits of FTL (light) and FTH (heavy) chains that associate in a spherical cage able to accumulate up to 4500 iron atoms. H-ferritin has a ferroxidase activity necessary for iron deposition as ferric oxy-hydroxide phosphate while L-ferritin promotes iron nucleation. It has been demonstrated that (in cells and in vitro) iron loads into ferritin through a metallochaperone molecule called (poly-(rC)-binding protein), an RNA binding protein with cytosolic and nuclear localization. In mammals, the proportion of H and L subunits can vary and depend on tissue function. Indeed ferritin found in heart and brain is rich in H chains to sequester and inactivate ferrous iron whereas in spleen and in liver predominates L-ferritin, a form of the macromolecule more stable which may contain a larger amount of iron (Arosio et al, 2009). Interestingly, ferritin predominantly of heavy chains has been also observed in nucleus and probably protects DNA from iron-induced damage (Surguladze et al, 2005).

The excess of intracellular iron can also be eliminated through Ferroportin carrier.

Iron levels in cells rely on proteins involved in its metabolism such as ferritin (storage), transferrin receptor (uptake) or ferroportin (export) and are regulated by iron-regulatory protein 1 and 2 (IRP 1/2). IRP1 and IRP2 are homologous to mitochondrial aconitase and have a cubane of Iron-Sulfur cluster (ISC) in their active site. They are also able to bind to specific stem-loop structures of 25-30 nucleotides called IRE -Iron Responsive Element- which are present in the 5' and 3' untranslated region (UTR) of lots of mRNAs (Wilkinson et al, 2014). Interaction of IRP proteins to hairpin structures in 5'UTR of mRNA (such as in ferritin, ALAS-2, ferroportin, HIF2 α) mainly decrease translation whereas in 3' UTR of mRNA (contained in TfR1, DMT1) stabilize translation.

In iron-replete cells, iron can ligate IRP1 as a Fe-S cluster keeping the protein in a close conformation unable to bind to IRE and can induce IRP2 proteasomal degradation through the stabilization of the Fbox and leucine rich repeat protein 5, FBxL5. In this circumstance, iron level lowers because ferroportin and ferritin mRNA are free to be translated providing iron storage and export whereas TfR1 mRNA is cleaved, blocking iron uptake. Differently, in iron deficient cells FbxL5-dependent degradation of IRP2 decreases and IRP1 adopts its IRE-binding conformation after the loss of the Fe-S cluster (Nakayama et al, 2011).

Iron levels can rapidly increase not only through the effect of IRP1/2-IRE binding but also through the mobilization of iron from deposits. Indeed, ferritin can be sequestered in double-membrane structures called autophagosomes and delivered to lysosomes for degradation and iron release. This new process is called ferritinophagy and involves NCOA4 (Nuclear receptor coactivator 4) protein as a cargo receptor for ferritin (Mancias et al, 2014; Dowle et al, 2014).

1.5 Iron levels and cell cycle: evidence of a an iron-dependent check-point

The orderly progression among the main phases of the cell cycle (G1-S-G2-M) is governed by CDK protein activities. These kinases recognize and phosphorylate their substrates when bound to cyclins, which expression peaks in a coordinated manner with transition from one phase to another (Figure 3)

During the low CDK activities period, from late mitosis through G1 phase, cell organizes the assembly of the pre-replication complexes (pre-RC) onto DNA. This first process, known as *licensing*, involves the cooperation among origin recognition complex (ORC), cell division cycle 6 (CDC6) and CDC10-dependent transcript 1 (CDT1) proteins to engage the DNA helicase complex MCM2-7 onto potential DNA replication origin. This loaded helicase is inactive at this stage.

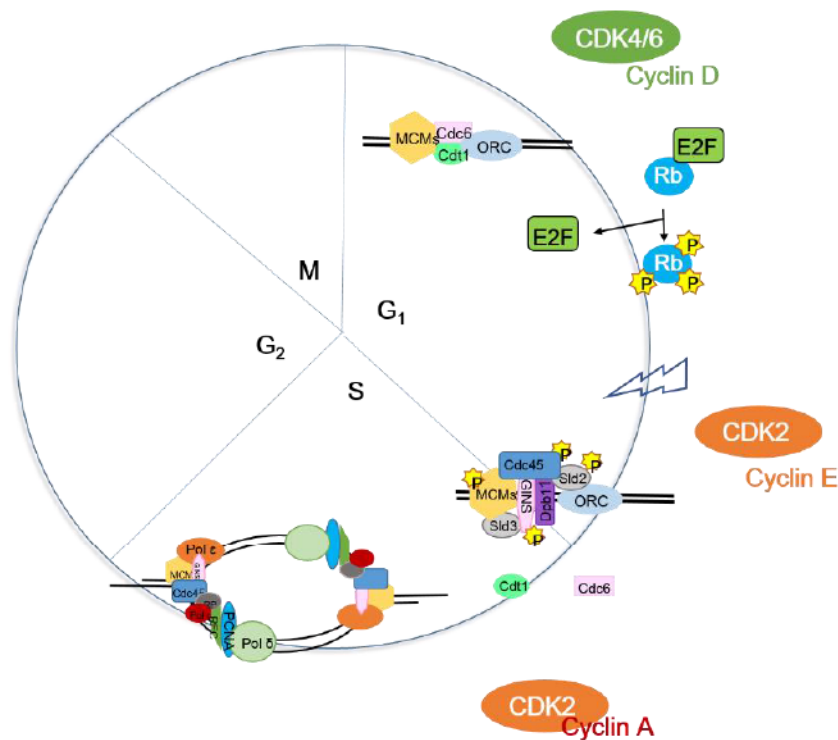


Figure 3. Schematic representation of cell cycle

Specific CDK-cyclin complexes are responsible for driving the various events known to take place during interphase in a sequential and orderly fashion.

When external signals stimulate cells to proliferate, cyclin D levels increase, enabling CDK4/6 to initiate Rb phosphorylation and inactivation. Thus, E2F transcriptional factors are freed to promote cyclin E transcription, allowing the complex CDK2-Cyclin E to activate a positive loop on RB-suppression/E2F activation and overcome the restriction point at the boundary of G1/S phase. Moreover, E2F factors promote transcription of genes responsible for DNA

synthesis (DNA pol α and δ , PCNA) and cyclin A to progress throughout the S-phase.

Activated CDKs (cyclin E/A with CDK2), together with Cdc7/DDK (Dbf4 and Drf1 dependent kinase) phosphorylate different members of the pre-replication complex, triggering the *origin firing* process in which the licensing factors CDC6 and CDT1 are released from chromatin (Delmolino et al, 2001; Li et al, 2003) and other replication factors, such as CDC45 and the GINS heterotetramer, (Psf1-3;Sld5) bind to licensed origins to form the Pre-IC (Pre-initiation complex) or CMG (Cdc45-MCM2-7-GINS) complex. The CMG represents the processive helicase able to unwind double strand DNA and open the replication bubble. There, RPA protein binds to single strand DNA, recruits DNA polymerases and allows, together with processive factor PCNA, the synthesis of DNA.

Finally, if all DNA is replicated correctly, cells can progress through G2 phase and prepare mitosis. The G2/M transition is marked by Cdc25 phosphatase activation and the removal of inhibitory phosphate on CDK1-cyclin B complexes.

Cells have evolved different regulatory pathways able to monitor the successful completion of each phase prior to proceeding to the next one (Hartwell et Weinert, 1989) and to arrest the cell cycle temporarily not only in case of damaged DNA but also in case of low nutrient availability. Besides basic organic macroelements such as glucose or lipids, also microelements are necessary. Iron is an essential microelement for fundamental biological processes in mitochondria, cytosol and nucleus. For example, numerous proteins involved in electron transfer but also in DNA replication and repair, like the three DNA polymerases (Pol alfa, Pol delta, Pol epsilon) or DNA helicases (XPD, FANCI, RAD3) and DNA primase (regulator subunit PRIM2) contain a conserved Fe-S domain necessary for their activity. Moreover, Ribonucleotide Reductases (RNRs) have a small subunit (R2) that continuously needs iron to form a diferric tyrosyl radical necessary to reduce ribonucleotides in deoxyribonucleotides (dNTPs), the building blocks of DNA (Zhang C. et al, 2014).

Thus, cells have to coordinate their proliferation also to intracellular iron levels. When quiescent cells are stimulated to re-enter the cell cycle, they increase iron uptake through enhanced TfR expression (Kwok et Richardson, 2002) and accordingly, depletion of the intracellular iron pool of cycling cells lead to cell cycle arrest (Le et Richardson, 2002).

Studies focused on the effects of iron chelators (deferrioxamine, DFO) have demonstrated that low iron blocks cells in late G1 phase suggesting the existence of a specific iron-sensitive cell cycle checkpoint. Indeed, analogous to the DNA damage checkpoint in which damaged DNA blocks replication in order to maintain genome stability, it would also be dangerous if cells began DNA synthesis without sufficient resources to complete the process.

The addiction of proliferating cells to iron is also underlined by the higher susceptibility of cancer cells, such as neuroblastoma cells, to iron deprivation, to

the point that iron chelators represent an alternative therapeutic strategy to treat some cancers.

The exact molecular mechanism underlining cell cycle arrest after iron depletion has not been fully understood. At first, it was thought that Fe chelation only inhibited RNR activity. In fact, recent studies have shown that other proteins involved in cell cycle progression are affected.

In iron deficiency, the expression levels of cyclin E, the specific catalytic subunit of CDK2, are reduced blocking cells in late G1 phase. Moreover, some CDKs inhibitors, such as p21 or p27 have been found to be up regulated in a p53-dependent manner after deferoxamine treatments. Indeed, iron chelation induces p53 phosphorylation at serine 15 and 37 preventing any association with mdm-2 and the subsequent proteosomal degradation. Stabilized p53, in turn functions as a positive transcriptional factor for CDKs inhibitors in order to arrest cell cycle. Interestingly, p53 also promotes the transcription of a specific subunit of RNR, p53R2 supplying the production of nucleotides in case of DNA damage (Tanaka H et al, 2000).

Low iron levels also mimics hypoxic state by interfering with Prolyl Hydroxylases functions, leading to increased stabilization of HIF1 α . Translocated to the nucleus, HIF1 α targets many genes by binding to the hypoxia-responsive element contained in their promoter, such as TfR1, which then functions to increase intracellular iron (Bianchi L et al. 1999). Moreover, HIF1 α also interacts and stabilizes p53 (An WG et al. 1999) and can promote apoptosis, upregulating pro-apoptotic factors such as BNIP3 (Bruick RK, 2000). Interestingly, it has been demonstrated that HIF1 α binds to Cdc6, a member of the pre-replication complex, inhibiting the phosphorylation induced by DDK and the formation of the active helicase represented by the CMG complex, in order to avoid DNA duplication (Hubbi et al, 2003)

1.6 NCOA4 protein: a multifunctional protein involved in iron metabolism and DNA replication

NCOA4 gene (also known as RFG, ELE1 or ARA70) encodes a 70-kDa protein that is ubiquitous expressed. Data obtained from our laboratory showed that NCOA4 is highly expressed in liver, duodenum, spleen and testis in adult mice (data not shown). The first role associated to NCOA4 protein was as a transcriptional coactivator for several nuclear receptors, including androgen receptor (AR), estrogen receptor (ER), peroxisome proliferator-activated receptor gamma (PPAR γ) (Yeh and Chang, 1996) and also thyroid hormone receptor (Moore JM et al, 2004). Indeed, it possesses two specific nuclear receptor binding motifs: LXXLL, mediating the interaction with TR and PPAR γ and FXXLF involved in AR and ER interactions. Moreover, the amino acid sequence of full length proteins reveals that there are no specific structural or functional domains except for the coiled-coil domain (cc) present in its N-

terminal portion, enabling the dimerization and oligomerization of the protein (Monaco et al, 2001).

This property is especially relevant for NCOA4-RET (or RET/PTC3), a chimeric protein resulting from a common paracentric inversion of the 10 chromosome firstly found in Papillary thyroid cancers (in 10-20 % of all PTCs) (Santoro et al, 1994). This recombination leads to the fusion of the first exons of NCOA4 gene with the last nine exons of RET gene, encoding the tyrosine kinase portion of RET receptor. It has been demonstrated that NCOA4-RET is directly involved in thyroid tumorigenesis and possesses oncogenic properties. Indeed, the dimerization mediated by the NCOA4 N-terminal portion leads to the ligand-independent activation of the catalytic portion of RET, and of the downstream signaling pathways such as MAP Kinase and PI3K-AKT cascades, promoting uncontrolled proliferation and survival.

The association of NCOA4-RET rearrangement to more aggressive PTC subtypes (Basolo et al, 2002) has suggested that not only the activity of RET oncogene but also the loss of NCOA4 protein could contribute to cellular transformation. Interestingly, NCOA4 expression is reduced in different prostate cancer cell lines (Tekur et al, 2001) and in a subset of HER2-positive breast cancer, identifying NCOA4 as a potential tumor suppressor.

To date, studies of sequencing of numerous tumor samples detected NCOA4-RET in non small cell lung cancer (adenocarcinomas) (Wang et al, 2012) and in colon carcinoma (Le Rolle et al, 2015).

Recently, our group has demonstrated that NCOA4, via its N-terminal portion, interacts with the mini chromosome maintenance protein MCM7, a component of the DNA helicase MCM2-7 (Bellelli et al, 2014). Via such interaction, NCOA4 blocks the CMG helicase activity and the opening of the replication bubble necessary to achieve DNA replication origin during S-phase. Through experiments in *Xenopus laevis* egg extracts, a cell-free system that recapitulate DNA replication after the addition of demembrated sperm nuclei, we observed that the recombinant full-length protein completely abolish DNA synthesis. Moreover mouse embryonic fibroblasts (MEFs) derived from a transgenic mouse Knock Out for NCOA4 display uncontrolled DNA origin activation and replication stress that lead to premature senescence. Thus, NCOA4 protein exerts a negative control over DNA duplication. Further studies are needed to understand how this mechanism is affected during cell cycle and which could be the cellular contexts requiring this additional form of regulation. Two different studies have also described NCOA4 involved in cellular iron metabolism, an apparently unrelated function for this unique protein. At molecular level NCOA4 can bind to H isoform of ferritin, through a specific tryptophan residue (W497) present in its C-terminal conserved portion and with certain proteins of the catabolic autophagic machinery (ATG8-like proteins such as GABARAP). Indeed, NCOA4 acts as a cargo receptor delivering ferritin to autophagosomes, little vesicles that fuse with lysosomes in order to mobilize iron from storages. This process, called *ferritinophagy* is affected by cellular iron levels and is mainly regulated by NCOA4 turnover (Mancias et al, 2016). Indeed,

in iron replete conditions, NCOA4 binds to iron, in a not fully understood way, folding into a conformation recognized by the E3 ubiquitin ligase, HERC2. Then NCOA4 levels lower whereas ferritin macromolecules accumulate to capture iron. On the contrary, in iron deficiency, NCOA4 interacts with the target ferritin and promotes its autophagic degradation restoring appropriate intracellular iron concentration.

2 AIMS OF THE STUDY

NCOA4 protein has been recently involved in different functions. It was firstly described as a coactivator of several nuclear receptors, including peroxisome proliferator activated receptors α and γ , receptors for steroid hormones and thyroid hormones, promoting their transcriptional activity.

NCOA4 also acts as a negative regulator of DNA synthesis binding to DNA replication origins and directly interfering with the MCM2-7 helicase function. Its ablation in mouse embryonic fibroblasts allows unscheduled DNA origin activation resulting in replicative fork stalling and genome instability that lead to cellular senescence.

On the other hand, cytosolic NCOA4 protein plays a crucial role in cellular iron metabolism acting as a cargo receptor for ferritin, the iron storage macromolecule. In iron-depleted conditions, NCOA4 accumulates, avoiding HERC2 ubiquitination and proteosomal degradation, and delivers ferritin to the autophagic catabolic route in order to restore iron levels. This new process, called *ferritinophagy* helps to establish the appropriate cellular iron levels, in addition to the IRP1 and IRP2-dependent control. However, the impact of this process in systemic iron homeostasis maintenance has not been investigated. In addition how iron levels may insist on activation of DNA replication origins via NCOA4 is still known.

First aims of this thesis was to study the role of NCOA4-mediated *ferritinophagy* in living animals carrying total ablation of NCOA4 gene and to evaluate how this process may affect systemic iron homeostasis in normal condition and also in iron deficiency and overload conditions.

To these aims we:

- Evaluated ferritin levels in key organs for iron metabolism (spleen, bone marrow, liver and duodenum), hematological parameters and key biochemical markers of iron status (serum iron, transferrin saturation) in NCOA4 deficient mouse model at basal level .

- Evaluated the hematological phenotype of NCOA4 deficient mouse and in particular erythropoiesis process after exposure to 5 and 7 months of low-iron diet in order to study iron mobilization from tissue stores in stress conditions

- Evaluated the phenotype of NCOA4 deficient mice fed with an iron-rich diet.

Second aims of this thesis was to clarify whether iron bioavailability affects DNA replication also through NCOA4 functions.

To this aim we:

- Evaluated NCOA4 nuclear localization and its binding to replisome in iron deficient condition

- Evaluate NCOA4 recruitment to DNA replication origins in HeLa cells by chromatin immunoprecipitation in iron deficient conditions

- Evaluate cell cycle progression in normal and NCOA4 deficient cells exposed to iron deficiency and whether changes in “IDR”, Iron Depletion Response, in NCOA4 null cells might affect cell viability.

3 MATERIALS AND METHODS

3.1 Cell Culture

HeLa cells were cultured in RPMI supplemented with 10% fetal bovine serum (FBS), 50 mg/ml penicillin-streptomycin, and 2 mM L-glutamine. WT and NCOA4-null MEFs were produced and cultured as described by Bellelli et al. (2014). To induce iron-overload conditions, MEFs were treated for 16 hours with 10 mg/ml of ferrum ammonium citrate (FAC), whereas, for growth under iron-deficient conditions, cells incubated for 24 hr in FAC were released in normal medium containing 50 mM deferoxamine (DFO).

Cell synchronization by nocodazole arrest. HeLa cells were incubated with 100 ng/ml nocodazole for 16 hours. Upon mitotic shake off, M-phase arrested cells were collected, washed 3 times with 1X phosphate-buffered saline (PBS) and plated in complete medium. Subsequently, cells were harvested at different time points or treated with DFO and subjected to fractionated protein extraction.

3.2 Cell fractionation

For subcellular fractionation cytosol /nucleosol, cells in the mid-exponential phase of growth were collected by scraping from the culture dish after two washings with 20 ml ice-cold 1X phosphate-buffered saline (PBS). Subcellular fractions were prepared using the NE-PER nuclear and cytoplasmic extraction kit (Pierce Biotechnology, Rockford, IL).

To isolate chromatin-bound proteins from cytosolic and nucleosolic proteins, cells were incubated on ice for 10 min with ice-cold CSK buffer (10 mM PIPES, pH 6.8, 100mM NaCl, 300 mM sucrose, 1mM MgCl₂, 1 mM EGTA, 1mM DTT, 1 mM phenylmethylsulfonyl fluoride, 10 μg/ml aprotinin) containing 0.5% Triton X-100 (Pierce Biotechnology, Rockford, IL). Chromatin-bound and unbound proteins were then separated by low speed centrifugation (3,000 rpm, 3 min at 4°C). To solubilize chromatin-bound proteins samples were incubated with Laemmli buffer (60 mM Tris-Cl pH 6.8, 2% SDS, 10% glycerol, 5% β-mercaptoethanol, 0.01% bromophenol blue) for 10 minutes at 99°C. For each fraction, protein amounts deriving from comparable number of cells were analysed by SDS-PAGE and Western blotting.

To obtain total protein extracts, cells and tissues were lysed in a buffer containing 50 mM N-2-hydroxyethylpiperazine-N'-2-ethanesulfonic acid (pH 7.5), 1% (vol/vol) Triton X-100, 150 mM NaCl, 5 mM EGTA, 50 mM NaF, 20 mM sodium pyrophosphate, 1 mM sodium vanadate, 2 mM phenylmethylsulphonyl fluoride and 1 μg/ml aprotinin. Lysates were clarified by centrifugation at 13200 rpm for 30 min. Lysates containing comparable amounts of proteins, estimated by Bradford assay (Bio-Rad, Munchen, Germany), were immunoprecipitated with the required antibody or subjected to direct Western

blotting. Immune complexes were detected with the enhanced chemiluminescence kit (Amersham Pharmacia Biotech, Little Chalfort, UK). Immunoblotting was carried out with specific antibodies.

For binding assay (pull-down), HeLa cell lysates were incubated with recombinant proteins immobilized to resin (glutathione sepharose 4B for GST-tagged protein and Ni-NTA Agarose matrix to purify NUS/His tagged protein). Bound proteins were detected by immunoblot analysis.

3.3 Chromatin Immunoprecipitation (ChIP)

Chromatin immunoprecipitation was performed from exponentially growing HeLa cells using purified anti-NCOA4. Cells were first cross-linked for 10 min by adding formaldehyde to a final concentration of 1%. Cross-linked cells were then blocked using glycine to a final concentration of 1.25 M, then lysed in SDS lysis buffer containing protease inhibitors and sonicated to reduce DNA to a length between 150 and 500 bp. The sheared chromatin extract was then frozen in aliquots at -80°C until required. The supernatants diluted 10-fold in ChIP dilution buffer with protease inhibitors and precleared with 60 μl salmon sperm DNA/protein A Agarose-50% slurry for 60 min at 4°C . Cross-linked chromatin was incubated overnight with 10 μg of antiNCOA4 antibody or control IgG in a total volume of 1 ml at 4°C . Antibody-protein-DNA complexes were isolated by immunoprecipitation with 60 μl salmon sperm DNA/protein A. After extensive washing, pellets were eluted by freshly prepared elution buffer (1% SDS, 0.1 M NaHCO_3). Formaldehyde cross-linking was reversed by 5-12-h incubation at 65°C after adding 20 μl 5 M NaCl. Samples were purified through phenol-chloroform extraction and used as a template in PCR. Primers for PCR were as follows:

Lamin B2 origin (ORI):

Forward GGCTGGCATGGACTTTTCATTTTCAG

Reverse GTGGAGGGATCTTTCTTAGACATC

Control region (CTR)

Forward CTGCCGCAGTCATAGAACCT

Reverse ATGGTCCCCAGGATACACAA

c-Myc origin:

Forward TATCTACACTAACATCCCACGCTCTG

Reverse CATCCTTGTCCTGTGAGTATAAATCA

Control region:

Forward TTCTCAACCTCAGCACTGGTGACA

Reverse GACTTTGCTGTTTGCTGTCAGGCT

Real-time PCR experiments were carried out in triplicate, using SYBR green mastermix (Bio-Rad, Munchen, Germany). NCOA4 Enrichments at origin region (ori) with respect to non origin containing region (non ori) region at each loci were calculated with delta Ct method.

3.4 Histology Analysis

Formalin-fixed, paraffin-embedded (FFPE) sections (5 mm thick) were stained with H&E by conventional methods or deparaffinized and rehydrated by passages through xylene and alcohol series for Perl's Prussian blue or immunohistochemical (IHC) staining. For Perl's blue staining, liver, duodenal and spleen section were incubated for 30 minutes with a solution 1:1 ferrocyanide and hydrochloric acid and then washed in water, counterstained with filtered fat red stain and mounted. For the IHC staining, endogenous peroxidase activity was blocked by treatment with 3% hydrogen peroxide (30 min at room temperature). Antigens were retrieved by incubating tissue sections for 15 min in boiling citrate buffer (1 mM, pH 6.0). Slides were blocked in 1% BSA for 1h at room temperature followed by o.n. incubation with primary antibodies anti FPN and for 30 min at room temperature with biotinylated goat anti-rabbit antibody (Vector Laboratories, Burlingame, CA, USA); the stain was visualized with 3,3'-Diaminobenzidine (DAB) (SIGMA-Aldrich).

3.5 RNA Extraction and RT-PCR

RNA was isolated from frozen mechanically fractured mouse liver by using TRIzol reagent (Invitrogen) and purified with chloroform and precipitated with isopropanol/ethanol passages. RNA (1 mg) was reverse-transcribed with a Quantitec reverse transcription kit (QIAGEN).

qRT-PCR reactions were done in triplicate, and fold changes were calculated with the following formula: $2^{-(\text{sample 1 DCt} - \text{sample 2 DCt})}$, where DCt is the difference between the amplification fluorescence threshold of the mRNA of interest and the mRNA of the gapdh used as an internal reference. The primer sequences used for qPCR are:

FPN Forward	CTACCATTAGAAGGATTGACCAGCTA
FPN Reverse	ACTGGAGAACCAAATGTCATAATCTG
FTH1 Forward	TGGAAGTGCACAACTGGCTACT
FTH1 Reverse	ATGGATTTACCTGTTCCTCAGATA
GAPDH Forward	CATGGCCTTCCGTGTTCCCTA
GAPDH Reverse	ATGCCTGCTTCACCACCTTCT
HAMP Forward	TGTCTCCTGCTTCTCCTCCT
HAMP Reverse	CTCTGTAGTCTGTCTCATCTGTTG
TfR Forward	GGTGATCCATACACCTGGCTT
TfR Reverse	TGATGACTGAGATGGCGGAA

3.6 Retrovirus-mediated MEFs transduction

pBABE Puro NCOA4 full length C and N terminal portion or the empty vector were transfected into Phoenix-eco cells and, after 48 hours, viral supernatants were harvested and used to infect primary *NCOA4* $+/+$ or $-/-$ MEFs. Forty-eight hours after infection cells were used to analyze ferritin accumulation and degradation upon FAC treatment and release in DFO as previously described.

3.7 Tissue and Serum Iron Determination

For iron concentration measurements, spleen and liver mouse tissues were dried overnight at 110°C, dissociated mechanically, weighed, and digested in 1 ml of 3M HCl and 0.6 M trichloroacetic acid for 20 hr at 65°C. The total non-heme iron content was then measured using the bathophenanthroline method. Serum iron and transferrin saturation (the ratio of serum iron and total iron binding capacity) were calculated using the serum iron/unsaturated iron binding capacity (UIBC) and the total iron binding capacity (TIBC) kits (Randox Laboratories) according to the manufacturer's instructions.

3.8 Flow Cytometric Analysis of Mouse Bone Marrow erythroblast precursors.

Flow cytometry was carried out with the FACSCanto™ flow cytometer (Becton Dickinson, San Jose, CA, USA). Bone marrow cells were stained with phycoerythrin rat anti-mouse Ter119 (BD Biosciences) and antigen-presenting cell rat anti-mouse CD44 (BD Biosciences) for 30 minutes in the dark at 4°C and then analyzed by flow cytometry within 1 hour.

Apoptosis was evaluated by using fluorescein isothiocyanate (FITC) Annexin V Apoptosis Kit I (BD Pharmingen 556547). Briefly, cells were washed twice with cold phosphate-buffered saline and then resuspend in 1X Binding Buffer at a concentration of 1×10^6 cells/mL. 1×10^5 cells were incubated with 5mL of FITC Annexin V and propidium iodide (PI) for 15 minutes at room temperature in the dark and then analyzed by flow cytometry within 1 hour.

4 RESULTS

4.1 Impaired ferritinophagy in NCOA4 deficient mice promotes tissue ferritin accumulation

In order to clarify the role of NCOA4-mediated ferritinophagy at systemic level, we evaluated ferritin in key tissues for iron metabolism in a mouse model carrying genetic inactivation of NCOA4 gene.

We analyzed protein extracts from liver, spleen, duodenum and bone marrow of NCOA4^{-/-} and wild type 8-week-old mice by western blotting. As shown in figure 4A, NCOA4^{-/-} mice displayed ferritin accumulation in all tissue analyzed compared to wild type mice. Moreover, iron content obtained from liver (Liver Iron Content, LIC) and spleen (Spleen Iron Content, SIC) biopsy of knockout mice was significantly higher than control mice (Fig. 4B).

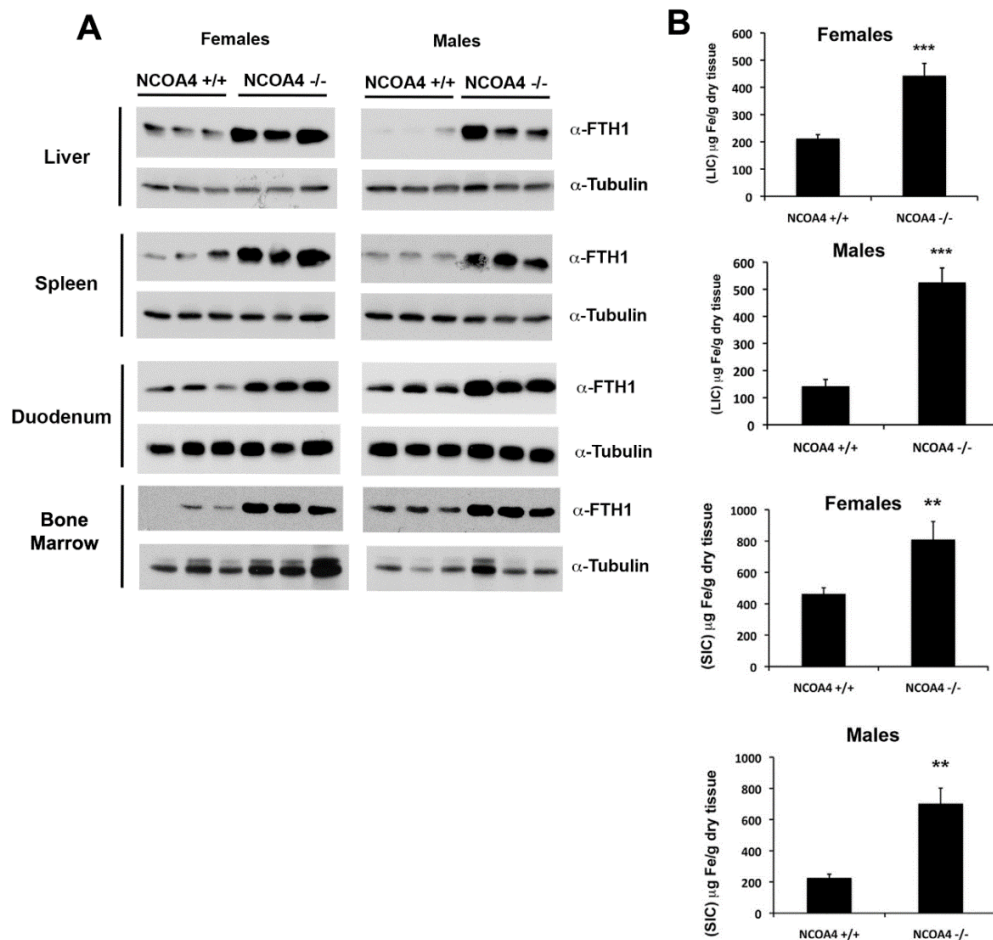


Figure 4. Total Ablation of NCOA4 Gene Results in Tissue Ferritin Accumulation

A. Western blot analysis of ferritin (FTH1) and tubulin protein levels derived from liver, spleen, duodenum and bone marrow of two-old months NCOA4 WT (+/+) and null (-/-) female and male mice.

B. Non-heme iron content were determined from spleen (SIC) and liver (LIC) of NCOA4 WT (+/+) and null (-/-) female and male mice. Mean values of 3 animals for genotype (control NCOA4+/+ and null mice NCOA4-/-) were graphed. Errors bars indicate standard error. Asterisks refer to a statistically significant difference: **P<0.01, ***P<0.001.

We also confirmed tissue iron loading in NCOA4 -/- mice by Perls' blue staining: in liver, spleen and duodenum sections of KO animals, strong blue staining reflected the increased ferritin accumulation (Fig. 5).

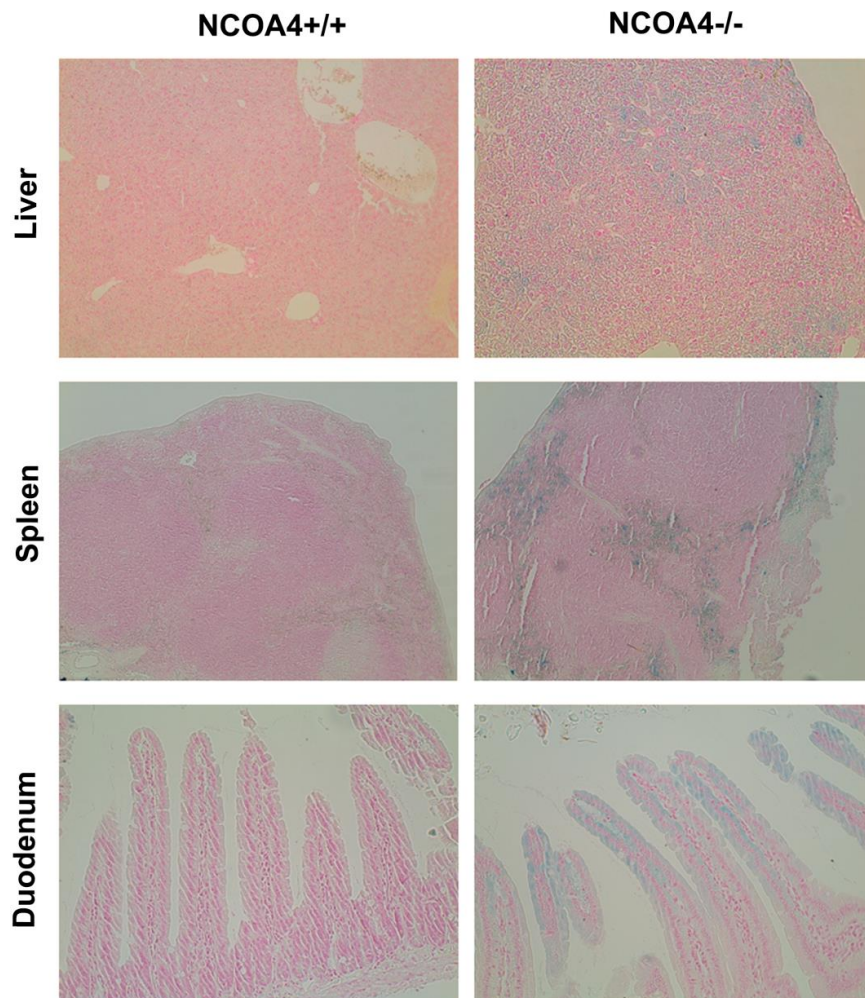


Figure 5. NCOA4 deficient mice display increased iron accumulation.

Representative Perls' Prussian Blue staining of liver, spleen and duodenum from section of NCOA4 -/- and +/+ mice. The blue staining reveal iron deposition.

We next analyzed markers of systemic iron status such as transferrin saturation, serum iron and serum ferritin. As shown in the graph (Fig. 6) serum iron level and transferrin saturation were higher in null mice compared to WT (p value <0,05). Accordingly with tissue iron loading, serum ferritin increased as well in

null mice with respect to wild type animals. The highest levels of circulating iron in knockout animals reflected tissue iron loading but could also suggest an impaired iron utilization.

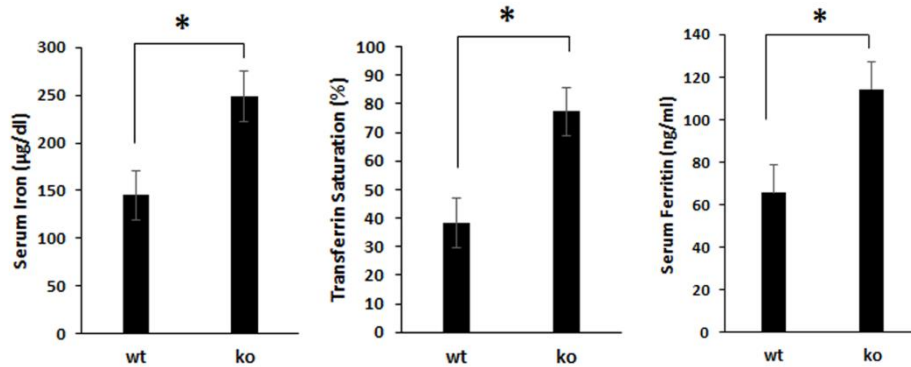


Figure 6. Increased Hematological Markers of Iron Status in NCOA4-Deficient Mice.

Serum iron concentration, serum ferritin concentration and percentage of transferrin saturation were evaluated from 2 months old mice. Mean values of 4 mice for genotype (control NCOA4 WT; null mice NCOA4 KO) were graphed. Errors bars indicate standard error. Asterisks refer to a statistically significant difference: *P<0.05.

4.2 The Hepcidin-ferroportin axis limits iron absorption in NCOA4 null mice

Since the impaired ferritinophagy in NCOA4 null mice increased tissue and serum iron levels, we focus our attention on the physiological response activated *in vivo* to counteract the iron overload, eg the Hepcidin-dependent downregulation of ferroportin (FPN). By Real Time PCR we found that the hepcidin gene transcription (HAMP) was significantly upregulated in the liver of NCOA4 null mice compared to control (fig. 7A).

As mentioned before, HAMP transcription is under control of multiple signaling. We evaluated phosphorylation status of SMAD proteins, which are activated by BMP6/HVJ signaling and MAP-kinase proteins activated by Tfr2 receptor in order to dissect the positive stimuli affecting HAMP expression. As shown by western blotting analysis (Fig.7 B), mice only ERK1/2 proteins (MAPK) resulted hyperphosphorylated and activated in comparison to WT, suggesting a stimulation by saturated transferrin on Tfr2 while the hepatic autocrine BMP6 signal seemed not to be involved. Similarly, IRP2 protein levels, which are affected by labile iron pool, were not increased in NCOA4 null mice liver (Fig 7C). Consistently, Tfr1 and FTH1 mRNA, whose stability is under IRPs control were not changed (Fig 7D).

As hepcidin expression increased, we investigated ferroportin level in duodeni of null mice. Immunohistochemical analysis of the duodenum clearly revealed the reduction of ferroportin levels in NCOA4 null mice (Fig. 7D) because of its

hepcidin-dependent degradation. These first data revealed that the impaired ferritinophagy in NCOA4 null mice increased iron deposits in key iron tissue such as liver and spleen. However, the hepcidin-mediated ferroportin downregulation and the consequent reduction of iron absorption, counteracted, at least in part, dangerous iron overload.

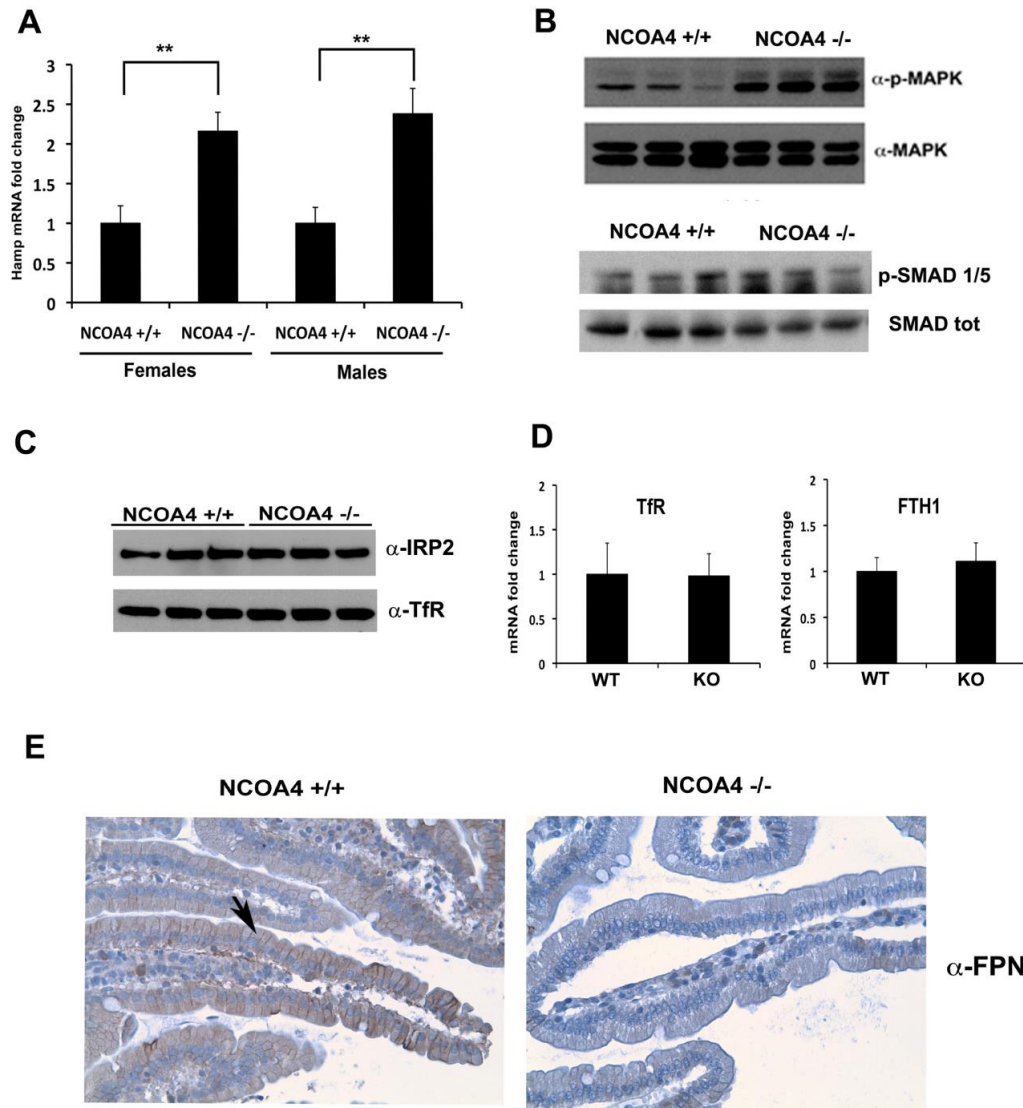


Figure 7. Up-regulation of HAMP gene mediated ferroportin downregulation in NCOA4 deficient mice.

A. Real time analysis RT-PCR of HAMP mRNA in livers from WT and NCOA4 null female and male mice. mRNA ratio was normalized to a WT control mice mean value of 1. Mean values of 4 mice for genotype (control NCOA4 WT; null mice NCOA4 KO) were graphed. Errors bars indicate standard error. Asterisks refer to a statistically significant difference: **P<0.01

B. Western blot analysis of p-MAPK and p-SMAD protein levels from liver extracts of 2 old female and male WT (+/+) and KO (-/-) mice. Total MAPK and total SMAD protein were used as loading control.

C. Western blot analysis of IRP2 and TfR1 protein levels from livers extracts as in B.

D. Real time analysis RT-PCR of TfR1 and FTH1 mRNA from livers as in A.

E. Representative immunohistochemical analysis of ferroportin (FPN) in duodenum sections from NCOA4 WT and null mice. The arrow indicates the basolateral presence of the carrier ferroportin.

4.3 NCOA4 null mice were unable to mobilize iron reserve under iron deprivation

Since the majority of body iron is used for hemoglobin synthesis during erythroid differentiation, we hypothesized that the inability to mobilize iron from ferritin storage could lead to inefficient erythropoiesis in NCOA4 -/- mice. Thus, we evaluated hematological parameters and red cell indices in NCOA4 null and WT mice under normal feeding condition.

Interestingly, all KO mice had a significantly lower values of hematocrit and hemoglobin compared to WT, and small red blood cells with low hemoglobin content (MCV and MCH reduced) reflecting a condition of mild microcytic anemia (Table 1).

Then, we decided to feed NCOA4 null and WT mice for five and seven months with an iron-low diet (2-3 mg/Kg) in order to force organism to release iron reserve to sustain erythropoiesis.

We analyzed ferritin levels in livers of NCOA4 null and WT mice by western blotting after 5 months of low-iron diet (Fig. 8A). As expected, iron deprivation induced a complete depletion of ferritin in WT mice subjected to hypoferric diet with respect to normal diet whereas a significant amount of ferritin was still present in NCOA4 null mice.

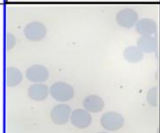
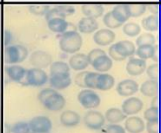
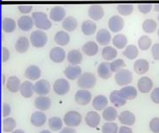
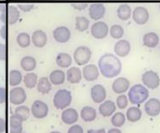
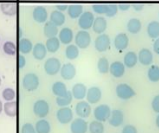
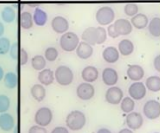
	Iron balance		Iron Deficiency			
			5 months		7 months	
	NCOA4+/+ Mice	NCOA4-/- Mice	NCOA4+/+ Mice	NCOA4-/- Mice	NCOA4+/+ Mice	NCOA4-/- Mice
Hct (%)	45.8 ± 1.1	42.2 ± 1.3*	36.7 ± 1.3*	28.6 ± 2.8*	36.0 ± 0.6*	28.8 ± 3.3*
Hb (g/dl)	15.1 ± 0.2	12.7 ± 0.6*	11.8 ± 0.3*	8.8 ± 1.7*	11.0 ± 0.5*	8.0 ± 1.8*
MCV (fl)	51.7 ± 0.5	46.3 ± 3.05*	47.5 ± 1.5*	38.5 ± 4.1*	43.7 ± 2.7*	36.5 ± 2.4*
MCH (pg)	16.3 ± 0.8	15.6 ± 0.2*	15.4 ± 1.2	10.3 ± 0.9*	14.1 ± 1.3*	10.4 ± 1.5*
MCHC (g/dl)	27.6 ± 0.4	28.2 ± 0.5	27.5 ± 0.3	26.1 ± 0.9*	26.7 ± 0.6	26.7 ± 0.6*
CH (pg)	14.9 ± 0.3	13.0 ± 0.5	13.1 ± 0.6*	9.92 ± 0.9*	10.12 ± 0.4*	9.57 ± 0.86*
RDW (%)	12.6 ± 0.5	15.1 ± 2.5	13.1 ± 0.7	23.4 ± 4.0*	30.12 ± 6.1*	28 ± 7.3*
Retics (103cell/μl)	498 ± 84	488 ± 170	419 ± 98	60 ± 2.8*	41 ± 15*	52 ± 0.8*
MCVr (fl)	55.2 ± 0.4	51 ± 1.84*	53.6 ± 1.9*	48.5 ± 5.4*	41.6 ± 5*	40.2 ± 2.8*
CHr (pg)	14.7 ± 0.8	13.8 ± 1.1	13.45 ± 1.5	11.0 ± 0.78*	13.5 ± 1.1	9.05 ± 1.3*
Perypheral Blood Smear						

Table 1.
Hematological parameters and red cell indices in NCOA4+/+ and NCOA4 -/- mice under iron balance and iron deficient diets.

Notably, a slightly reduction of ferritin levels after low iron diet was also seen in KO animals, suggesting that NCOA4-independent process might promote iron release from ferritin in livers.

The hypoferric diet efficiently induced mobilization of iron reserve in WT mice as demonstrated by maintenance of normal levels of transferrin saturation and serum iron in these animals whereas in KO animals circulating iron was significantly lower (Fig 8B). As a consequence of the greater iron need, in KO animals the hepcidin-ferroportin axis was completely suppressed. Indeed, as shown by real time analysis (Fig. 8C) liver Hepcidin expression was lower in NCOA4 deficient mice respect to WT animals, and, consequently, ferroportin was highly present in spleen macrophages as demonstrated by immunoistochemical analysis (Fig. 8D).

All together, these data strongly confirmed the impairment of iron storage mobilization and recycling in NCOA4 null mice, also after a prolonged low iron diet.

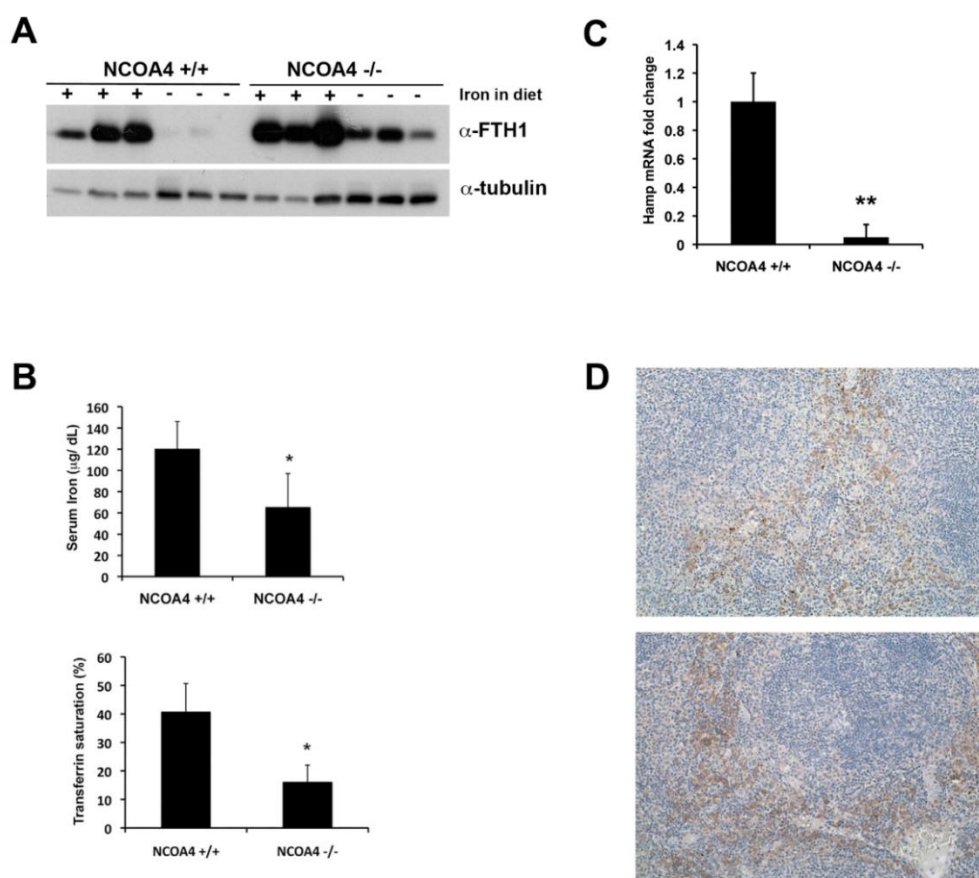


Figure 8. NCOA4 deficient mice display impaired iron mobilization under iron restricted diet feeding condition.

A Western blot analysis of ferritin (FTH1) protein levels of WT and NCOA4 deficient mice under iron balance and iron deficient diets (5 months). Tubulin was used as loading control.

B Serum iron concentration and percentage of transferrin saturation were evaluated in NCOA4 null and WT mice fed an iron deficient diet (5 months). Data are shown as a mean \pm standard deviation. (*P<0.05)

C Real time analysis RT-PCR of HAMP mRNA from livers of WT and NCOA4 mice fed an iron low diet for five months. Normalized data were expressed relative to the corresponding value for a WT control mice under iron deprivation.

D Representative immunohistochemical analysis of ferroportin (FPN) in spleen sections from NCOA4 WT and null mice fed an iron deficient diet (5 months).

4.4 NCOA4 null mice display ineffective erythropoiesis and an impaired terminal erythroid differentiation under iron poor diet

Next, we decided to analyze erythropoiesis in iron deprivation conditions. As shown in the table, knock out animals after 5 months of low iron diet worsened their mild anemia displaying all red cell indices, such as MCV, MCH, MCHC, statistically decreased with respect to the WT. Moreover, null mice presented a lower number of reticulocytes in peripheral blood respect to the WT and an increased RDW (red cell distribution width), indicating that the small number of erythroid precursor able to complete differentiation had a variable size (anisocytosis; see also the representative staining of peripheral blood smear in Table 1). These analyses revealed a condition of severe hypochromic microcytic hyporegenerative anemia in NCOA4^{-/-} mice that worsened after 7 months of low iron diet. Conversely, the WT mice developed a mild anemia after five months of diet, reaching a hyporegenerative anemia only after seven months of low iron diet.

Then, to analyze in detail erythropoiesis, in collaboration with Professor Lucia De Franceschi from Verona University, we monitored terminal erythroid differentiation, by FACS analysis. Terminal erythroid differentiation is a specific stage of erythropoiesis in which proerythroblast differentiates into morphologically distinct populations: basophilic, polychromatic and orthochromatic erythroblasts. This ordered process requires a decrease in cell size, chromatin condensation, hemoglobinization and a complete change in membrane protein composition. Thus, we discriminated and isolated erythroblast populations at each stage of development by flow cytometry, analyzing the expression levels of TER119 (a molecule associated with glycophorin A, that specifically marks the late stages of murine erythroid lineage), CD44 (membrane adhesion molecule that decreased during terminal erythroid differentiation) and cell size (forward scatter parameter).

As shown in Fig. 6A, the viable murine erythroblasts from bone marrow (impermeable to Propidium iodide and positive for Ter119) analyzed with respect to the expression levels of CD44 and forward scatter, separated five erythroid population: proerythroblasts (I), basophilic erythroblasts (II), polychromatic erythroblasts (III), orthochromatic erythroblasts and immature reticulocytes (IV) and mature red cells (V).

Under an iron balance diet, no significant difference were seen between WT and NCOA4 null mice differentiation (Fig. 6B). However, the erythropoiesis profile of bone marrow in KO mice was completely affected after five and seven months of iron deprivation, revealing a block in late stage of terminal differentiation (see IV population in Fig.6B). Indeed, the percentage of orthochromatic erythroblast/reticulocytes was significantly lower in NCOA4 null compared to WT mice after seven months of low iron diet (Fig.9C) and was associated to increased apoptosis, as demonstrated by analysis of Annexin V binding in IV population (Fig.9D).

Overall, these data revealed that in NCOA4 KO mouse model the block of iron release (from hepatic storages) and iron recycle (from splenic macrophages) affects erythropoiesis, especially in iron depletion condition, when NCOA4 mediated ferritinophagy seems to be crucial for the terminal erythroid differentiation.

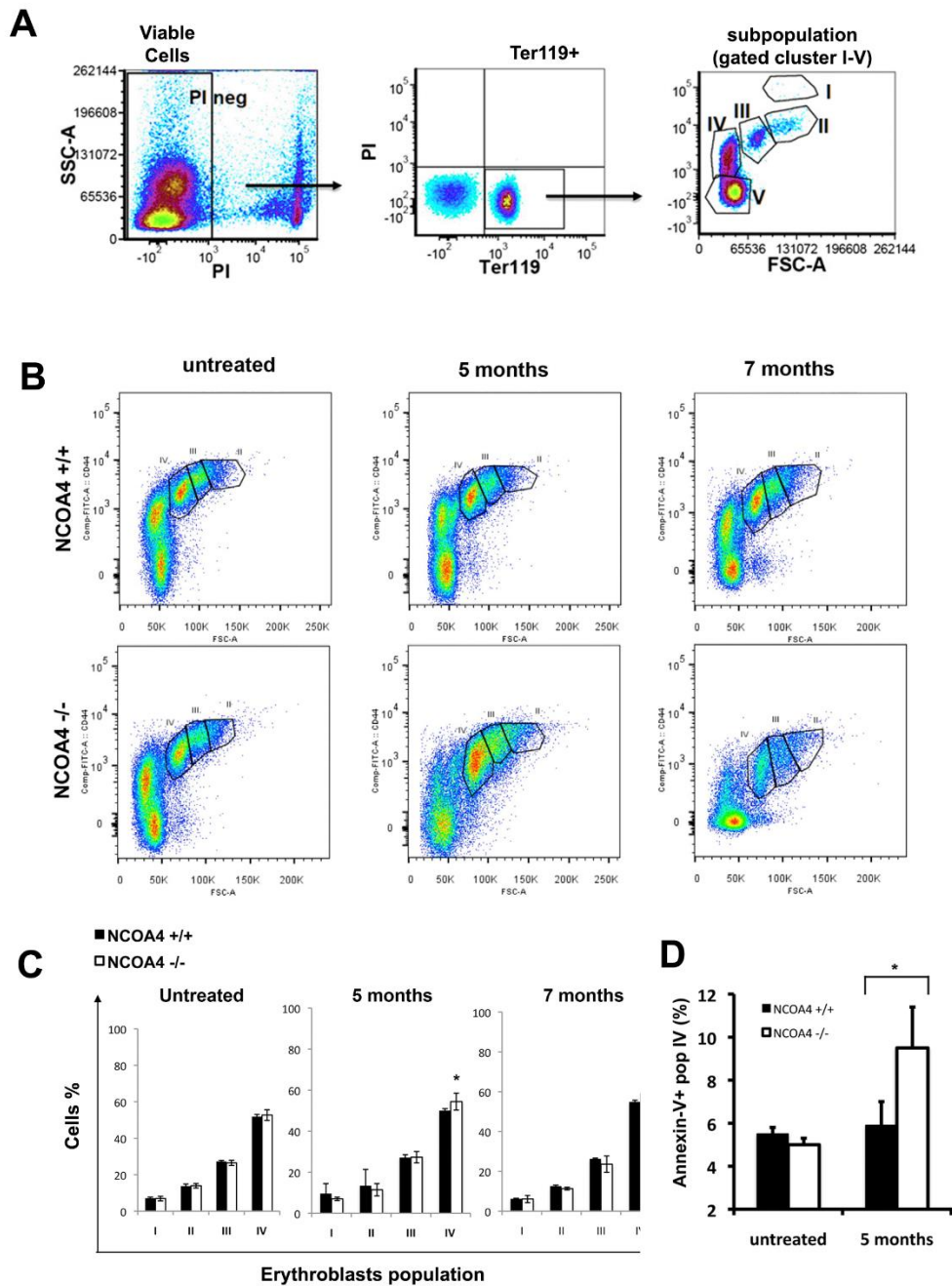


Figure 9. Iron deficiency affects terminal erythroid differentiation in NCOA4 null mice

A. Representative gating strategy for Ter119 subpopulation. Viable cells from bone marrow are impermeable to Propidium Iodide and are analyzed for Ter119 expression. Ter119 positive cells are further discriminated for CD44 surface expression and cell size parameter (FSC) in order to obtain distinct population.

B. Flow cytometry strategy explained in A combining CD44, Ter119 and FSC as markers to sort erythroid precursors from BM of NCOA4 WT and null mice iron-repleted (untreated) or iron depleted diets (five and seven months).

C. Percentage of erythroid precursors at each developmental stage sorted as in B. Errors bars indicate standard error. Asterisks refer to a statistically significant difference: *P<0.05.

D. The survival of orthochromatic erythroblast was examined for annexin V binding to assess apoptosis.

4.5 NCOA4^{-/-} mice develop fatal liver damage under hyperferric diet

Given that NCOA4^{-/-} mice were unable to degrade ferritin, accumulating a potential dangerous amount of iron, we examined the effect of iron overload in these animals when feeding a high-iron diet (1 g. After 15 days of high-iron diet, NCOA4 null mice continued to display higher hepatic levels of ferritin protein and higher hepatic iron content with respect to the WT (fig 10 A and 10 B).

Since free iron can promote oxidative stress through Fenton reactions, we then focus our attention on the expression levels of antioxidant enzyme such as hepatic superoxide dismutase (SOD) and glutathione peroxidase (GPx). As shown in the graph (fig 10 C), real time analysis confirmed a higher expression of SOD and GPx genes in NCOA4 null mice compared to the WT. Although the activation of anti-oxidative defense in liver NCOA4^{-/-} mice, we found serum levels of the hepatic enzyme alanine and aspartate liver transferase (AST and ALT) significantly increased in null mice, reflecting a condition of liver damage (Fig 10 E). Consistently, after 1 month of hyperferric diet, hematoxylin and eosin staining of NCOA4^{-/-} liver sections showed a diffuse damage, with sign of a marked steatosis respect to the WT mice (Fig.10 D). Indeed, more numerous and bigger vacuoles in NCOA4^{-/-} sections, revealed pronounced fatty degeneration and impairment of normal cellular metabolism compared to WT liver sections. Finally, most NCOA4 mice started to die after 75 days of high iron diet and were all dead within 2 weeks after 100 days of diet, with a mean survival of 89 days. Notable, WT mice started to die only after 100 days after hyperferric diet, with a mean survival of 104 days. Overall, these data demonstrated that NCOA4 null mice, displaying an iron tissue loading, were hypersensitive to iron rich diet and died prematurely respect to the WT mice.

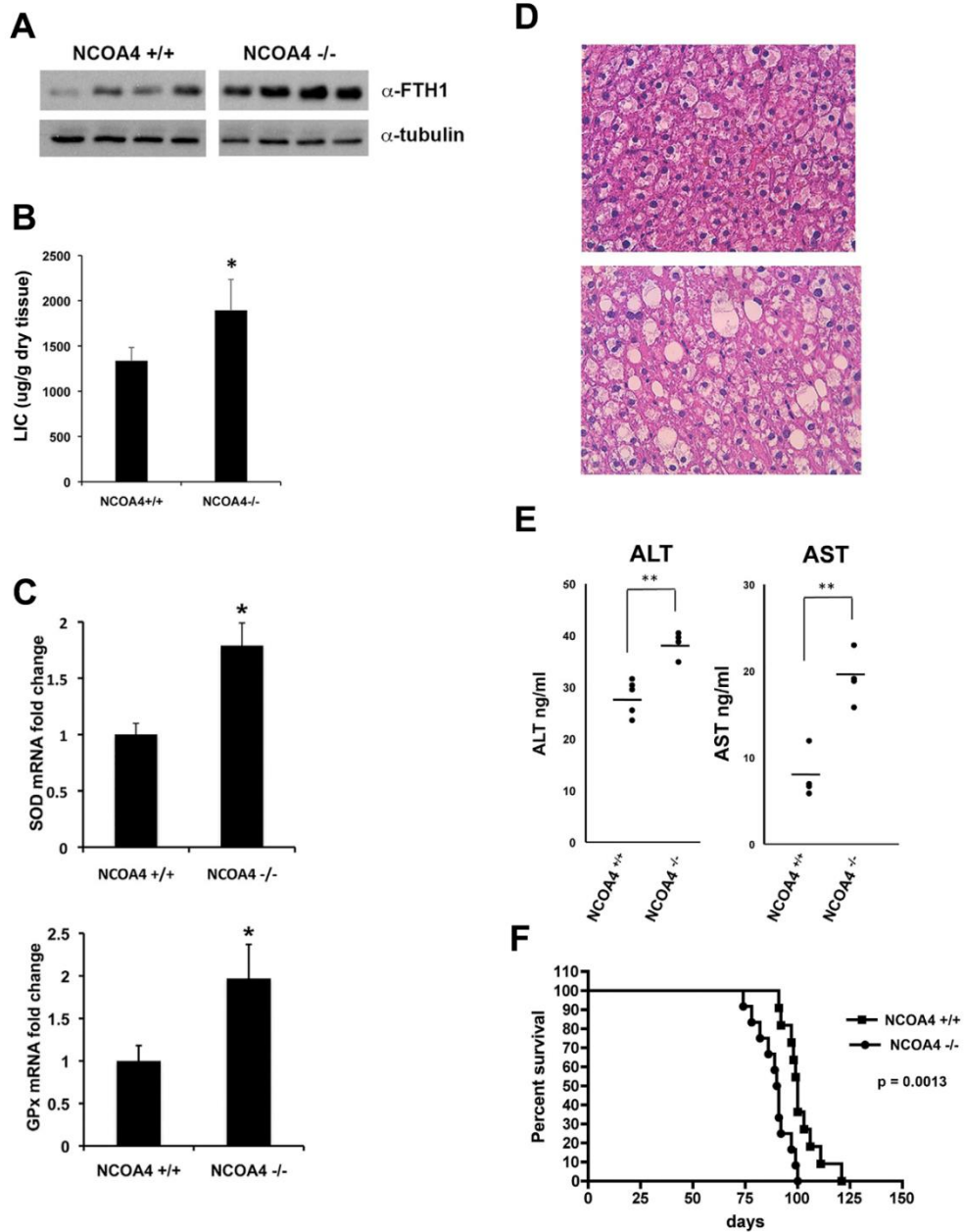


Figure 10. NCOA4^{-/-} mice develop fatal liver damage under hyperferric diet.
 A. Western blot analysis of FTH1 protein levels from livers of NCOA4 null and WT mice after 15 days of high iron diet. Tubulin was used as loading control.
 B. Liver non-heme iron content of NCOA4 null and WT mice fed a high iron diet for 15 days. Data are mean values \pm standard deviation from 4 independent sample. Asterisks refer to a statistically significant difference: * $P < 0.05$.
 C. Real time RT-PCR analysis of superoxide dismutase (SOD) and glutathione peroxidase (GPx) mRNA expression of NCOA4 null and WT mice fed a high iron diet for a month. (* $P < 0.05$)
 D. Representative histological analysis of NCOA4 null and WT mice liver sections stained with Hematoxylin and Eosin. The larger, white vesicles indicate droplets of fat.

E. Serum levels of the hepatic enzyme alanine and aspartate liver transferase (AST and ALT) from NCOA4 null and WT mice after 1 month of high iron diet. AST and ALT levels were evaluated from serum using a commercial Elisa Kit.

F. Analysis of the fraction of 10 NCOA4 deficient mice and 10 NCOA4 WT mice surviving under high iron rich diet were represented by Kaplan-Meier survival curve. P value is indicated.

4.6 NCOA4 protein controls ferritinophagy through its C-terminal portion

In order to characterize and identify the molecular determinants of NCOA4 involved in ferritinophagy process, we performed an *in vitro* pull down-assay using HeLa cell protein extracts and recombinant full-length, N-terminal (1-238) or C-terminal (239-318) NCOA4 proteins fused to NusA tag. As shown in Fig. 8A, both Nus-NCOA4 and (C)-NCOA4 were able to pull down the heavy chain of ferritin (FTH1). On the contrary, no signal was detected in pull down experiments with (N)-NCOA4 or Nus moiety alone. Then, in order to evaluate which portion of NCOA4 is involved in the specific binding to autophagosome-associated proteins, such as GABARAP and GABARAPL1, we performed another pull down using, as a bait, recombinant protein GABARAP, GABARAPL1 and LC3B fused to GST. HEK293T cells, transiently expressing MYC-tagged NCOA4, HA-tagged NCOA4 (N) and NCOA4 (C) protein, were used as protein source (Fig. 11B e 11C). Again, as for ferritin, NCOA4 full length and the C-terminal portion of NCOA4 were also purified from GABARAP and GABARAPL1 recombinant proteins whereas no interaction was detected for LC3B recombinant protein.

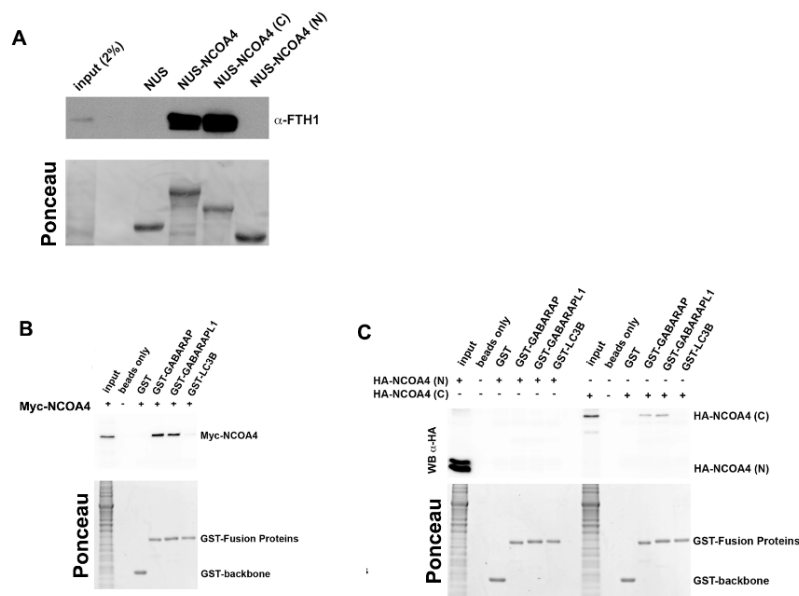


Figure 11. NCOA4 C-terminal is involved in ferritin and ATG8-like protein binding

A. NUS, NUS NCOA4 (N), NUS NCOA4 (C) and full length NUS NCOA4 were used as bait recombinant proteins immobilized on resin and incubated with protein extracts from HeLa cells.

The pulled down ferritin was analyzed by western blotting. The filter was colored with ponceau staining to visualize the input of recombinant proteins.

B. and C. GST alone or GST- tagged GABARAP, GABARAP-L1 and LC3B recombinant protein immobilized on resin were incubated with protein extracts from 293T cells transiently transfected with Myc-NCOA4, Ha-tagged NCOA4(N) or (C) encoding vector. The pulled-down proteins were analyzed by western blotting.

Since the C-terminal portion of NCOA4 was sufficient for ferritin and ATG8-like protein binding, we asked whether NCOA4 (C) portion alone could sustain ferritin degradation. We used Mouse Embryonic Fibroblasts (MEF) derived from NCOA4 deficient and wild type mice and firstly, verified the ferritinophagy process. As expected, NCOA4 null MEFs displayed higher levels of Ferritin protein respect to the WT at basal conditions, with no significant changes in iron labile pool as demonstrated by similar IRP2 proteins levels (Fig.12A). Then, we monitored ferritin degradation in NCOA4 null and WT MEFs. We first cultured fibroblasts in the presence of Ferric Ammonium Citrate (FAC) for 16 hours in order to induce iron accumulation into ferritin and then we treated cells for increasing time with the iron chelator Deferoxamine to promote iron mobilization from storage. Western blot analysis revealed that ferritin was rapidly degraded in WT MEFs and began undetectable after 6 hours of DFO treatment. Differently, more than 50% of ferritin was present after 9 hours of DFO in NCOA4 $-/-$ MEFs reflecting a slower kinetic of degradation (Fig.12B). We finally evaluated whether, in NCOA4 null MEFs the isolated C-terminal portion of NCOA4 allowed ferritin degradation in response to iron depletion. We infected NCOA4 null MEFs with retrovirus expressing full length, C-terminal or N-terminal fragments of NCOA4 and analyzed ferritin content after FAC/DFO release treatments. As shown in Fig. 12C, the (C)-terminal fragment of NCOA4 was able to induce ferritin turnover in low iron condition similarly to the full-length protein. On the contrary, MEFs infected with (N)-NCOA4 fragment displayed impaired ferritin digestion as the null MEFs. Altogether, these experiments showed that NCOA4 protein controls ferritin delivery to autophagosomes to induce iron release using its C-terminal domain, which is distinct from the one necessary to interact with MCM2-7 complex and control DNA replication.

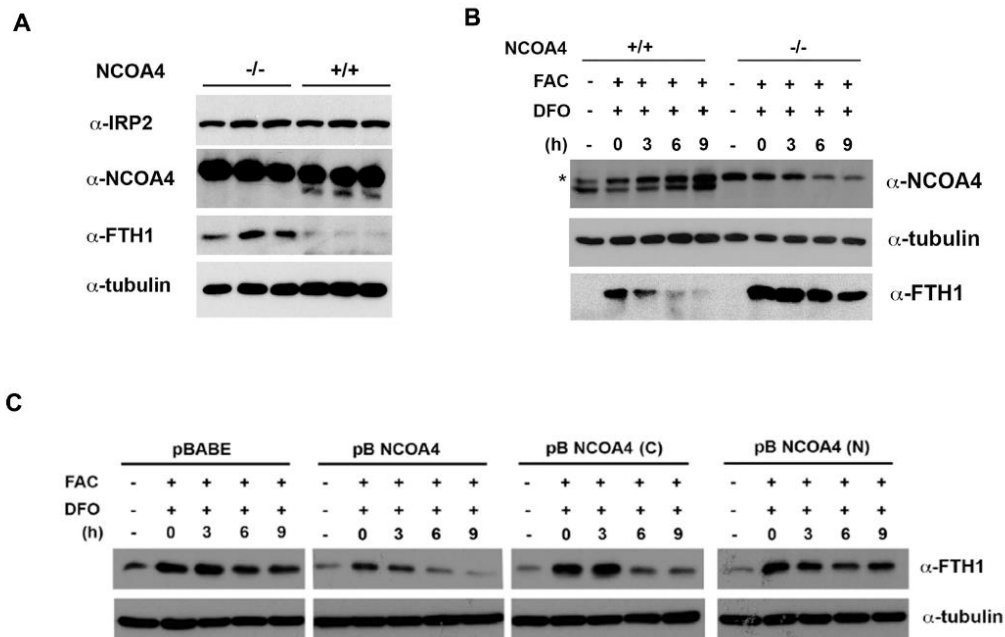


Figure 12. The C-terminal portion of NCOA4 protein is sufficient to allow ferritin degradation

A. Western blot analysis with the indicated antibody of protein extracts from immortalized Mouse Embryonic Fibroblasts derived from NCOA4 null and WT mice. The asterisk indicated an unspecific band.

B. Western blot analysis of NCOA4 and Ferritin proteins in NCOA4 null and WT MEFs subjected to iron depletion. MEFs were first incubated o/n with FAC to allow ferritin accumulation and then release in medium containing the iron chelator DFO and harvested at the indicated time point.

C. NCOA4 null MEFs were infected with retrovirus expressing full length, C-terminal or N-terminal NCOA4 vector or an empty vector (pBABE), then subjected to FAC/DFO treatment as in B to verify ferritin degradation.

4.8 Iron bioavailability affects intracellular NCOA4 levels and cell cycle progression

Besides ferritinophagy, it has been already demonstrated that NCOA4 protein exerts a negative control over DNA replication. Since iron levels affect cell cycle progression inducing a DNA replication arrest (Le N. et al, 2002), we sought to verify whether, in response to iron bioavailability, NCOA4 could regulate/inhibit DNA origins activation.

We initially studied NCOA4 and ferritin levels during cell cycle, upon subcellular fractionation of HeLa cells and analysis of the soluble fraction (cytosol and nucleoplasm) and the insoluble fraction (chromatin). During early-mid G1 phase (2-6 hours after Nocodazole release) NCOA4 increased in insoluble fraction (figure 13 A), reaching a peak prior to the onset of the S-

phase, which occurs after 8-10 hours as shown by Cyclin E protein peaking. Soon after, when PCNA became detectable onto chromatin to allow processive polymerases activity and thus, DNA replication, chromatin-bound NCOA4 protein levels started to decrease. Ferritin protein was detected only in soluble fraction and its levels interestingly decreased in S-phase when cytosolic NCOA4 was stabilized and could mediate ferritinophagy, supporting the idea that the progression through G1 phase towards S phase requires appropriate iron levels, firstly necessary for dNTP synthesis. Indeed, depletion of iron using Deferoxamine for 8 and 16 hours in asynchronous HeLa cells affected cell cycle distribution, enriching cells with a G1-phase DNA content (2n) (from 74,4% to 88,4% of cells in G1 phase after 16 h of DFO) and reducing the S-phase population (from 9,7 to 5,1% of cells in S-phase), as shown by flow cytometry profile in Fig.10B.

At molecular level, increased incubation with DFO induced a stabilization of NCOA4 cytosolic levels that soon accumulated in order to promote ferritin degradation via autophagy, as demonstrated by western blotting analysis (Fig 13 C, cytosol fraction). Moreover, after 2 hours of iron chelator treatment, NCOA4 levels also increased in nucleosol (Fig13 C), strongly enriching its loading onto chromatin (Fig.13 D, insoluble fraction).

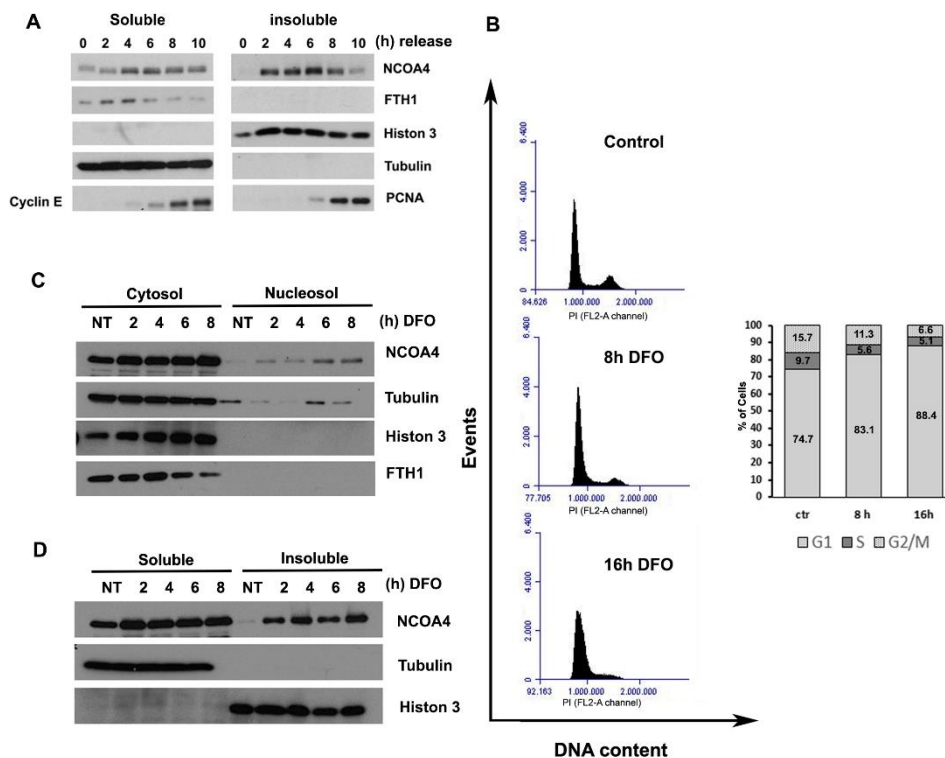


Figure 13. Iron bioavailability affects cell cycle progression and intracellular NCOA4 levels.

A. HeLa cells released from Nocodazole arrest were harvested at the indicated time points (h). Synchronized cells were then subjected to subcellular fractionation in order to obtain a soluble

fraction (cytosol and nucleosol) and an insoluble fraction (chromatin-bound protein) and analyzed by western blotting using the indicated antibody. Histon 3 and Tubulin were used as fractionation control.

B. Asynchronous HeLa cells were treated with 50 μ M Deferoxamine (DFO) for 8 and 16 hours, stained with Propidium Iodide and analyzed using flow cytometry. Cell cycle profiles of processed cells were shown and percentage of cells in each phase were reported as bar graph.

C. Asynchronous HeLa cells were treated with 50 μ M DFO and harvested at the indicated time points. Cells were then subjected to cytosol/nucleosol fractionation (using NePer kit) and analyzed by Western blotting.

D. HeLa cells were treated with DFO as in C. Samples were subjected to biochemical fractionation obtaining a soluble (cytosol and nucleosol) and an insoluble fraction (chromatin-bound protein), then analyzed by western blotting with different antibodies.

To exclude that the NCOA4-enrichment in chromatin fraction was an indirect effect of the iron-dependent G1-cell cycle arrest and a consequent blockage of DNA origins activation (failure of NCOA4 release from replisome), we monitored chromatin-bound and soluble proteins depleting iron specifically in G1-phase or in S-phase of the cell cycle. We synchronized HeLa cells in M-phase with Nocodazole (an inhibitor of microtubule polymerization) then release cells in complete medium to allow cycle re-entry and treated or not cells with DFO in early G1 phase (2 h after Nocodazole release) (Fig 14 A). As expected, under normal condition, western blotting analysis of chromatin fraction proteins revealed a reduction of NCOA4 levels in S-phase (8-14 hours after Nocodazole release) whereas PCNA levels increased and DNA replication progressed. Iron depletion in early G1 phase blocked S-phase progression, as demonstrated by the lower levels of cyclin E and the almost undetectable levels of PCNA onto chromatin. In addition, we also found Chk1, a kinase effector of the DNA Damage Response activated, as demonstrated by the increased phosphorylation status of Chk1 in response to iron chelation (Fig. 14 A, lower panel), confirming the activation of the replication checkpoint due to decrease levels of iron (IDR, Iron Deficiency Response). Consistently, NCOA4 remained stable onto chromatin for hours after DFO treatment, reaching even higher levels onto chromatin in comparison to the untreated cells (Fig. 11 A bottom panel and B see quantification of chromatin bound NCOA4).

Then, we depleted iron from cells during S-phase (at 8 hours from Nocodazole release), when many DNA origins had already fired and NCOA4 chromatin bound was reduced (Fig 14 C). Again, iron chelation affected cell cycle progression, as demonstrated by the lower levels of cyclin B and the stabilized levels of cyclin E compared to the untreated cells (Fig. 14 C, top panel.) Surprisingly, iron depletion also induced a significant increase in NCOA4 loading onto chromatin (Fig 14, bottom panel) whereas PCNA levels immediately decreased, indicating a blockage of further DNA replication origins activation. Taken together, these data indicated that NCOA4 responded to iron depletion, increasing its protein levels in both cytosol and nuclear fraction.

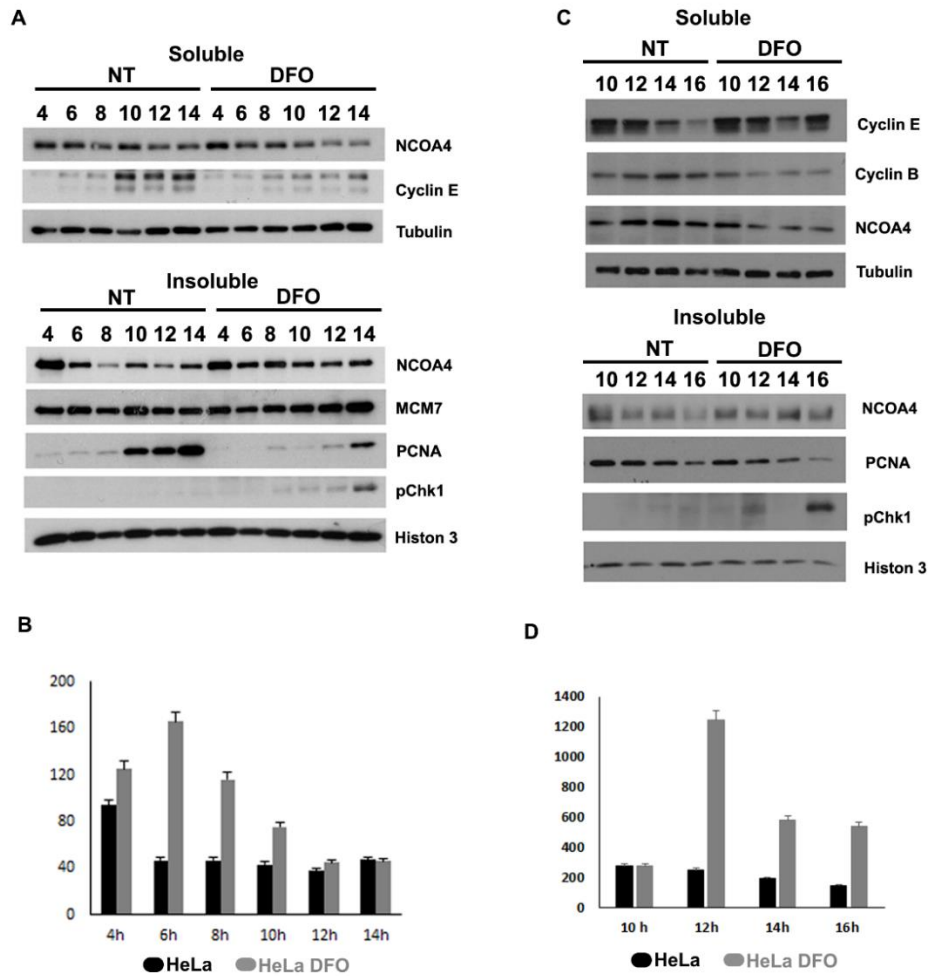


Figure 14. NCOA4 increases the binding to chromatin in iron depletion

A. HeLa cells were treated with Deferoxamine (DFO) 2 hours after Nocodazole release (in early G1 phase) and then were harvested at the indicated time points (h). Soluble (cytosol and nucleosol) and insoluble (chromatin-bound) extracts were subjected to western blotting analysis using the indicated antibodies.

B. Densitometric analysis of normalized, Chromatin-bound NCOA4 of the insoluble fraction of A was performed using ImageQuant. Data are shown as a mean \pm SD of two independent experiments.

C. HeLa cells were treated with Deferoxamine (DFO) 8 hours later Nocodazole release (in S-Phase), then were harvested at the indicated time points (h). Soluble (cytosol and nucleosol) and insoluble (chromatin-bound) extracts were subjected to western blotting analysis using the indicated antibodies.

D. Densitometric analysis of normalized, Chromatin-bound NCOA4 of the insoluble fraction of C was performed using ImageQuant. Data are shown as a mean \pm SD of two independent experiments

4.9 NCOA4 is enriched at DNA replication origins in response to iron depletion

We next sought to determine the biological significance of the iron dependent enrichment of nuclear NCOA4. Because NCOA4 exerts a negative regulation over DNA synthesis during cell cycle, interfering with DNA helicase by a direct interaction with MCM7, we hypothesized that iron depletion could control DNA origins activation through NCOA4 activity on MCM2-7.

First, we evaluated NCOA4 interaction with MCM7 in normal and iron depleted condition by coimmunoprecipitation assay. As shown in figure 15 A, MCM7 immunoprecipitated from chromatin together with NCOA4 and after 2 hours of iron depletion, this interaction increased.

Furthermore, we tested the enrichment of NCOA4 after DFO treatment at known canonical replication origins, mapped close to Myc and Lamin B2 genes, by Chromatin immunoprecipitation (ChIP) analysis. As shown in the graph, NCOA4 preferentially bound near origin regions (Fig. 15 B e C) with respect to distant, control regions. After iron chelation, NCOA4 binding to replication origins increased of 2 and 3 fold with respect to the control region, in myc and lamin B2 origins respectively.

The data obtained revealed a stronger NCOA4 binding to DNA origins via presumably its MCM7-interactor in iron depletion.

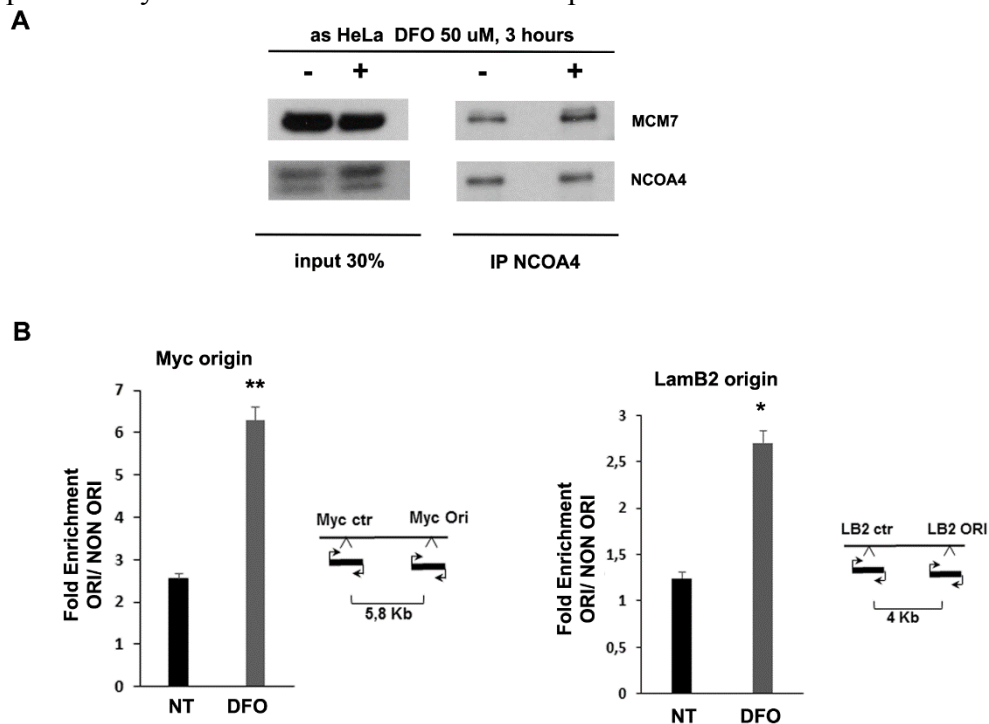


Figure 15. NCOA4 enrichment at canonical DNA replication origins in iron depletion

A. Total Protein extracts from asynchronous HeLa cells treated with Deferoxamine (DFO), were subjected to immunoprecipitation with α NCOA4 and immunoblotted with the indicated antibodies.

B. and C Chromatin immunoprecipitation on human myc and lamin B2 loci was performed using anti-NCOA4. On the left, bar graphs showed fold enrichment of NCOA4 at Origin region with respect to control region precipitated with NCOA4 antibody from ChIP experiments. On the right, schematic representation of genomic Myc and Lamin B2 loci together with PCR fragments and primer sets (converging arrows) used for quantitative real-time PCR analysis. Each amplified region span respectively 5.8 and 4 Kb around the described loci. Results are shown as means of duplicates +/- SD.

4.10 NCOA4 mediates DNA replication arrest during iron depletion

Finally, we sought to verify whether NCOA4 mediates DNA replication arrest during iron depletion monitoring DNA replication in transiently silenced HeLa cell lines.

After synchronization of control and silenced cells, we depleted iron during S-phase (at 8 hours from Nocodazole release) and monitored protein levels in chromatin fraction by western blotting (Fig. 16 A). As already mentioned, in control cells, NCOA4 and PCNA-chromatin bound were inversely related in normal and iron depleted condition, with the increase of PCNA levels and the opposite decrease of NCOA4 as long as replication progressed. To note, in silenced cells the expression of NCOA4 was not completely abrogated and NCOA4 levels in chromatin fraction became detectable after iron depletion. Interestingly, after DFO treatment, PCNA levels in NCOA4 silenced cells were higher compared to the control cells, suggesting that numerous origins continued to fire despite iron depletion. Moreover, this unscheduled origins activation in NCOA4 deficient cells promoted replication stress, strongly activating the DNA damage response as demonstrated by phosphorylation of Chk1 protein. The improper DNA replication of NCOA4 depleted cells under iron depleted condition was also confirmed by the higher and significant BrdU incorporation in silenced cells compared to control cells after 2 hours of DFO treatment (Fig. 16 B and C) as demonstrated by FACS analysis and confocal microscopy.

Based on these results, we concluded that reduction of NCOA4 activity affected the DNA replication arrest activated by iron depletion, promoting uncontrolled DNA origin firing, replication stress and the consequent activation of DNA damage response.

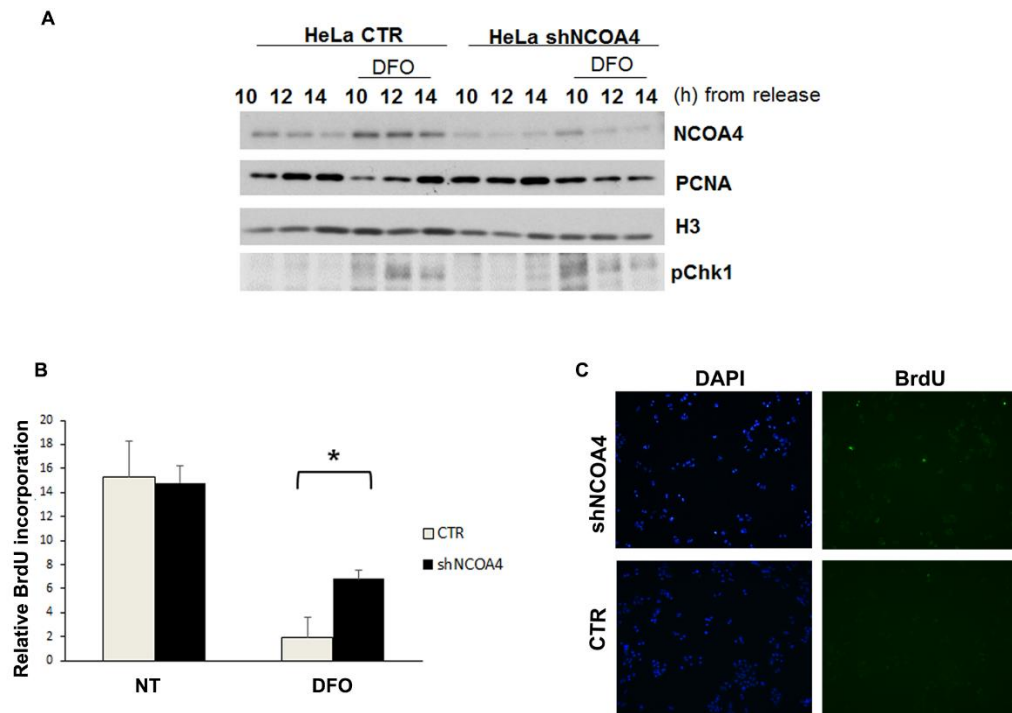


Figure 16. The iron-dependent arrest of DNA replication fails in NCOA4-silenced cells

A. HeLa cells were transfected with shNCOA4 or SH control for 48 hours then were synchronized in G2/M transition with Nocodazole; 8 hours later Nocodazole release (in S-Phase) cells were treated with Deferoxamine (DFO), then harvested at the indicated time points (h). Soluble (cytosol and nucleosol) and insoluble (chromatin-bound) extracts were subjected to western blotting analysis using the indicated antibodies.

B. Bar graph showing the relative BrdU (halogenated nucleotide) incorporation of NCOA4 silenced and control HeLa cells in normal (NT) and iron depleted (DFO) condition. Cells were release from Nocodazole block and treated with DFO in S-phase (8 hours) for 2 hours. Halogenated nucleotides was added for 30 minutes. Mean values \pm standard deviation of 2 experiments are represented.

C. Representative Fluorescence image of NCOA4 silenced and control cells after DFO treatment as described in B.

5 DISCUSSION

NCOA4 is a novel player in cellular iron metabolism. It is an iron sensing protein that, in iron depleted condition, accumulates, avoiding the HERC2-dependent proteosomal degradation, and promotes, via its c-terminal portion, the autophagic degradation of ferritin (the ferritinophagy process) in order to restore appropriate iron levels. We have explored the impact of ferritinophagy at systemic level using a mouse model carrying total genetic ablation of NCOA4 gene. In addition, we have explored the role of NCOA4 in controlling DNA replication in relation to iron metabolism in order to couple these diverse functions of the protein.

NCOA4 absence leads to ferritin accumulation in several key organs involved in iron metabolism of NCOA4 null mice, such as duodenum, liver and spleen. NCOA4 null mice also display higher transferrin saturation and serum ferritin respect to the WT mice, reflecting the tissue iron loading. As response of highest TfR saturation, in NCOA4 null mice liver hepcidin expression increases in order to reduce duodenal iron absorption via ferroportin degradation and limits, as a compensating mechanism, dangerous iron overload. However, although the activated Hepcidin-ferroportin regulatory circuit, NCOA4 null mice died prematurely when fed an iron rich diet showing signs of liver damage. The increased basal levels of ferritin in NCOA4 null mice probably deplete earlier the antioxidant defense with respect to control mice, making these mice hypersensitive to iron overload. Notably, NCOA4 deficient mice represent a peculiar case of hemochromatosis because tissue iron overload occurs in the contest of a functional Hepcidin-mediated response.

Despite tissue iron loading, NCOA4 null mice suffer anemia with reduced hemoglobin and microcytic erythrocytes (low MCH and MCV), resembling an iron deficient anemia. Under iron-restricted diet, NCOA4 null mice were unable to mobilize iron reserve from ferritin and worsened their condition, developing a severe hypochromic microcytic anemia and ineffective erythropoiesis, as demonstrated by the impaired terminal erythroid differentiation and apoptosis of orthoblastic population. Interestingly, NCOA4 has been already identified among the highest expressed gene during terminal erythroid differentiation, especially in orthochromatic erythroblasts (Gallegher et al, 2014). Therefore, NCOA4-mediated ferritinophagy seems to be crucial for hemoglobinization and the correct development of erythroblasts.

Besides controlling ferritinophagy, NCOA4 exerts a negative control over DNA replication. Indeed, during cell cycle, nuclear NCOA4 binds to replisome, through a direct interaction with a member of the DNA helicase, MCM7, and blocks DNA origins activation. At the onset of S-phase, NCOA4 reduces its binding to chromatin allowing DNA replication whereas cytosolic NCOA4 is stabilized and, interestingly, ferritin levels decreased, probably to release iron and sustain iron needs during S-phase.

Many proteins, playing key role in DNA metabolism utilize iron as cofactor. As fundamental microelement, disruption of iron homeostasis by chelators impairs

normal cell cycle progression and evokes a complex signaling causing a G1-arrest, which can be referred to as IDR, iron depletion response. NCOA4 is also affected by iron bioavailability, acting as an effector of this iron sensitive checkpoint. Indeed, in a cell cycle independent manner NCOA4 responds to low iron, translocating into the nucleus and increasing its binding to replisome, via MCM7. The finding that nuclear NCOA4 is enriched at canonical DNA replication origins loci when iron levels are low, suggest that NCOA4, by controlling DNA helicase, could avoid dangerous origins firing and prevent DNA synthesis when no sufficient resources are available to complete the process. However, nuclear NCOA4 senses iron also when replication has started and many origins have already fired, increasing its loading onto chromatin. In these circumstances, iron depletions could affect DNA synthesis, slowing and stalling DNA replication forks and could activate the DNA damage checkpoint responsible for the inhibition of further origin firing (Diffley et al, 2013). Thus, NCOA4 could participate also in this signaling and block late origins firing maintaining its binding to pre-RC.

The iron-dependent blockage of DNA replication fails in absence of NCOA4 and DNA origins continue to fire although iron depletion, as demonstrated by the persistent incorporation of halogenated nucleotides and the higher levels of PCNA in NCOA4 silenced cell respect to control. However, the simultaneous and uncontrolled origins activation in NCOA4-silenced cells is likely to depauperate nucleotides and replication factors in iron depletion leading to replication stress and probably to a permanent cell cycle blockage-senescence as observed when replication is promoted by oncogene activation (OIS). Our data indicate NCOA4 as a unique iron-sensing protein able to correlate DNA replication with iron levels. In low iron condition, NCOA4 inhibits DNA origins activation to avoid replication stress as well as contributes to restore the appropriate iron levels promoting ferritinophagy. Its ablation affects this iron-dependent checkpoint and probably impairs cell proliferation. Thus, we can not exclude that the impairment of erythropoiesis in NCOA4 null mice could be, at least in part dependent on the alteration of NCOA4 nuclear function.

6 CONCLUSIONS

Intracellular iron levels are tightly controlled to sustain crucial cellular processes such as DNA synthesis and repair as well as to avoid the iron-dependent toxic effects. Iron deficiency is not tolerated and cells have evolved complex responses to block cellular growth until iron levels are restored, a checkpoint response that we named IDR, Iron Depletion Response.

Here we report that NCOA4 is a novel key iron responsive protein, able to correlate iron bioavailability to cellular proliferation. NCOA4 accumulates when iron levels lowers in order to promote iron release from ferritin storage and to block DNA replication origins firing, avoiding replication stress. NCOA4 regulatory role provides the direct connection between DNA metabolism and iron homeostasis and indicates NCOA4 as an effector of the IDR.

Further analysis are needed to reveal the signaling pathways responsible for NCOA4 nuclear localization under iron depletion. It remains to be clarify whether NCOA4 regulates late firing origin under iron depletion condition, participating to the global checkpoint-dependent inhibition of origin activation as response to replication stress. Moreover, it should be investigating whether NCOA4-modulation of MCM2-7 helicase occurs at replication bubble as well to prevent forks collapse upon stalling because of iron depletion. Finally, it will be interesting define and map the genomic region where NCOA4 binds in response to iron depletion.

REFERENCES

- An WG, Kanekal M, Simon MC, Maltepe E, Blagosklonny MV, Neckers LM. Stabilization of wild-type p53 by hypoxia-inducible factor 1 α . *Nature* 1998; 392:405-8.
- Andrews NC, Schmidt PJ. Iron homeostasis. *Annu Rev Physiol*. 2007;69:69-85. Review.
- Basolo F, Giannini R, Monaco C, Melillo RM, Carlomagno F, Pancrazi M, Salvatore G, Chiappetta G, Pacini F, Elisei R, Miccoli P, Pinchera A, Fusco A and Santoro M. Potent Mitogenicity of the RET/PTC3 Oncogene Correlates with Its Prevalence in Tall-Cell Variant of Papillary Thyroid Carcinoma. *American Journal Of Pathology*, 02/2002; 160(1):247-54.
- Bianchi L, Tacchini L, Cairo G. HIF-1-mediated activation of transferrin receptor gene
- Brissot P, Ropert M, Le Lan C, Loréal O. Non-transferrin bound iron: a key role in iron overload and iron toxicity. *Biochim Biophys Acta*. 2012 Mar;
- Bruick RK. Expression of the gene encoding the proapoptotic Nip3 protein is induced by hypoxia. *Proc Nat Acad Sci USA* 2000; 97:9082-7
- Dowdle WE, Nyfeler B, Nagel J, Elling RA, Liu S, Triantafellow E, Menon S, Wang Z, Honda A, Pardee G, Cantwell J, Luu C, Cornella-Taracido I, Harrington E, Fekkes P, Lei H, Fang Q, Digan ME, Burdick D, Powers AF, Helliwell SB, D'Aquin S, Bastien J, Wang H, Wiederschain D, Kuerth J, Bergman P, Schwalb D, Thomas J, Ugwonalu S, Harbinski F, Tallarico J, Wilson CJ, Myer VE, Porter JA, Bussiere DE, Finan PM, Labow MA, Mao X, Hamann LG, Manning BD, Valdez RA, Nicholson T, Schirle M, Knapp MS, Keaney EP, Murphy LO. Selective VPS34 inhibitor blocks autophagy and uncovers a role for NCOA4 in ferritin degradation and iron homeostasis in vivo. *Nat Cell Biol*. 2014 Nov;16(11):1069-79.
- Farzaneh F, Hediger MA, Hentze MW, Simpson RJ. A novel duodenal iron-regulated transporter, IREG1, implicated in the basolateral transfer of iron to the circulation. *Mol Cell*. 2000 Feb;5(2):299-309.
- Feder JN, Tsuchihashi Z, Irrinki A, Lee VK, Mapa FA, Morikang E, Prass CE, Starnes SM, Wolff RK, Parkkila S, Sly WS, Schatzman RC. The hemochromatosis founder mutation in HLA-H disrupts beta2-microglobulin interaction and cell surface expression. *J Biol Chem*. 1997 May 30;272(22):14025-8.
- Gkouvatsos K, Papanikolaou G, Pantopoulos K. Regulation of iron transport and the role of transferrin. *Biochim Biophys Acta*. 2012 Mar; 1820(3):188-202.
- Gozzelino R, Arosio P. Iron Homeostasis in Health and Disease. *Int J Mol Sci*. 2016 Jan 20;17(1).
- Gunshin H, Mackenzie B, Berger UV, Gunshin Y, Romero MF, Boron WF, Nussberger S, Gollan JL, Hediger MA. Cloning and characterization of a mammalian proton-coupled metal-ion transporter. *Nature*. 1997 Jul 31

Hartwell, L.H., Weinert, T.A., 1989. Checkpoints: controls that ensure the order of cell cycle events. *Science* 246, 629/634.

Hediger MA. Cloning and characterization of a mammalian proton-coupled metal-ion transporter. *Nature*. 1997 Jul 31;388(6641):482-8.

Heinlein CA1, Ting HJ, Yeh S, Chang C. Identification of ARA70 as a ligand-enhanced coactivator for the peroxisome proliferator-activated receptor gamma. *J Biol Chem*. 1999 Jun 4;274(23):16147-52.

Hentze MW, Muckenthaler MU, Galy B, Camaschella C. Two to tango: regulation of Mammalian iron metabolism. *Cell*. 2010 Jul 9;142 (1):24-38.

Kautz L, Jung G, Valore EV, Rivella S, Nemeth E, Ganz T. Identification of erythroferrone as an erythroid regulator of iron metabolism. *Nat Genet*. 2014 Jul;46(7):678-84.

Kollara A, Kahn HJ, Marks A, Brown TJ. Loss of androgen receptor associated protein 70 (ARA70) expression in a subset of HER2-positive breast cancers. *Breast Cancer Res Treat*. 2001 Jun;67(3):245-53.

Krause, A., Neitz, S., Magert, H.J., Schulz, A., Forssmann, W.G., Schulz-Knappe, P. and Adermann, K. LEAP-1, a novel highly disulfide-bonded human peptide, exhibits antimicrobial activity. *FEBS Lett*. 480, 147–150 (2000)

Kwok JC, Richardson DR. The iron metabolism of neoplastic cells: alterations that facilitate proliferation? *Crit Rev Oncol Hematol*. 2002 Apr;42(1):65-78.

Lakhal S1, Schödel J, Townsend AR, Pugh CW, Ratcliffe PJ, Mole DR. (2011) Regulation of type II transmembrane serine proteinase TMPRSS6 by hypoxia-inducible factors: new link between hypoxia signaling and iron homeostasis. *J Biol Chem*. 11;286(6):4090-7. doi: 10.1074/jbc.M110.173096.

Le NT, Richardson DR. The role of iron in cell cycle progression and the proliferation of neoplastic cells. *Biochim Biophys Acta*. 2002. Review.

Le Rolle A, Klempner S, Garrett C, Seery T, Sanford E, Balasubramanian S, Ross J, Stephens P, Miller V, Ali S and Chiu V. Identification and characterization of *RET* fusions in advanced colorectal cancer. *Oncotarget*. 2015 Oct 6; 6(30): 28929–28937.

Liuzzi JP, Aydemir F, Nam H, Knutson MD, Cousins RJ. Zip14 (Slc39a14) mediates non-transferrin-bound iron uptake into cells. *Proc Natl Acad Sci U S A*. 2006 Sep 12;103(37):13612-7. Epub 2006 Sep 1.

Mancias JD, Wang X, Gygi SP, Harper JW, Kimmelman AC. Quantitative proteomics identifies NCOA4 as the cargo receptor mediating ferritinophagy. *Nature*. 2014 May 1;509(7498):105-9

McKie AT, Marciani P, Rolfs A, Brennan K, Wehr K, Barrow D, Miret S, Bomford A, Peters TJ, Farzaneh F, Hediger MA, Hentze MW, Simpson RJ. A novel duodenal iron-regulated transporter, IREG1, implicated in the basolateral transfer of iron to the circulation. *Mol Cell*. 2000 Feb

McKie, A.T The role of Dcytb in iron metabolism: an update. 2008 *Biochem. Soc. Trans*. 36, 1239–1241.

Moore JM, Galicia SJ, McReynolds AC, Nguyen NH, Scanlan TS, Guy RK. Quantitative proteomics of the thyroid hormone receptor-coregulator interactions. *J Biol Chem*. 2004 Jun 25;279(26):27584-90. Epub 2004 Apr 19.

Moroishi T1, Nishiyama M, Takeda Y, Iwai K, Nakayama KI. The FBXL5-IRP2 axis is integral to control of iron metabolism in vivo. *Cell Metab.* 2011 Sep 7;14(3):339-51.

Nemeth, E., Tuttle, M.S., Powelson, J., Vaughn, M.B., Donovan, A., Ward, D.M., Ganz, T., and Kaplan, J. Heparin regulates cellular iron efflux by binding to ferroportin and inducing its internalization. *Science* 306, 2090–2093. 2004

Pantopoulos K, Porwal SK, Tartakoff A, Devireddy L. Mechanisms of mammalian iron homeostasis. *Biochemistry.* 2012 Jul 24 2012 Jul 9.

Pigeon, C., Ilyin, G., Courselaud, B., Leroyer, P., Turlin, B., Brissot, P. and Loreal, O. A new mouse liver-specific gene, encoding a protein homologous to human antimicrobial peptide hepcidin, is overexpressed during iron overload. *J. Biol. Chem.* 276, 7811–7819 (2001)

Silvestri L, Pagani A, Nai A, De Domenico I, Kaplan J, Camaschella C. 2008 The serine protease matriptase-2 (TMPRSS6) inhibits hepcidin activation by cleaving membrane hemojuvelin. *Cell Metab.* (6):502-11.

Surguladze N, Patton S, Cozzi A, Fried MG, Connor JR. Characterization of nuclear ferritin and mechanism of translocation. *Biochem J.* 2005 Jun 15;388 (Pt 3):731-40.

Taher AT, Musallam KM, Inati A. Iron overload: consequences, assessment, and monitoring. *Hemoglobin.* 2009; 33 Suppl 1:S46-57

Tanaka H, Arakawa H, Yamaguchi T, Shiraishi K, Fukuda S, Matsui K, Takei Y, Nakamura Y. A ribonucleotide reductase gene involved in a p53-dependent cell-cycle checkpoint for DNA damage. *Nature* 2000; 404:42-9.

Tanno T, Porayette P, Sripichai O, Noh SJ, Byrnes C, Bhupatiraju A, Lee YT, Goodnough JB, Harandi O, Ganz T, Paulson RF, Miller JL. Identification of TWSG1 as a second novel erythroid regulator of hepcidin expression in murine and human cells. *Blood.* 2009 Jul 2;114(1):181-6.

Tekur S, Lau KM, Long J, Burnstein K, Ho SM. Expression of RFG/ELE1alpha/ARA70 in normal and malignant prostatic epithelial cell cultures and lines: regulation by methylation and sex steroids. *Mol Carcinog.* 2001 Jan;30(1):1-13

Tomas Ganz J Macrophages and systemic iron homeostasis *Innate Immun.* 2012;4(5-6):446-53.

Wang R, Hu H, Pan Y, Li Y, Ye T, Li C, Luo X, Wang L, Li H, Zhang Y, Li F, Lu Y, Lu Q, Xu J, Garfield D, Shen L, Ji H, Pao W, Sun Y and Chen H. RET Fusions Define a Unique Molecular and Clinicopathologic Subtype of Non-Small-Cell Lung Cancer. *Journal of Clinical Oncology* 2012. doi: 10.1200/JCO.2012.45.8240

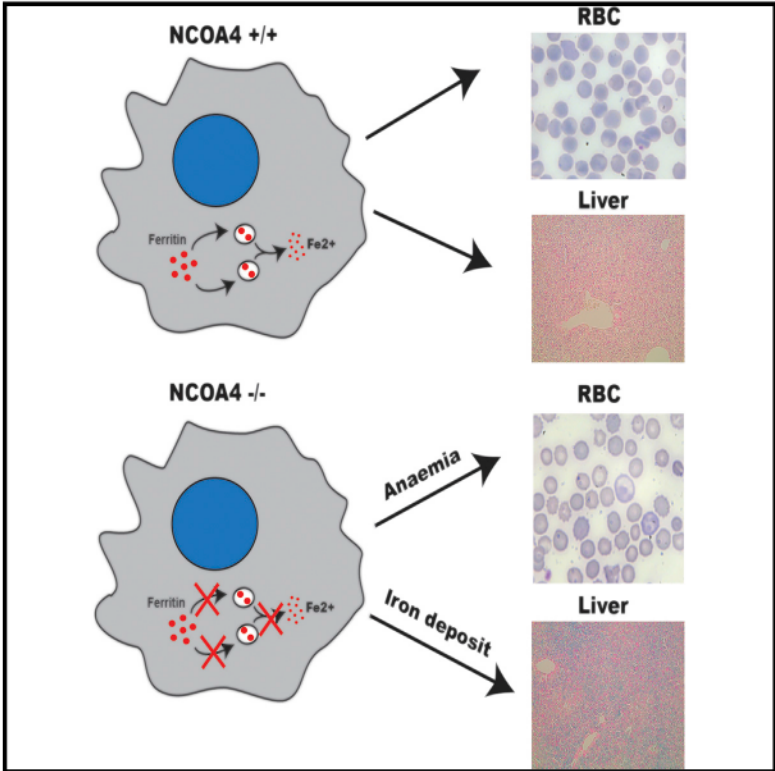
Wilkinson N, Pantopoulos K. The IRP/IRE system in vivo: insights from mouse models. *Front Pharmacol.* 2014 Jul 28; 2014.

Zhang C. Essential functions of iron-requiring proteins in DNA replication, repair and cell cycle control. *Protein Cell.* 2014 Oct;5(10):750-60.

Zhao N1, Zhang AS, Enns CA. Iron regulation by hepcidin. *J Clin Invest.* 2013 Jun 3;123(6):2337-43.

NCOA4 Deficiency Impairs Systemic Iron Homeostasis

Graphical Abstract



Authors

Roberto Bellelli, Giorgia Federico, Alessandro Matte', ..., Massimo Santoro, Lucia De Franceschi, Francesca Carlomagno

Correspondence

francesca.carlomagno@unina.it

In Brief

NCOA4 is crucial for autophagic ferritin degradation. Bellelli et al. find that genetic disruption of NCOA4 causes ferritin accumulation in tissues and defective iron mobilization from storage. NCOA4-null mice display impaired erythropoiesis associated with microcytic and hypochromic anemia, which is more pronounced in mice fed an iron-depleted diet.

Highlights

- Genetic disruption of NCOA4 causes ferritin accumulation in tissues
- NCOA4 deficiency blocks iron mobilization from ferritin storage and induces anemia
- NCOA4-null mice are hypersensitive to iron overload

NCOA4 Deficiency Impairs Systemic Iron Homeostasis

Roberto Bellelli,^{1,5} Giorgia Federico,¹ Alessandro Matte,² David Colecchia,³ Achille Iolascon,^{1,4} Mario Chiariello,³ Massimo Santoro,¹ Lucia De Franceschi,² and Francesca Carlomagno^{1,*}

¹Dipartimento di Medicina Molecolare e Biotecnologie Mediche, Università degli Studi di Napoli Federico II, and Istituto di Endocrinologia ed Oncologia Sperimentale del Consiglio Nazionale delle Ricerche, 80131 Napoli, Italy

²Dipartimento di Medicina, Università degli Studi di Verona–Azienda Ospedaliera Universitaria Integrata Verona, 37134 Verona, Italy

³Istituto Toscano Tumori–Core Research Laboratory and Consiglio Nazionale delle Ricerche–Istituto di Fisiologia Clinica, 53100 Siena, Italy

⁴Centro di Ingegneria Genetica–Advanced Biotechnologies, 80145 Naples, Italy

⁵Present address: DNA Damage Response Laboratory, Clare Hall Laboratory, The Francis Crick Institute, South Mimms EN6 3LD, UK

*Correspondence: francesca.carlomagno@unina.it

<http://dx.doi.org/10.1016/j.celrep.2015.12.065>

This is an open access article under the CC BY-NC-ND license (<http://creativecommons.org/licenses/by-nc-nd/4.0/>).

SUMMARY

The cargo receptor NCOA4 mediates autophagic ferritin degradation. Here we show that NCOA4 deficiency in a knockout mouse model causes iron accumulation in the liver and spleen, increased levels of transferrin saturation, serum ferritin, and liver hepcidin, and decreased levels of duodenal ferroportin. Despite signs of iron overload, NCOA4-null mice had mild microcytic hypochromic anemia. Under an iron-deprived diet (2–3 mg/kg), mice failed to release iron from ferritin storage and developed severe microcytic hypochromic anemia and ineffective erythropoiesis associated with increased erythropoietin levels. When fed an iron-enriched diet (2 g/kg), mice died prematurely and showed signs of liver damage. Ferritin accumulated in primary embryonic fibroblasts from NCOA4-null mice consequent to impaired autophagic targeting. Adoptive expression of the NCOA4 COOH terminus (aa 239–614) restored this function. In conclusion, NCOA4 prevents iron accumulation and ensures efficient erythropoiesis, playing a central role in balancing iron levels in vivo.

INTRODUCTION

Iron is essential for oxygen transport, oxidation-reduction reactions, and metabolite synthesis (Andrews and Schmidt, 2007; Ganz and Nemeth, 2012). However, because of its high chemical reactivity and ability to generate reactive hydroxyl radicals through Fenton chemistry, iron concentration must be tightly controlled in tissues, cells, and blood (Papanikolaou and Pantopoulos, 2005). Notably, iron is stored in transport (transferrin) or deposit (ferritin) protein complexes to protect it from the deleterious effects of Fenton reactions. Ferritin is a ubiquitously expressed cytosolic multimeric protein complex constituted of 24 H- and L-polypeptide subunits that self-organize in different ratios in a tissue-dependent fashion and form a shell-like nanocage in which iron is stored. Each “cage” accommodates up to 4,500 iron atoms in the Fe(III) state (Arosio et al., 2009). Iron concentra-

tion in mammals is mainly regulated by a set of interlocking regulatory circuits involving hepcidin, hypoxia-inducible factor 2 α (HIF2 α), and iron regulatory proteins (IRPs) (Hentze et al., 2010).

Serum and tissue iron levels are principally regulated by iron absorption. Dietary heme iron is absorbed efficiently via membrane transport mechanisms that have yet to be fully characterized. Non-heme iron is transported into enterocytes by the divalent metal transporter 1 (DMT1), which is the apical transporter of iron ions. Most of the iron taken up is stored in ferritin and lost upon sloughing of senescent enterocytes. The basolateral transporter ferroportin (FNP) carries iron from enterocytes to the blood. Transferrin then transports iron to peripheral tissues via a receptor-mediated uptake process. Two transferrin receptors have been identified: a high-affinity, widely expressed receptor, transferrin receptor 1 (TfR1), which is required for cellular iron uptake, and a bone marrow/liver-specific low-affinity receptor, TfR2, which is mainly involved in the regulation of iron homeostasis in the liver and bone marrow (Nai et al., 2015).

The main hormone regulating intestinal iron uptake and release from splenic macrophages is hepcidin, whose production in the liver is controlled by serum iron concentrations, erythropoiesis, and inflammation. By promoting internalization and ubiquitin-mediated degradation of the iron transporter ferroportin 1 (Fnp1), hepcidin reduces iron absorption and its recycling from red blood cell breakdown. Hepcidin expression is regulated by systemic iron availability. Therefore, a high concentration of Fe(III)-saturated transferrin activates the TfR2 receptor in complex with the HFE (High Iron Fe) protein, which, in turn, promotes hepcidin transcription through the BMP/Smad and, probably, the extracellular signal-related kinase (ERK)/mitogen-activated protein kinase (MAPK) signaling pathways. In addition, increased tissue iron activates the Smad pathway by increasing BMP6 production. By binding BMP receptors in complex with the hemojuvelin protein, BMP6 activates the Smad pathway, leading to increased hepcidin production (Babitt et al., 2006). The expression of iron transporters in the duodenum is also regulated by the transcription factor HIF2 α , which binds to hypoxia-responsive elements in the promoters of ferroportin and DMT1 (Mastrogiannaki et al., 2009).

Dysregulation of hepcidin production, because of a plethora of genetic defects of iron homeostasis, causes iron overload and results in a systemic disease known as “hereditary

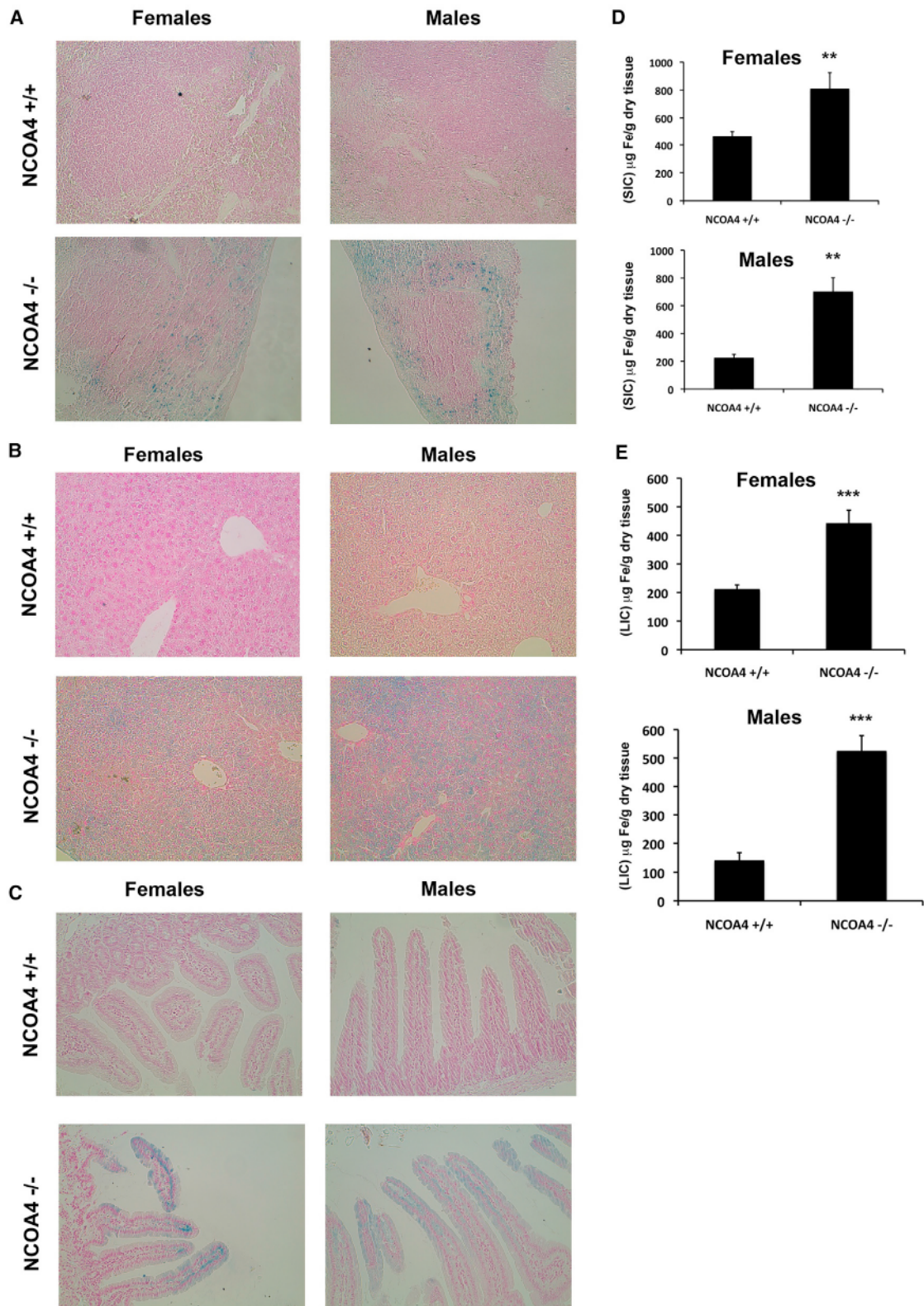


Figure 1. Increased Iron Accumulation in NCOA4-Null Mouse Liver, Spleen, and Duodenum

(A) Representative Perls' Prussian blue staining of WT (+/+) and NCOA4-null (-/-) spleen sections from 2-month-old female and male mice. Magnification, $\times 20$.
(B) Representative Perls' Prussian blue staining of WT (+/+) and NCOA4-null (-/-) liver sections from 2-month-old female and male mice. Magnification, $\times 20$.

(legend continued on next page)

hemochromatosis," which is characterized by tissue iron accumulation, iron-mediated injury, and organ dysfunction (Fleming and Ponka, 2012). Mouse models of hereditary hemochromatosis correctly recapitulate various human diseases (Hentze et al., 2010).

To avoid iron overload, cells shelter iron in ferritin. Consequently, a high concentration of iron promotes the translation of ferritin subunits by inactivating the iron regulatory protein (IRP)/iron-responsive element (IRE) machinery (Zhang et al., 2014; Zhao et al., 2013). On the contrary, under conditions of iron deficiency or increased iron requirement, mobilization of iron from ferritin deposits is supported via autophagy ("ferritinophagy") (Mancias et al., 2014).

Protein NCOA4, which interacts with and co-activates several nuclear hormone receptors and controls DNA replication origin activation, thereby preserving genome stability (Bellelli et al., 2014; Heinlein et al., 1999; Lanzino et al., 2005; Yeh and Chang, 1996), has been identified recently as a crucial player in ferritinophagy (Dowdle et al., 2014; Mancias et al., 2014). Therefore, NCOA4 functions as a cargo receptor that, by interacting with ferritin, promotes its transport to autophagosomes via interaction with ATG8-like proteins such as GABARAP and GABARAPL1, sustaining iron release under both basal and iron starvation conditions. Inactivation of NCOA4 in cells causes an increase in ferritin deposits (Dowdle et al., 2014; Mancias et al., 2014).

The aim of this study was to explore the involvement of NCOA4 in ferritinophagy *in vivo* using an NCOA4^{-/-} mouse model. To determine the role of NCOA4 in maintaining *in vivo* iron homeostasis, we exposed NCOA4^{-/-} mice to a high- or low-iron diet. We also evaluated the ability of mouse embryonic fibroblasts (MEFs) from NCOA4-null mice to target ferritin to autophagolysosomal digestion under basal and iron-depleted conditions.

RESULTS

NCOA4-Null Animals Display Ferritin Accumulation

To determine whether ferritin deposits were enhanced in NCOA4-null animals as a consequence of impaired ferritinophagy, we analyzed protein extracts from the liver, spleen, duodenum, bone marrow, and kidney of NCOA4^{-/-} and wild-type (WT) animals by western blotting. As shown in Figure S1, ferritin content (FTH1) was significantly higher in NCOA4-null mice than in WT mice in all analyzed tissues. Perls' Prussian blue staining of the liver, spleen, and duodenum confirmed this finding (Figures 1A–1C). Consistently, iron concentrations were significantly higher in the spleens and livers of NCOA4-null than in WT animals (Figures 1D and 1E).

NCOA4-Null Animals Display Increased Serum Iron, Transferrin Saturation, and Hepcidin Upregulation

The percentages of transferrin saturation and serum ferritin levels were increased slightly but significantly in NCOA4-null

versus WT animals (Figures S2A and S2B). This indicates that tissue iron in the knockout animals is in equilibrium with circulating iron. Generally, increased transferrin saturation activates a signaling pathway in hepatocytes that leads to increased hepcidin gene (HAMP) transcription to reduce iron absorption. At real-time PCR, HAMP mRNA expression was 2-fold higher in NCOA4-null livers versus WT tissues (Figure S2C). Western blotting with anti-phospho Smad1/5/8 antibody did not show increased phosphorylation of Smad proteins in the livers of knockout animals (data not shown) but, rather, increased phosphorylation of proteins ERK1/2 (Figure S2D). Consistent with increased HAMP expression, FPN protein expression was lower in the duodeni of NCOA4-null mice than in those of WT animals (Figure S3A). NCOA4 deficiency did not significantly affect the expression of protein HIF2 α or of FPN mRNA in duodenum enterocytes (Figures S3B and S3C). Furthermore, IRP2 protein levels were not increased in NCOA4-null mouse livers. This finding strongly suggests that, notwithstanding the increase in ferritin content in various tissues, the IRP/IRE and HIF2 systems, which are mainly influenced by alteration of labile intracellular iron, were not affected (Figure S3D). Accordingly, levels of TFR1 mRNA (containing multiple IRE elements in the 3' UTR) and protein were similar in the livers of NCOA4-null and WT mice (Figures S3D and S3E), as was FTH1 mRNA expression (Figure S3E). In summary, NCOA4-null mice, despite their ability to activate the hepcidin/ferroportin pathway, accumulated iron in tissues. Notably, no gender differences were observed.

NCOA4-Null Mice Display Hypochromic Microcytic Anemia that Is Exacerbated by a Low Dietary Iron Intake

To determine whether the failure of NCOA4-null mice to degrade ferritin and mobilize stored iron affects erythropoiesis, we evaluated red blood parameters in NCOA4-null and WT mice at baseline and after prolonged exposure to a low-iron diet; namely, for 5 and 7 months. As shown in Table 1, at baseline, compared with WT animals, NCOA4-null mice had significantly lower values of hematocrit, hemoglobin, mean corpuscular volume, and mean corpuscular hemoglobin, a condition compatible with microcytic anemia.

To examine defective erythropoiesis in greater detail, we analyzed ferritin deposits by western blotting in knockout and WT animals fed an iron-poor diet (2–3 mg/kg) for 5 months, which is sufficient time to allow iron mobilization from ferritin. As shown in Figures 2A and S4A, although, after 5 months of iron depletion, ferritin deposits were completely exhausted in WT livers and spleens, a large amount of ferritin was still present in NCOA4-null mice. Indeed, liver and spleen iron content was significantly higher in knockout than in WT animals (Figure 2B). On the contrary, serum iron and transferrin saturation, which, under a normal diet, were higher in NCOA4-null than in WT animals (Figure S2A; data not shown), were significantly lower under a low-iron diet in NCOA4-null than in WT animals (Figure 2C).

(C) Representative Perls' Prussian blue staining of WT (+/+) and NCOA4-null (-/-) duodenum sections from 2-month-old female and male mice. Magnification, $\times 20$.

(D) Splenic non-heme iron content (SIC) of WT (+/+) and NCOA4-null (-/-) female and male mice. Data are shown as mean \pm SD from 4–5 independent samples.

(E) Liver non-heme iron content (LIC) of WT (+/+) and NCOA4-null (-/-) female and male mice. Data are shown as mean \pm SD from 4–5 independent samples.

** $p < 0.01$, *** $p < 0.001$. See also Figures S1, S2, and S3.

Table 1. Hematological Parameters and Red Cell Indices in NCOA4^{+/+} and NCOA4^{-/-} MICE under Standard and Iron-Deficient Diets

	Baseline		Iron-Deficient Diet			
	NCOA4 ^{+/+} Mice (n = 6)	NCOA4 ^{-/-} Mice (n = 6)	5 Months		7 Months	
			NCOA4 ^{+/+} Mice (n = 6)	NCOA4 ^{-/-} Mice (n = 6)	NCOA4 ^{+/+} Mice (n = 3)	NCOA4 ^{-/-} Mice (n = 4)
Hct (%)	45.8 ± 1.1	42.2 ± 1.3*	36.7 ± 1.3°	28.6 ± 2.8°*	36.0 ± 0.6°	28.8 ± 3.3°*
Hb (g/dl)	15.1 ± 0.2	12.7 ± 0.6*	11.8 ± 0.3°	8.8 ± 1.7°*	11.0 ± 0.5°	8.0 ± 1.8°*
MCV (fl)	51.7 ± 0.5	46.3 ± 3.05*	47.5 ± 1.5°	38.5 ± 4.1°*	43.7 ± 2.7°	36.5 ± 2.4°*
MCH (pg)	16.3 ± 0.8	15.6 ± 0.2*	15.4 ± 1.2	10.3 ± 0.9°*	14.1 ± 1.3°	10.4 ± 1.5°*
MCHC (g/dl)	27.6 ± 0.4	28.2 ± 0.5	27.5 ± 0.3	26.1 ± 0.9°*	26.7 ± 0.6	26.7 ± 0.6°
CH (pg)	14.9 ± 0.3	13.0 ± 0.5	13.1 ± 0.6°	9.92 ± 0.9°*	10.12 ± 0.4°	9.57 ± 0.86°
RDW (%)	12.6 ± 0.5	15.1 ± 2.5	13.1 ± 0.7	23.4 ± 4.0°*	30.12 ± 6.1°	28 ± 7.3°*
Retics (10 ³ cell/μl)	498 ± 84	488 ± 170	419 ± 98	60 ± 2.8°*	41 ± 15°	52 ± 0.8°
MCVr (fl)	55.2 ± 0.4	51 ± 1.84*	53.6 ± 1.9°	48.5 ± 5.4°*	41.6 ± 5°	40.2 ± 2.8°
CHr (pg)	14.7 ± 0.8	13.8 ± 1.1	13.45 ± 1.5	11.0 ± 0.78°*	13.5 ± 1.1	9.05 ± 1.3°*

Hct, hematocrit; Hb, hemoglobin; MCV, mean corpuscular volume; MCH, mean corpuscular hemoglobin; MCHC, mean corpuscular hemoglobin concentration; CH, hemoglobin concentration; RDW, red cell distribution width; Retics, reticulocytes; MCVr, reticulocyte mean corpuscular volume; CHr, reticulocyte hemoglobin concentration. *p < 0.05 compared with WT mice; °p < 0.05 compared with baseline.

Consistent with this finding, hepcidin mRNA levels were suppressed completely in NCOA4^{-/-} livers, whereas ferroportin protein expression was increased significantly in spleen macrophages despite the accumulation of ferritin in the spleen (Figures S4B and S4C).

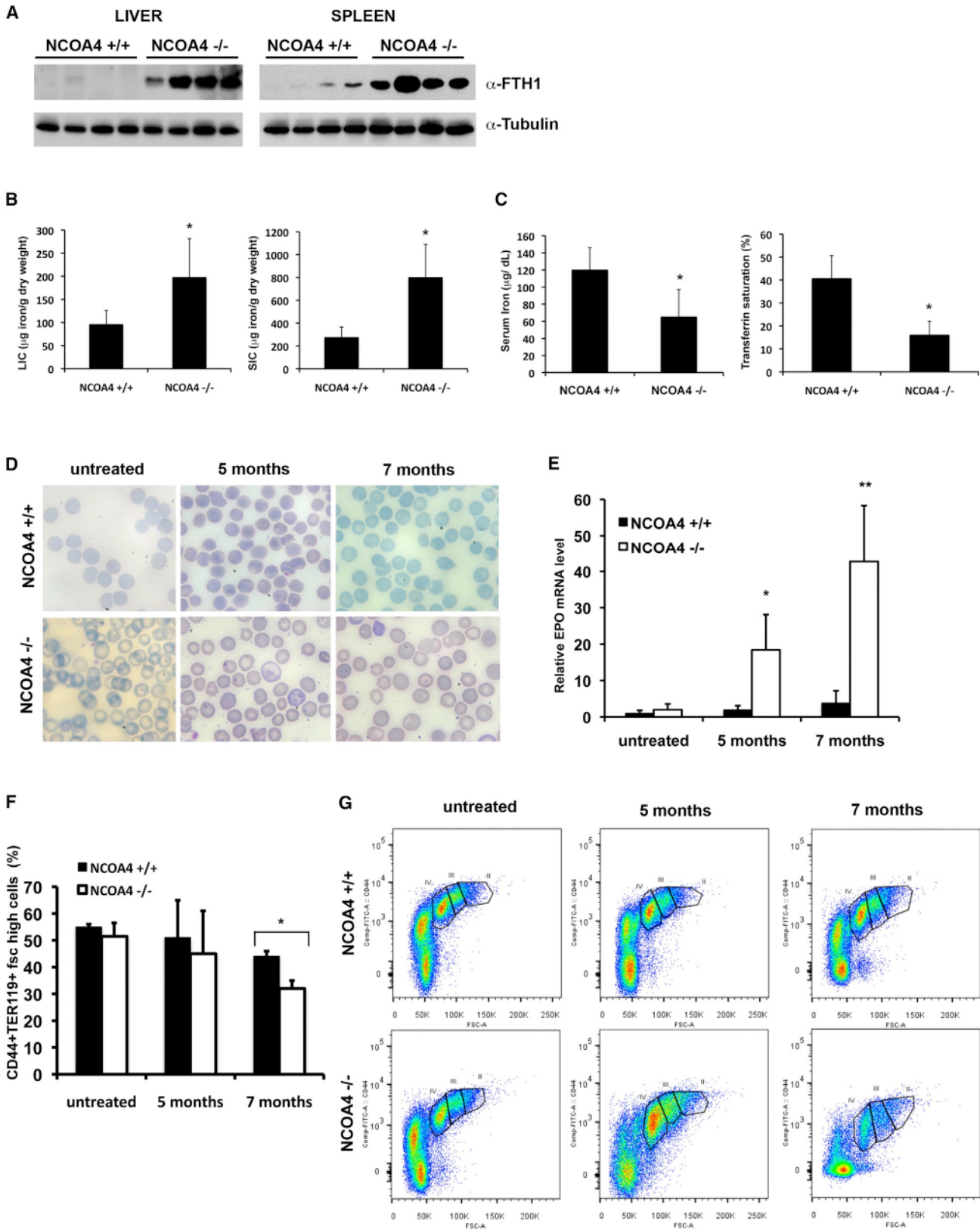
These data strongly indicated that NCOA4-null animals were unable to mobilize iron from ferritin deposits when subjected to an iron depletion regimen. Therefore, we explored the effects of a low-iron diet on red cells and erythropoiesis. After 5 months of a low-iron diet, NCOA4-null mice developed severe hypochromic microcytic hyporegenerative anemia and anisopoikilocytosis (Figure 2D). This was associated with significantly lower values of hemocrit, hemoglobin, mean corpuscular volume, mean corpuscular hemoglobin, mean corpuscular hemoglobin concentration, hemoglobin concentration, reticulocytes, and a significantly lower reticulocyte mean corpuscular volume in NCOA4-null than in WT mice (Table 1). After 7 months of a low-iron diet, the hypochromic microcytic anemia became more severe in NCOA4^{-/-} mice, and the reticulocyte hemoglobin concentration was significantly lower than in WT mice. These results indicate a severe reduction in the availability of iron required for cell hemoglobinization (Figure 2D; Table 1). Notably, WT mice developed only mild hypochromic anemia after 5 months of a low-iron diet and severe microcytic and hypo-regenerative anemia after 7 months of a low-iron diet (Figure 2D; Table 1). Consistently, erythropoietin expression was significantly higher in NCOA4-null than in WT animals after both 5 and 7 months of a low-iron diet (Figure 2E).

To characterize the different forms of anemia, we explored NCOA4-null mice erythropoiesis using a recently developed flow cytometry strategy. This strategy combines CD44 and TER119 positivity with cell size to quantify terminal erythroid differentiation by sorting bone marrow erythroid precursors at each distinct developmental stage (population I, pro-erythroblasts; population II, basophilic erythroblasts; population III, polychro-

matic erythroblasts; population IV, orthochromatic erythroblasts) (Liu et al., 2013). As shown in Figure 2F, after 7 months of a low-iron diet, the decrease in Fsc^{high} CD44⁺ Ter119⁺ cells was more pronounced in NCOA4-null mice than in WT animals. The process of terminal erythroid differentiation did not differ substantially between untreated NCOA4-null and WT mouse bone marrow (Figure S4D). However, at the same time point, orthochromatic erythroblasts were significantly fewer in NCOA4-null mice than in WT animals (Figure 2G). The decrease in orthochromatic erythroblasts was associated with significantly higher amounts of apoptotic orthochromatic erythroblasts in NCOA4-null mice than in WT mice already after 5 months of diet (Figure S4E). The number of apoptotic orthochromatic erythroblasts increased in WT mice only after 7 months of a low-iron diet (data not shown). Overall, these data indicate that genetic inactivation of NCOA4 impairs the mobilization of iron from liver and spleen deposits, thereby promoting anemia, particularly under conditions of iron deficiency.

NCOA4-Null Animals Are Hypersensitive to an Iron-Rich Diet

Increased iron deposits in NCOA4-null mice tissues (Figure 1; Figure S1) suggested that these animals might poorly tolerate an increased iron intake. To explore this possibility, knockout and WT animals were fed chow containing 2 g/kg iron. After 15 days of a hyperferric diet, both FTH1 protein levels and iron content were higher in NCOA4^{-/-} liver extracts than in the WT counterparts (Figures 3A and 3B). Furthermore, Perl's Prussian blue staining was more intense and diffuse in NCOA4^{-/-} than in WT livers (Figure 3C). Saturation of ferritin deposits presumably leads to an increase of free iron concentration and Fenton reaction-mediated oxidative stress, which causes hepatocyte damage and, eventually, cell death. Hepatocytes react to oxidative stress by activating the transcription of scavenger proteins such as superoxide dismutase (SOD) and glutathione peroxidase (GPx) (Vanoaica et al., 2010). Consistent with an increased



(legend on next page)

reactive oxygen species (ROS) concentration in NCOA4^{-/-} hepatocytes, SOD and GPx gene expression was significantly higher in NCOA4^{-/-} than in WT hepatocytes (Figure 3D). To verify hepatocyte cell damage, we measured the concentrations of alanine and aspartate liver transferases (ALT and AST, respectively), which are considered a bona fide measure of liver damage, in NCOA4-null and WT animals after 1 month of a hyperferric diet. As shown in Figure 3E, both enzymes were significantly higher in NCOA4-null animals than in WT mice, indicating precocious hepatic damage in knockout animals. Indeed, after 2 months of a hyperferric diet, fatty degeneration, which is a sign of hepato-steatosis, was more pronounced in livers of NCOA4-null than in those of WT mice, indicating more severe tissue damage in the former animals (Figure 3F). Finally, NCOA4-null animals started to die 75 days after diet onset, whereas WT animals started to die only after 100 days. Mean survival was 89 days in NCOA4-null animals and 104 days in WT animals, which corresponds to a 15% reduction in the mean survival of NCOA4-null mice (Figure 3G).

NCOA4-Null Mouse Embryonic Fibroblasts Display Impaired Ferritinophagy

To functionally verify the above results, we immortalized MEFs from NCOA4-null and WT mice in culture and evaluated their ability to target ferritin to autophagolysosomal digestion under both basal and iron-depleted conditions. Initially, we studied the intracellular localization of ferritin by confocal immunofluorescence analysis of MEFs treated with chloroquine, which, by inhibiting autophagosome-lysosome fusion and lysosomal protein degradation, reveals proteins contained in autophagosomes (Klionsky et al., 2012). As shown in Figure 4A, ferritin co-localized with LC3B-positive autophagosomes in WT MEFs, whereas ferritin was dispersed in the cytoplasm of NCOA4-null cells. In addition, western blotting showed that ferritin accumulation at steady-state was higher in NCOA4-null MEFs than in WT MEFs, which suggests reduced targeting of ferritin to autophagy in the former animals (Figure 4B). Consistently, when treated with ferric ammonium citrate (to induce iron accumulation in ferritin deposits) followed by the iron chelator deferoxamine (to promote iron release by ferritin digestion), WT MEFs rapidly degraded

more than 80% of ferritin within 6 hr, whereas the kinetics of ferritin digestion in NCOA4-null cells was much slower, with more than 50% of deposits being present 9 hr after treatment (Figure 4C).

NCOA4 promotes ferritinophagy by directly interacting with the ATG8-like proteins GABARAP and GABARAPL1, localized on the membrane of autophagic vesicles, but not with the ATG8-like protein LC3B (Mancias et al., 2014). To study the molecular determinants of NCOA4-mediated interaction with the autophagosome receptors, we performed pull-down experiments with HEK293 cell extracts exogenously expressing the myc-tagged full-length NCOA4, the hemagglutinin (HA)-tagged N-terminal (N) NCOA4 (1–238 amino acids [aa]), and the C-terminal (C) NCOA4 (239–618 aa) using glutathione S-transferase (GST)-fused recombinant proteins of the ATG8-like polypeptides LC3B, GABARAP, and GABARAPL1. As reported by Mancias et al. (2014), full-length NCOA4 was pulled down by GABARAP and GABARAPL1 but not by LC3B (Figure S5A). Interestingly, only the NCOA4 (C), but not the NCOA4 (N) fragment, was able to bind to both GST-GABARAP and GST-GABARAPL1 (Figure S5B). To identify the NCOA4 protein domain responsible for interaction with ferritin, we then performed pull-down experiments using NUS-NCOA4, NUS-NCOA4 (C), and NUS-NCOA4 (N) recombinant proteins together with the isolated NUS moiety. As shown in Figure S5C, both NUS-NCOA4 and NUS-NCOA4 (C) were able to pull down ferritin whereas NUS and NUS-NCOA4 (N) were not, suggesting that the C-terminal fragment of NCOA4 protein mediates interaction with both ferritin and the autophagosomal machinery.

Confocal microscopy of EGFP-GABARAP- and EGFP-GABARAPL1-transfected HeLa cells confirmed that, like the full-length NCOA4 protein, the NCOA4 COOH-terminal fragment was able to localize to autophagosomes whereas the NCOA4 NH2-terminal fragment was not (Figures S5D and S5E). Finally, like the WT protein, the NCOA4 COOH-terminal fragment was able to complement NCOA4-null MEF-impaired ferritinophagy whereas the NCOA4 N-terminal fragment was not (Figure 4D). In summary, these data indicate that the NCOA4 COOH-terminal fragment is necessary and sufficient for interaction with both ferritin and autophagosomes and for promoting ferritinophagy.

Figure 2. Defective Iron Release from Ferritin Storage and Impaired Erythropoiesis in NCOA4-Null Mice

- (A) Western blot analysis of FTH1 protein levels from WT (+/+) and NCOA4-null (-/-) female mice fed an iron-depleted diet for 5 months (2–3 mg Fe/kg of food). Tubulin was used as loading control.
- (B) Left: LIC of WT (+/+) and NCOA4-null (-/-) mice fed an iron-depleted diet (5 months). Right: SIC of WT (+/+) and NCOA4-null (-/-) mice fed an iron-depleted diet (5 months). Data are shown as mean \pm SD of 4 independent samples (**p* < 0.05).
- (C) Left: serum iron concentration of WT (+/+) and NCOA4-null (-/-) mice fed an iron-depleted diet (5 months). Right: percentage of transferrin saturation of WT (+/+) and NCOA4-null (-/-) mice fed an iron-depleted diet (5 months). Data are shown as mean \pm SD of 4 independent samples (**p* < 0.05).
- (D) Representative May-Grünwald-Giemsa staining of peripheral blood smears from WT (+/+) and NCOA4-null (-/-) mice subjected or not subjected for 5 or 7 months to a low-iron (2–3 mg Fe/kg of food) diet. Original magnification, \times 40.
- (E) Relative erythropoietin mRNA expression in kidneys from WT (+/+) and NCOA4-null (-/-) mice under basal conditions (+/+, two females and five males; -/-, two females and six males) and after 5 months (+/+, three females; -/-, three females) or 7 months (+/+, three males; -/-, four males) of an iron-deficient diet (**p* < 0.05, ***p* < 0.01).
- (F) Percentage of CD44⁺/CD119⁺/fsc-high bone marrow cells in WT (+/+) and NCOA4-null (-/-) mice under basal conditions (+/+, three females and three males; -/-, three females and three males) and after 5 months (+/+, three females and three males; -/-, three females and three males) or 7 months (+/+, three males; -/-, four males) of iron-deficient diet (**p* < 0.05).
- (G) Flow cytometry analysis combining CD44, CD119, and cell size as markers to sort erythroid precursors at each distinct developmental stage (population I, pro-erythroblasts; population II, basophilic erythroblasts; population III, polychromatic erythroblasts; population IV, orthochromatic erythroblasts). See also Figure S4.

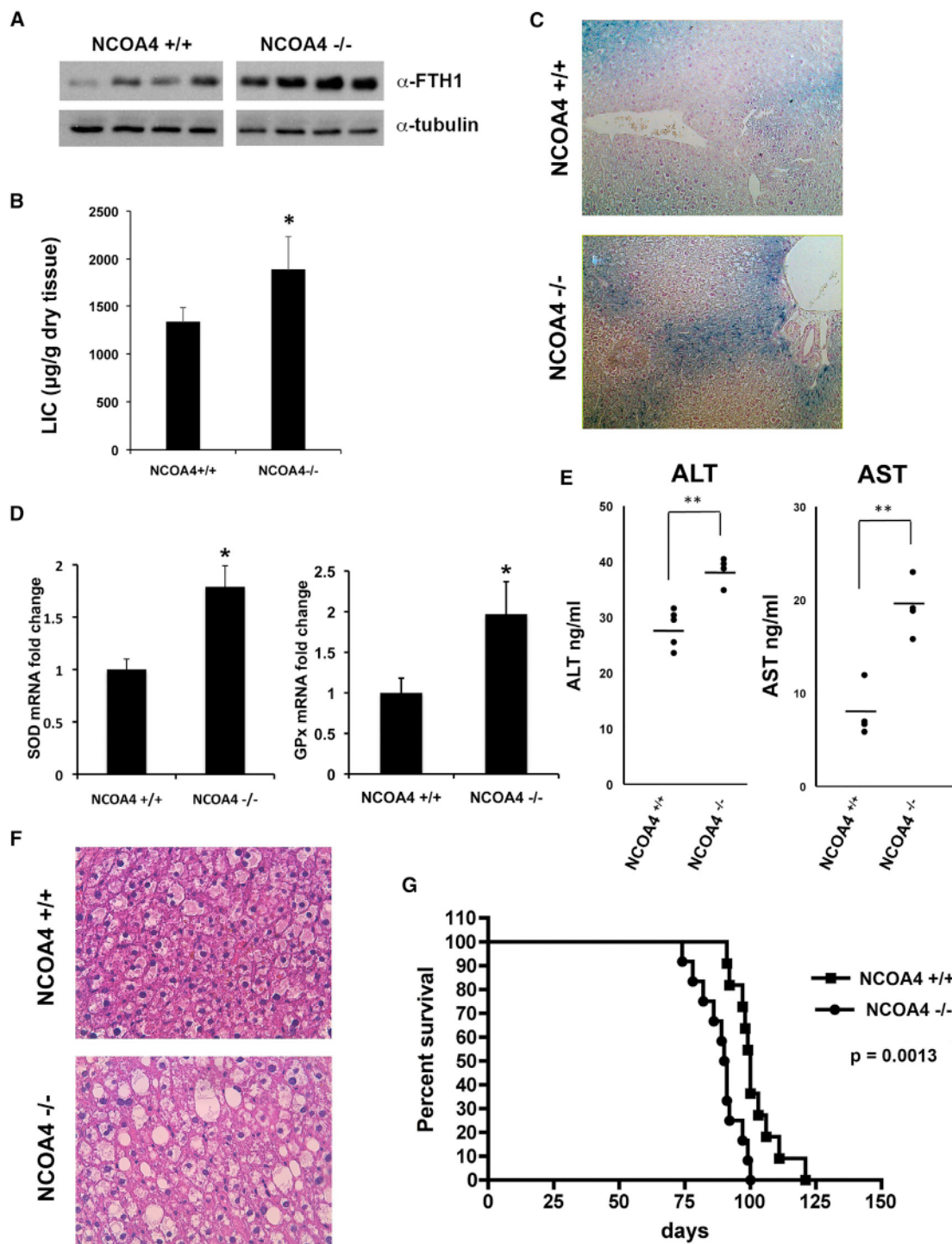


Figure 3. Iron Overload Leads to Liver Damage and Reduces Survival of NCOA4-Null Mice

(A) Western blot analysis of FTH1 protein levels from WT (+/+) and NCOA4-null (-/-) mice fed an iron-rich diet for 15 days. Tubulin was used as a loading control. The samples were run on the same SDS-PAGE gel and transferred and hybridized on the same filter. They were mounted separately because we did not include unrelated samples that were loaded in the central wells of the gel.

(B) LIC of WT (+/+) and NCOA4-null (-/-) mice subjected to a high-iron diet for 15 days. Data are shown as mean \pm SD from 4–5 independent samples. (* $p < 0.05$).

(C) Representative Perls' Prussian blue staining of WT (+/+) and NCOA4-null (-/-) liver sections from mice subjected to an iron-rich diet for 15 days. Magnification, $\times 20$.

(D) Real-time PCR of SOD and GPx mRNA expression in livers from NCOA4^{+/+} and NCOA4^{-/-} mice subjected to a hyperferric diet for 1 month (* $p < 0.05$).

(legend continued on next page)

DISCUSSION

NCOA4 promotes autophagic ferritin degradation to mobilize iron from deposits under both normal and iron-depleted conditions *in vitro* (Mancias et al., 2014; Dowdle et al., 2014). Here we describe the role of NCOA4 in controlling iron homeostasis *in vivo*. Loss of NCOA4 function induced ferritin accumulation in all analyzed tissues. Therefore, liver and spleen iron content were significantly higher in knockout than in WT animals. Transferrin saturation and serum ferritin were significantly higher in knockout than in WT animals and were probably sustained by iron overload in tissues. This phenotype resembles that described by Iolascon et al. (2006) in a patient carrying genetic inactivation of the DMT1 gene and displaying hepatic iron overload, microcytic hypochromic anemia, and increased levels of transferrin saturation. Increased transferrin saturation in NCOA4-null mice presumably leads to increased hepcidin mRNA levels, possibly consequent to activation of the Tfr2/HFE receptor complex, as suggested by the increased activation of the ERK pathway. In turn, increased hepcidin reduces FPN levels in duodenal enterocytes, limiting iron absorption. Such a compensating mechanism could be responsible for the mild nature of the iron overload phenotype displayed by NCOA4-null animals.

Despite their ability to produce hepcidin to compensate for tissue iron overload, NCOA4-null mice subjected to a high iron content diet displayed early signs of steatohepatitis, as witnessed by increased serum transaminase levels and increased liver fat deposition. The low survival time of knockout animals on a hyperferric diet is probably due to the enhanced levels of basal tissue iron, which may accelerate saturation of the detoxification pathways that protect cells against the deleterious effects of iron-dependent oxidative reactions. All previous mouse models of hereditary hemochromatosis are based on the absence of either hepcidin production or resistance to hepcidin action, whereas NCOA4-null animals are fully competent for hepcidin production and activity on duodenal ferroportin, as shown by decreased levels of ferroportin in NCOA4-null duodenal enterocytes (Figure S3A). Therefore, to our knowledge, NCOA4-null mice represent the first example of a hepcidin-independent model of tissue hemochromatosis. Although no NCOA4 mutations have yet been identified in patients, this gene might represent a candidate modifier of iron overload diseases, which are often associated with a variable phenotype and incomplete penetrance (Fleming and Ponka, 2012).

Our data also indicate that impaired NCOA4 function predisposes to iron deficiency anemia, especially in animals fed a low-iron diet. Various observations have implicated NCOA4 in erythropoiesis. For instance, NCOA4 is highly expressed in erythroid precursors (<https://genome-euro.ucsc.edu/>). It is also particularly expressed during erythropoiesis in zebrafish mutants harboring defects of specific stages of hematopoiesis (Weber

et al., 2005). Lastly, Mancias et al. (2015) have shown recently that NCOA4 plays an essential role in erythropoiesis in zebrafish embryos and cultured erythrocytes. Our mouse model suggests that the absence of NCOA4 also favors anemia in adult animals and under unstressed erythropoietic conditions. In fact, the use of iron deposits is impaired in NCOA4-null animals, inducing a peculiar mild hypochromic microcytic anemia associated with increased tissue iron content and transferrin saturation. These data suggest that, during erythroblast development, when liberated from transferrin, iron is, at least in part, stored intermediately in ferritin. In the absence of NCOA4, use of the ferritin-bound iron pool would be limited. Under hypoferric conditions, NCOA4-null mice develop severe anemia because of a remarkable reduction in circulating iron and ineffective erythropoiesis associated with reduction of the erythroid mass and increased apoptosis of orthochromatic erythroblasts. In this view, NCOA4 might also represent a modifier of genetic predisposition to iron deficiency.

Besides controlling ferritinophagy, NCOA4 has also been described as a coactivator of nuclear receptors and, in particular, of androgen receptor-, estrogen receptor-, and peroxisome proliferator-activating receptor γ (Heinlein et al., 1999; Yeh and Chang, 1996). We showed recently that NCOA4 controls DNA replication origin activation by inhibiting the processive helicase of the replication fork; i.e., the MCM2-7 complex, via its NH2-terminal portion (Bellelli et al., 2014). Interestingly, in their proteomic screening for NCOA4-interacting polypeptides, Mancias et al. (2014) and Dowdle et al. (2014) identified several MCM2-7 complex components. Moreover, the protein HERC2, which is an important player in the DNA damage response and in DNA replication origin activation, has been found to bind NCOA4 in an iron-dependent manner, promoting its ubiquitination and proteosomal degradation (Bekker-Jensen et al., 2010; Izawa et al., 2011; Mancias et al., 2015).

In structure-function experiments, we observed that the COOH-terminal portion of NCOA4 was necessary and sufficient to interact with both ferritin and ATG8-like proteins and that it was also able to complement ferritinophagy in NCOA4-null MEFs. This is in line with Mancias et al. (2015), who recently demonstrated that NCOA4 binding to FTH requires residues I489 and W497, both of which are contained in the COOH-terminal portion of the protein. Our data also indicate that the NCOA4 oligomerization motif contained within the protein's NH2-terminal portion is dispensable for ferritinophagy. Therefore, the two NCOA4 functions are separated structurally: the NH2-terminal portion interacts with DNA replication machinery, and the COOH-terminal portion interacts with the players crucial for ferritinophagy. Whether and how these distinct functions might crosstalk is unknown. It is conceivable that the regulation of intracellular iron concentrations needs to be coordinated with features of DNA metabolism; namely replication and transcription. In this context, it should be noted that many enzymes involved in DNA replication contain iron and that, during DNA

(E) AST and ALT levels in WT (+/+) and NCOA4-null (-/-) mice subjected to a hyperferric diet for 1 month (**p < 0.01).

(F) Representative H&E staining of liver sections from WT (+/+) and NCOA4-null (-/-) mice subjected to a hyperferric diet for 2 months.

(G) Kaplan-Meier survival curve of ten WT (+/+) (two females and eight males) and ten NCOA4-null (-/-) (two females and eight males) 4-week-old mice subjected to a hyperferric diet (2 g Fe/kg of food).

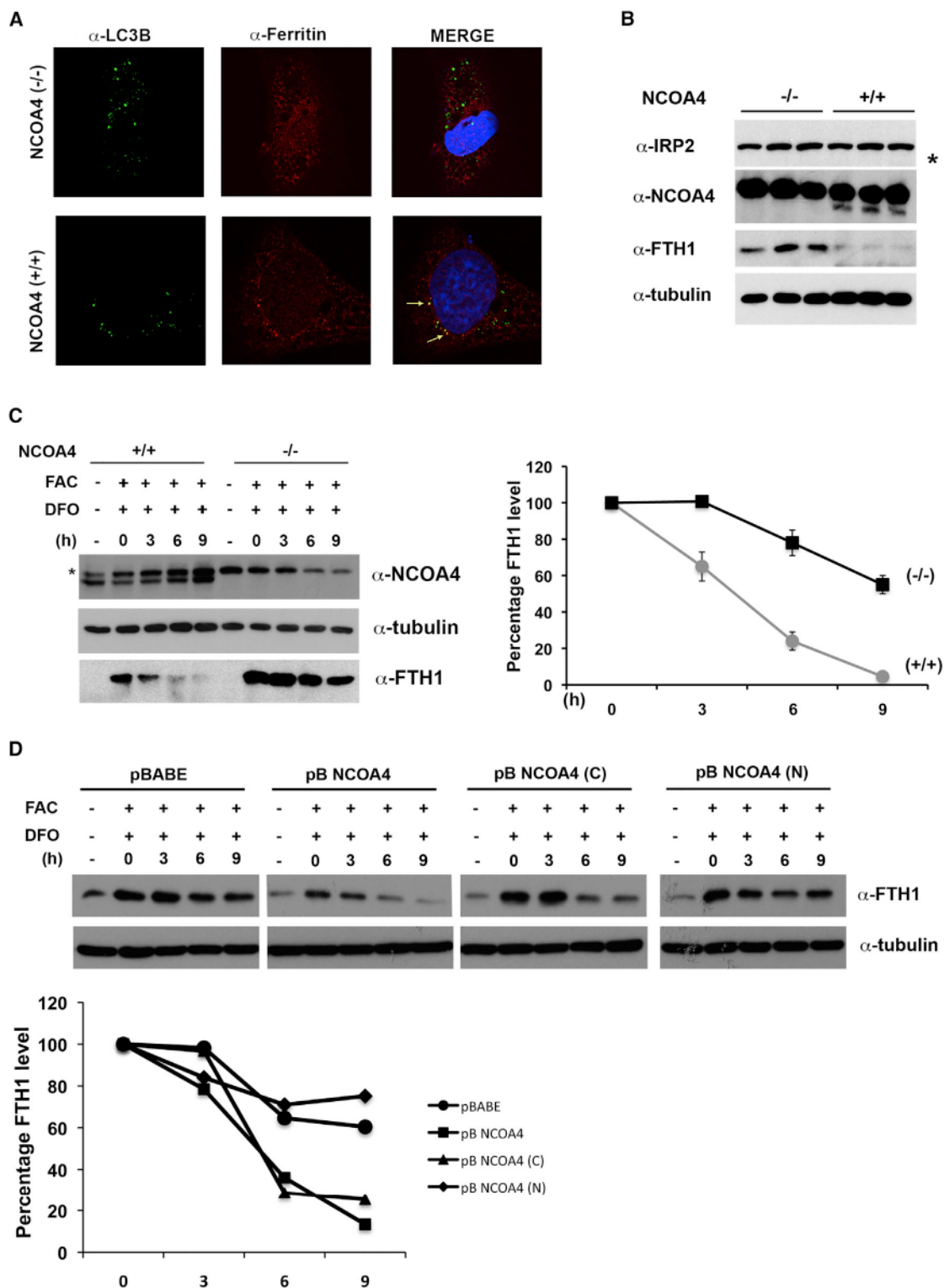


Figure 4. NCOA4-Null MEFs Show Defective Ferritinophagy

(A) Immunofluorescence analysis of LC3B (green) and Ferritin (red) co-localization in NCOA4 WT (+/+) and NCOA4-null (-/-) cells treated with chloroquine. Arrows indicate co-localization in merged images.

(B) Western blot analysis of IRP2, NCOA4, and FTH1 expression in three different WT (+/+) and NCOA4-null (-/-) MEF clones. The asterisk indicates an un-specific band. Tubulin was used as a loading control.

(legend continued on next page)

and RNA synthesis, the double helix is more sensitive to oxidative damage, being less sheltered by chromatin proteins. In addition, erythropoiesis has been linked directly to iron availability. Indeed, iron deficiency blocks erythrocyte production (Kim and Nemeth, 2015). Our data suggest that NCOA4 might be involved in coupling the proliferation of erythroblasts with iron availability so that, under conditions of iron depletion, the lack of NCOA4 results in severe impairment of erythropoiesis.

EXPERIMENTAL PROCEDURES

NCOA4^{-/-} Mice

Generation of NCOA4^{-/-} mice is described in Bellelli et al. (2014).

Details about animal care and management are provided in the Supplemental Experimental Procedures.

Cell Culture

WT and NCOA4-null MEFs were produced and cultured as described by Bellelli et al. (2014). HeLa cells were cultured in DMEM supplemented with 10% fetal bovine serum (FBS), 50 μg/ml penicillin-streptomycin, and 2 mM L-glutamine. To induce iron-replete conditions, MEFs were treated with 10 μg/ml of ferrum ammonium citrate (FAC), whereas, for growth under iron-deficient conditions, cells incubated for 24 hr in FAC were released in normal medium containing 50 μM deferoxamine (DFO). Chloroquine (Sigma-Aldrich) was used at a final concentration of 25 μM.

Histology

Formalin-fixed, paraffin-embedded (FFPE) sections (5 μm thick) were stained with H&E by conventional methods or deparaffinized and rehydrated by passages through xylene and alcohol series for Perl's Prussian blue or immunohistochemical (IHC) staining. The IHC staining protocol is described in the Supplemental Experimental Procedures.

Hematological Parameters and Red Cell Indices

Blood was collected by retro-orbital venipuncture in anesthetized mice using heparinized microcapillary tubes. Hematological parameters were evaluated on a Bayer Technicon Analyzer ADVIA. Hematocrit and hemoglobin were determined manually as described previously (Franco et al., 2014). Blood smears were stained with May-Grünwald-Giemsa (Sigma-Aldrich) for morphological analysis. Images were captured using a Nikon EclipseE600 microscope.

Flow Cytometric Analysis of Mouse Bone Marrow and Spleen

Precursors

Flow cytometric analysis of erythroid precursors from mouse bone marrow was carried out as described by Liu et al. (2013). The cell staining and analysis procedures are reported in the Supplemental Experimental Procedures.

RNA Extraction and RT-PCR

RNA was isolated from snap-frozen mouse tissues by using TRIzol reagent (Invitrogen) and purified with the RNeasy purification kit (QIAGEN). RNA (1 μg) was reverse-transcribed with a Quantitect reverse transcription kit (QIAGEN). qRT-PCR reactions were done in triplicate, and fold changes were calculated with the following formula: $2^{-(\text{sample 1 } \Delta\text{Ct} - \text{sample 2 } \Delta\text{Ct})}$, where ΔCt is the differ-

ence between the amplification fluorescence threshold of the mRNA of interest and the mRNA of the β -actin used as an internal reference. The primer sequences used for qPCR are available upon request.

Protein Studies

Details regarding the preparation of protein cell lysates, immunoprecipitation, and western blotting can be found in the Supplemental Experimental Procedures. Densitometric analysis of signal was performed using ImageQuant.

Antibodies

Anti-IRP2 antibody was from Santa Cruz Biotechnology. Anti-FTH1, anti-MAPK, and anti-pMAPK were from Cell Signaling Technology, and anti-transferrin receptor was from Invitrogen. Anti-FPN for IHC was from Alpha Diagnostics International, and anti-HIF2 α was from Novus Biologicals. Anti-tubulin was from Sigma-Aldrich. Anti-NCOA4 is an affinity-purified rabbit polyclonal antibody raised against the C-terminal protein fragment of human NCOA4 (amino acids 239–614) (Bellelli et al., 2014). Secondary antibodies coupled to horseradish peroxidase were from Santa Cruz Biotechnology.

Tissue and Serum Iron Determination

For iron concentration measurements, mouse spleen and liver tissues were dried overnight at 110°C, dissociated mechanically, weighed, and digested in 1 ml of 3M HCl and 0.6 M trichloroacetic acid for 20 hr at 65°C. The total non-heme iron content was then measured using the bathophenanthroline method as described by Torrance and Bothwell (1968). Serum iron and transferrin saturation (the ratio of serum iron and total iron binding capacity) were calculated using the serum iron/unsaturated iron binding capacity (UIBC) and the total iron binding capacity (TIBC) kits (Randox Laboratories) according to the manufacturer's instructions.

Transduction of Retrovirus-Mediated MEFs

pBABE Puro NCOA4, NCOA4 (N), and NCOA4 (C) or the empty vector were transfected into Phoenix-eco cells, and, 48 hr later, viral supernatants were harvested and used to infect primary NCOA4-null MEFs. Forty-eight hours after infection, cells were selected with Puromycin (2.5 mg/ml) and used to analyze ferritin accumulation and degradation upon FAC treatment and release in DFO, as reported under Cell Culture.

Immunofluorescence Staining

For indirect immunofluorescence, cells were fixed in 4% paraformaldehyde, permeabilized with 0.2% Triton X-100 (5 min on ice), and then incubated with the appropriate antibodies. The immunofluorescence staining procedure is reported in the Supplemental Experimental Procedures.

Recombinant Proteins

NUS-NCOA4, NUS-NCOA4(N), and NUS-NCOA4(C) recombinant proteins were generated as described by Bellelli et al. (2014) and produced in *Escherichia coli* using standard protocols. GST-GABARAP, GST-GABARAPL1, and GST-LC3B recombinant proteins are described by Colecchia et al. (2012).

Statistics

Two-tailed unpaired Student's t test was used for statistical analysis. All p values were two-sided, and differences were considered significant when p was less than 0.05. All statistical analyses were carried out using GraphPad Instat software (version 3.06.3).

(C) Left: western blot analysis of FTH1 in WT (+/+) and NCOA4-null (-/-) cells under iron-depleted conditions. Cells were incubated for 24 hr with FAC and then released at the reported time points in medium containing the iron chelator DFO. NCOA4 and tubulin western blots are shown. The asterisk indicates an unspecific band. Right: curves showing FTH1 degradation kinetics in WT (+/+) and NCOA4-null (-/-) MEFs. Values are represented as the mean \pm SD of three experiments performed in triplicate.

(D) Top: western blot analysis of FTH1 degradation in primary NCOA4-null MEFs infected with retrovirus expressing empty vector (pBABE), NCOA4 WT (pB NCOA4), or the C-terminal (pB NCOA4 (C)) or N-terminal (pB NCOA4 (N)) NCOA4 deletion mutants. Bottom: FTH1 degradation kinetics in NCOA4-null MEFs infected with the described constructs. The percentage of protein levels compared with the control was measured by densitometric analysis using ImageQuant. See also Figure S5.

SUPPLEMENTAL INFORMATION

Supplemental Information includes Supplemental Experimental Procedures and five figures and can be found with this article online at <http://dx.doi.org/10.1016/j.celrep.2015.12.065>.

AUTHOR CONTRIBUTIONS

Conceptualization and Design, R.B., F.C., and M.S.; Investigation, R.B., G.F., A.M., D.C., M.C., and L.D.F.; Formal Analysis, R.B., F.C., M.S., M.C., A.I., and L.D.F.; Resources, A.I., M.C., M.S., and L.D.F.; Writing, F.C., M.S., and L.D.F.

ACKNOWLEDGMENTS

We thank Nina A. Dathan for providing NCOA4 recombinant proteins. We also thank Clara Camaschella and Laura Silvestri for useful discussions and Giancarlo Troncone and Antonino Iaccarino for technical support in the IHC studies. We are grateful to Jean Ann Gilder (Scientific Communication) for editing of the text. This study was funded by the Associazione Italiana per la Ricerca sul Cancro (AIRC), by MOVIE and OCKEY grants from the Regione Campania, and by a CREME grant from the Ministero dell'Istruzione dell'Università e della Ricerca (MIUR).

Received: August 14, 2015

Revised: October 31, 2015

Accepted: December 13, 2015

Published: January 14, 2016

REFERENCES

- Andrews, N.C., and Schmidt, P.J. (2007). Iron homeostasis. *Annu. Rev. Physiol.* **69**, 69–85.
- Arosio, P., Ingrassia, R., and Cavadini, P. (2009). Ferritins: a family of molecules for iron storage, antioxidation and more. *Biochim. Biophys. Acta* **1790**, 589–599.
- Bablitt, J.L., Huang, F.W., Wrighting, D.M., Xia, Y., Sidis, Y., Samad, T.A., Campagna, J.A., Chung, R.T., Schneyer, A.L., Woolf, C.J., et al. (2006). Bone morphogenetic protein signaling by hemojuvelin regulates hepcidin expression. *Nat. Genet.* **38**, 531–539.
- Bekker-Jensen, S., Rendtlew Danielsen, J., Fugger, K., Gromova, I., Nerstedt, A., Lukas, C., Bartek, J., Lukas, J., and Mailand, N. (2010). HERC2 coordinates ubiquitin-dependent assembly of DNA repair factors on damaged chromosomes. *Nat. Cell Biol.* **12**, 80–86, 1–12.
- Bellelli, R., Castellone, M.D., Guida, T., Limongello, R., Dathan, N.A., Merolla, F., Cirafici, A.M., Affuso, A., Masai, H., Costanzo, V., et al. (2014). NCOA4 transcriptional coactivator inhibits activation of DNA replication origins. *Mol. Cell* **55**, 123–137.
- Colecchia, D., Strambi, A., Sanzone, S., Iavarone, C., Rossi, M., Dall'Armi, C., Piccioni, F., Verrotti di Pianella, A., and Chiariello, M. (2012). MAPK15/ERK8 stimulates autophagy by interacting with LC3 and GABARAP proteins. *Autophagy* **8**, 1724–1740.
- Dowdle, W.E., Nyfeler, B., Nagel, J., Elling, R.A., Liu, S., Triantafellow, E., Menon, S., Wang, Z., Honda, A., Pardee, G., et al. (2014). Selective VPS34 inhibitor blocks autophagy and uncovers a role for NCOA4 in ferritin degradation and iron homeostasis *in vivo*. *Nat. Cell Biol.* **16**, 1069–1079.
- Fleming, R.E., and Ponka, P. (2012). Iron overload in human disease. *N. Engl. J. Med.* **366**, 348–359.
- Franco, S.S., De Falco, L., Ghaffari, S., Brugnara, C., Sinclair, D.A., Matte', A., Iolascon, A., Mohandas, N., Bertoldi, M., An, X., et al. (2014). Resveratrol accelerates erythroid maturation by activation of FoxO3 and ameliorates anemia in beta-thalassemic mice. *Haematologica* **99**, 267–275.
- Ganz, T., and Nemeth, E. (2012). Iron metabolism: interactions with normal and disordered erythropoiesis. *Cold Spring Harb. Perspect. Med.* **2**, a011668.
- Heinlein, C.A., Ting, H.J., Yeh, S., and Chang, C. (1999). Identification of ARA70 as a ligand-enhanced coactivator for the peroxisome proliferator-activated receptor gamma. *J. Biol. Chem.* **274**, 16147–16152.
- Hentze, M.W., Muckenthaler, M.U., Galy, B., and Camaschella, C. (2010). Two to tango: regulation of Mammalian iron metabolism. *Cell* **142**, 24–38.
- Iolascon, A., d'Apolito, M., Servedio, V., Cimmino, F., Piga, A., and Camaschella, C. (2006). Microcytic anemia and hepatic iron overload in a child with compound heterozygous mutations in DMT1 (SCL11A2). *Blood* **107**, 349–354.
- Izawa, N., Wu, W., Sato, K., Nishikawa, H., Kato, A., Boku, N., Itoh, F., and Ohta, T. (2011). HERC2 interacts with Claspin and regulates DNA origin firing and replication fork progression. *Cancer Res.* **71**, 5621–5625.
- Kim, A., and Nemeth, E. (2015). New insights into iron regulation and erythropoiesis. *Curr. Opin. Hematol.* **22**, 199–205.
- Klionsky, D.J., Abdalla, F.C., Abeliovich, H., Abraham, R.T., Acevedo-Aroza, A., Adeli, K., Agholme, L., Agnello, M., Agostinis, P., Aguirre-Ghiso, J.A., et al. (2012). Guidelines for the use and interpretation of assays for monitoring autophagy. *Autophagy* **8**, 445–544.
- Lanzino, M., De Amicis, F., McPhaul, M.J., Marsico, S., Panno, M.L., and Andò, S. (2005). Endogenous coactivator ARA70 interacts with estrogen receptor alpha (ERalpha) and modulates the functional ERalpha/androgen receptor interplay in MCF-7 cells. *J. Biol. Chem.* **280**, 20421–20430.
- Liu, J., Zhang, J., Ginzburg, Y., Li, H., Xue, F., De Franceschi, L., Chasis, J.A., Mohandas, N., and An, X. (2013). Quantitative analysis of murine terminal erythroid differentiation *in vivo*: novel method to study normal and disordered erythropoiesis. *Blood* **121**, e43–e49.
- Mancias, J.D., Wang, X., Gygi, S.P., Harper, J.W., and Kimmelman, A.C. (2014). Quantitative proteomics identifies NCOA4 as the cargo receptor mediating ferritinophagy. *Nature* **509**, 105–109.
- Mancias, J.D., Pontano Vaites, L., Nissim, S., Biancur, D.E., Kim, A.J., Wang, X., Liu, Y., Goessling, W., Kimmelman, A.C., and Harper, J.W. (2015). Ferritinophagy via NCOA4 is required for erythropoiesis and is regulated by iron dependent HERC2-mediated proteolysis. *eLife* **4**, 4.
- Mastrogiannaki, M., Matak, P., Keith, B., Simon, M.C., Vaulont, S., and Peyssonnaud, C. (2009). HIF-2alpha, but not HIF-1alpha, promotes iron absorption in mice. *J. Clin. Invest.* **119**, 1159–1166.
- Nai, A., Lidonnici, M.R., Rausa, M., Mandelli, G., Pagani, A., Silvestri, L., Ferrari, G., and Camaschella, C. (2015). The second transferrin receptor regulates red blood cell production in mice. *Blood* **125**, 1170–1179.
- Papanikolaou, G., and Pantopoulos, K. (2005). Iron metabolism and toxicity. *Toxicol. Appl. Pharmacol.* **202**, 199–211.
- Torrance, J.D., and Bothwell, T.H. (1968). A simple technique for measuring storage iron concentrations in formalinised liver samples. *S. Afr. J. Med. Sci.* **33**, 9–11.
- Vanoaica, L., Darshan, D., Richman, L., Schumann, K., and Kühn, L.C. (2010). Intestinal ferritin H is required for an accurate control of iron absorption. *Cell Metab.* **12**, 273–282.
- Weber, G.J., Choe, S.E., Dooley, K.A., Paffett-Lugassy, N.N., Zhou, Y., and Zou, L.I. (2005). Mutant-specific gene programs in the zebrafish. *Blood* **106**, 521–530.
- Yeh, S., and Chang, C. (1996). Cloning and characterization of a specific coactivator, ARA70, for the androgen receptor in human prostate cells. *Proc. Natl. Acad. Sci. USA* **93**, 5517–5521.
- Zhang, D.L., Ghosh, M.C., and Rouault, T.A. (2014). The physiological functions of iron regulatory proteins in iron homeostasis - an update. *Front. Pharmacol.* **5**, 124.
- Zhao, N., Zhang, A.S., and Enns, C.A. (2013). Iron regulation by hepcidin. *J. Clin. Invest.* **123**, 2337–2343.

Cell Reports

Supplemental Information

NCOA4 Deficiency Impairs Systemic Iron Homeostasis

Roberto Bellelli, Giorgia Federico, Alessandro Matte', David Colecchia, Achille Iolascon, Mario Chiariello, Massimo Santoro, Lucia De Franceschi, and Francesca Carlomagno

SUPPLEMENTAL INFORMATION

Supplemental Experimental Procedures

NCOA4^{-/-} Mice. Animals were maintained under a standard diet of 480 mg iron/kg (Harlan Teklad, Madison, WI, USA) or subjected to iron-depleted diet (2-3 mg iron/kg, Harlan Teklad) or iron overload (2 g iron/kg, Harlan Teklad) starting from 4 weeks of age. Mice were maintained under specific pathogen-free conditions in the animal facility of the Dipartimento di Medicina Molecolare Biotecnologie Mediche (University of Naples Federico II). All studies were conducted in accordance with the Italian regulations for experiments involving animals. Genetic screening of mice and MEFs was conducted by genomic PCR as described in Bellelli et al. (2014).

Histology. Endogenous peroxidase activity was blocked by treatment with 3% hydrogen peroxide (30 min at room temperature). Antigens were retrieved by incubating tissue sections for 15 min in boiling citrate buffer (1 mM, pH 6.0). Slides were blocked in 1% BSA for 1h at room temperature followed by o.n. incubation with primary antibodies and for 30 min at room temperature with biotinylated goat anti-rabbit antibody (Vector Laboratories, Burlingame, CA, USA); the stain was visualized with 3,3'-Diaminobenzidine (DAB) (SIGMA-Aldrich).

Flow Cytometric Analysis of Mouse Bone Marrow and Spleen Precursors. CD16/CD32 (BD Biosciences, Mountain View, CA, USA), CD44-FITC (eBioscience, San Diego, CA USA), TER-119 APC (eBioscience), CD45 APC-eFluor 780 (eBioscience), GR1 APC-Cy7 (BD Biosciences), CD11b APC-Cy7 (BD Biosciences) were used. The 7AAD Viability staining solution (eBioscience) was used to remove dead cells from the analysis. Flow cytometry was carried out with the FACSCanto™ flow cytometer (Becton Dickinson, San Jose, CA, USA) equipped with the FACSDiva software (Becton Dickinson). Data were analyzed with the FlowJo software (Tree Star, Ashland, OR, USA). Apoptotic orthochromatic erythroblasts were analysed in the CD44-Ter-119 gated cells using the Annexin-V PE Apoptosis detection kit (eBioscience) following the manufacturer instructions. Flow cytometry was carried out with the FACSCanto™ flow cytometer (Becton Dickinson) as described in Franco et al. 2014.

Protein Studies. Cells and tissues were lysed in a buffer containing 50 mM N-2-hydroxyethylpiperazine-N'-2-ethanesulfonic acid pH 7.5, 1% (vol/vol) Triton X-100, 150 mM NaCl, 5 mM EGTA, 50 mM NaF, 20 mM sodium pyrophosphate, 1 mM sodium vanadate, 2 mM phenylmethylsulphonyl fluoride and 1 µg/ml aprotinin. Lysates were clarified by centrifugation at 10,000 x g for 20 min. Lysates containing comparable amounts of proteins, estimated by a modified Bradford assay (Bio-Rad, Munchen, Germany), were immunoprecipitated with the required antibody or subjected to direct Western blotting. Immune complexes were detected with the enhanced chemiluminescence kit (Amersham Pharmacia Biotech, Little Chalfort, UK). Immunoblotting was carried out with specific antibodies. For binding assay (pull-down), HeLa cell lysates were incubated with 5 µg of immobilized fusion proteins. Bound proteins were detected by immunoblot analysis.

Immunofluorescence Staining. For indirect immunofluorescence, cells were fixed in 4% paraformaldehyde, permeabilized with 0.2% Triton X-100 (5 min on ice), and then incubated with anti-LC3B (Cell Signalling Technologies) and anti-Ferritin (Rockland, Limerick, PA, Ireland) or anti-Myc tag (Santa Cruz Biotechnology) for 1h at room temperature. Coverslips were washed and incubated with Alexa Fluor 488 goat anti-rabbit or anti-mouse antibodies (Invitrogen) for 30 min at room temperature. After 5 min of DRAQ5 (Cell Signalling Technologies) or Hoechst 33258 (Sigma-Aldrich) counterstaining, coverslips were mounted in glycerol/PBS (1:1) and observed with a Zeiss LSM 510 META confocal microscope (Carl Zeiss, Jena, Germany).

Supplemental Figure Legends

Figure S1. Increased Ferritin Protein Levels in NCOA4-Null Mice Tissues. Supplemental to Figure 1

Left: Western blot analysis of FTH1 protein levels in the indicated tissues from 2 months old wild type (+/+) and NCOA4-null (-/-) female and male mice. Tubulin was used as loading control. Right: Bar graph showing the relative fold increase in FTH1 level in NCOA4^{-/-} mice compared to wild type. Densitometric analysis was performed using ImageQuant. Data are shown as mean ± SD (*p<0.05, **p<0.01).

Figure S2. Increased Transferrin Saturation, Serum Ferritin Levels and Hcpidin Expression in NCOA4-Null Mice. Supplemental to Figure 1

(A) Bar graphs showing percentage of transferrin saturation from wt (+/+) and NCOA4-null (-/-) 2 months old female and male mice. Data are shown as mean ± SD from 4 independent samples. (*p<0.05). (B) Bar graphs showing serum ferritin levels from wt (+/+) and NCOA4-null (-/-) 2 month old female and male mice. Data are shown as mean ± SD from 4 independent samples. (*p<0.05, ** p<0.01). (C) Bar graphs showing liver hepcidin (HAMP) mRNA expression levels from wt (+/+) and NCOA4-null (-/-) 2 months old female and male mice. Data

are shown as mean of 3 experiments \pm SD (** $p < 0.01$). (D) Western blot analysis of p-MAPK from liver extracts of wt (+/+) and NCOA4-null (-/-) 2 months old female and male mice. Total MAPK levels were used as control.

Figure S3. Ferroportin, HIF2 α , IRP2 and TfR Levels in NCOA4-Null and Wild-Type Mice. Supplemental to figure 1

(A) Representative immunohistochemical analysis of ferroportin (FPN) in duodenum sections from 6 months old NCOA4 +/+ and -/- mice. (B) Western blot analysis of HIF2 α protein levels in NCOA4 +/+ and -/- duodenum from 2 months old female and male mice. (C) Real-time RT-PCR of FPN mRNA from wild type (+/+) and NCOA4 null (-/-) 2 months old female and male mice. Data are the mean \pm SD of triplicate experiments. (D) Western blot analysis of IRP2 and TfR protein levels in livers from wild type (+/+) and NCOA4 null (-/-) 2 months old female and male mice. (E) Real-time RT-PCR of the indicated liver mRNAs from wild type (+/+) and NCOA4 null (-/-) female 2 months old mice. Data are the mean \pm SD of two experiments performed in triplicate.

Figure S4. Defective Iron Mobilization and Analysis of Erythroid Precursors in NCOA4 WT and Null Mice. Supplemental to Figure 2

(A) left: Western blot analysis of FTH1 protein levels in NCOA4 +/+ and -/- liver extracts from mice subjected to a normal or hypoferric (2-3 mg iron/kg of food) diet for three months. Right: Bar graph showing the relative fold change in FTH1 levels in NCOA4 +/+ and -/- livers from mice subjected or not to a hypoferric diet. Densitometry was performed using ImageQuant. Data are shown as mean \pm SD. (B) Real-time PCR for Hamp mRNA levels in livers from NCOA4 +/+ and -/- mice subjected to a hypoferric diet for three months. Data are shown as mean \pm SD. (C) Representative immunohistochemical staining for ferroportin (FPN) of NCOA4 +/+ and -/- spleens from mice subjected to a hypoferric diet for three months. (D) Percentage of erythroid precursors at each developmental stage (population I: pro-erythroblasts; population II: basophilic erythroblasts; population III: polychromatic erythroblasts; population IV: orthochromatic erythroblasts) are indicated. Cells were sorted by flow cytometry analysis combining CD44, CD119 and cell size as markers. (E) Bar graphs showing percentage of Annexin V-positive cells in population IV (orthochromatic erythroblast) from bone marrow of 6 months old wt (+/+) and NCOA4-null (-/-) mice under basal conditions (+/+ : 3 females and 3 males; -/- : 3 females and 3 males) or after 5 months of iron-deficient diet (+/+ : 3 females and 3 males; -/- : 3 females and 3 males) (* $p < 0.05$).

Figure S5. NCOA4 (C) Protein Fragments Interact With Ferritin and ATG8-Like Proteins. Supplemental to Figure 6

(A and B) Protein extracts from HEK 293 cells exogenously expressing myc-tagged full-length NCOA4, HA-tagged NCOA4 (N) and NCOA4 (C) proteins were pulled-down using the LC3B, GABARAP and GABARAPL1 GST-fused recombinant proteins. Isolated proteins were subjected to Western blotting using the indicated antibodies (upper panels). The gel was coloured with Coomassie staining to visualize the input of recombinant proteins (lower panels). (C) HeLa cell protein extracts were subjected to pull-down assay with the indicated recombinant proteins. Isolated proteins were subjected to Western blotting using the indicated antibody (upper panel). The filter was coloured with Ponceau staining to visualize the input of recombinant proteins (lower panel). (D and E) Confocal microscopy of HeLa cells transiently transfected with EGFP-GABARAP or EGFP-GABARAPL1 together with myc-tagged full-length NCOA4, HA-tagged NCOA4 (N) and NCOA4 (C) expressing vectors stained with the indicated antibodies. On the right is a merge of the same sections stained with α -GABARAP or GABARAPL1 (green) and α -myc or HA (red). Arrows indicate co-localization (yellow).

Figure S1

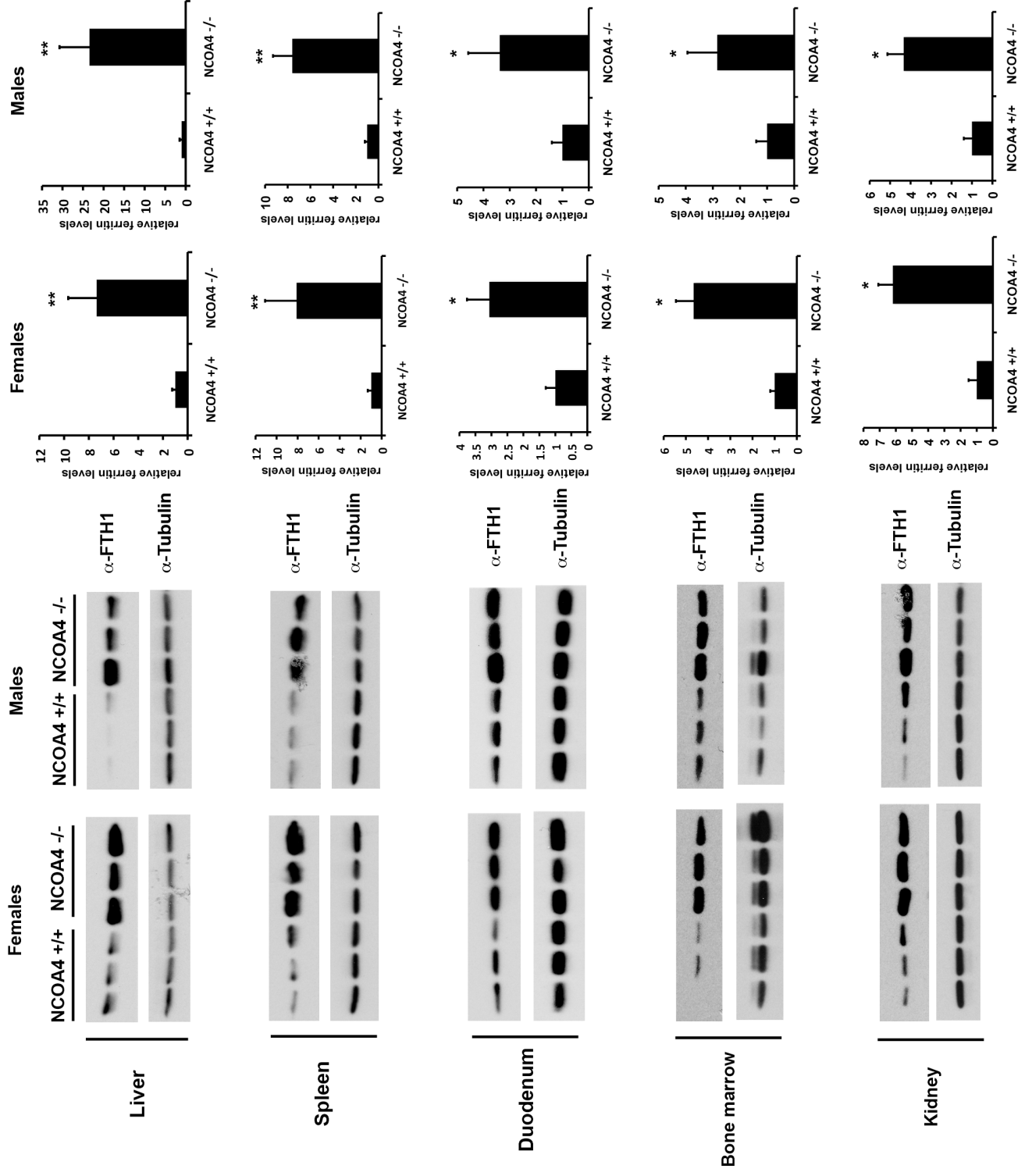


Figure S2

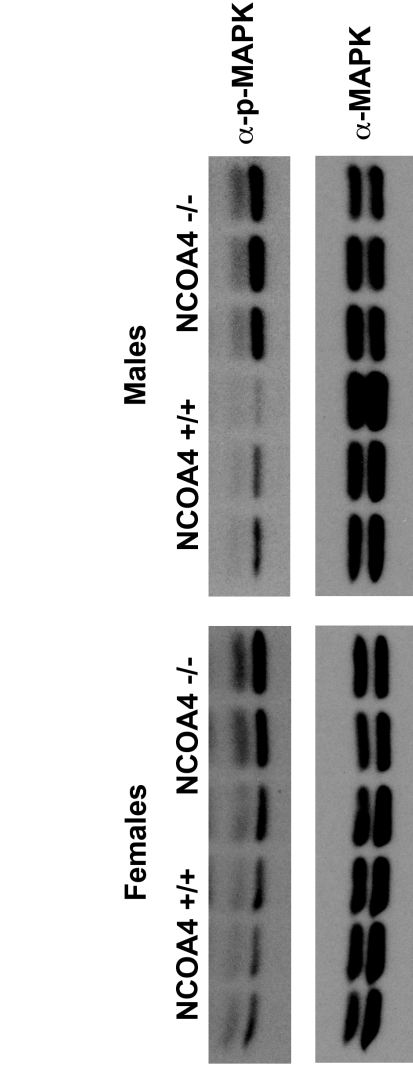
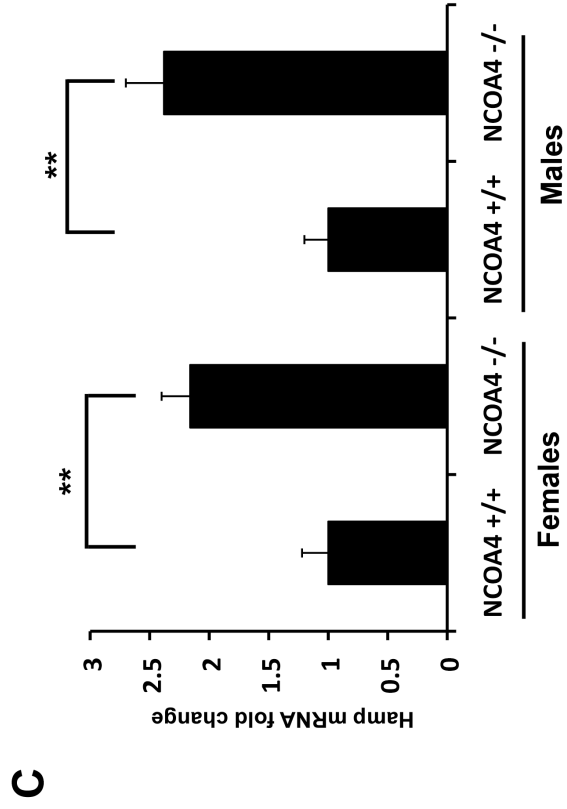
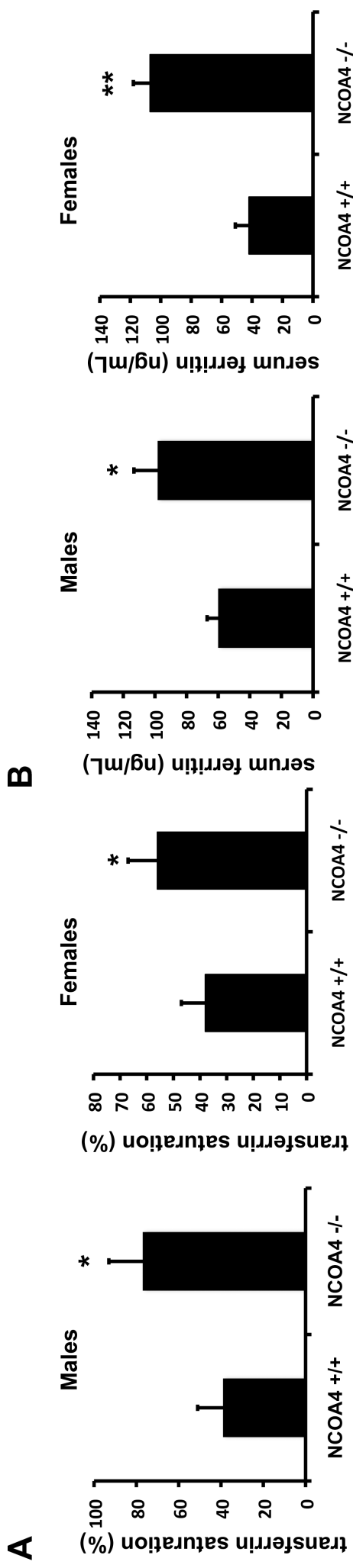


Figure S3

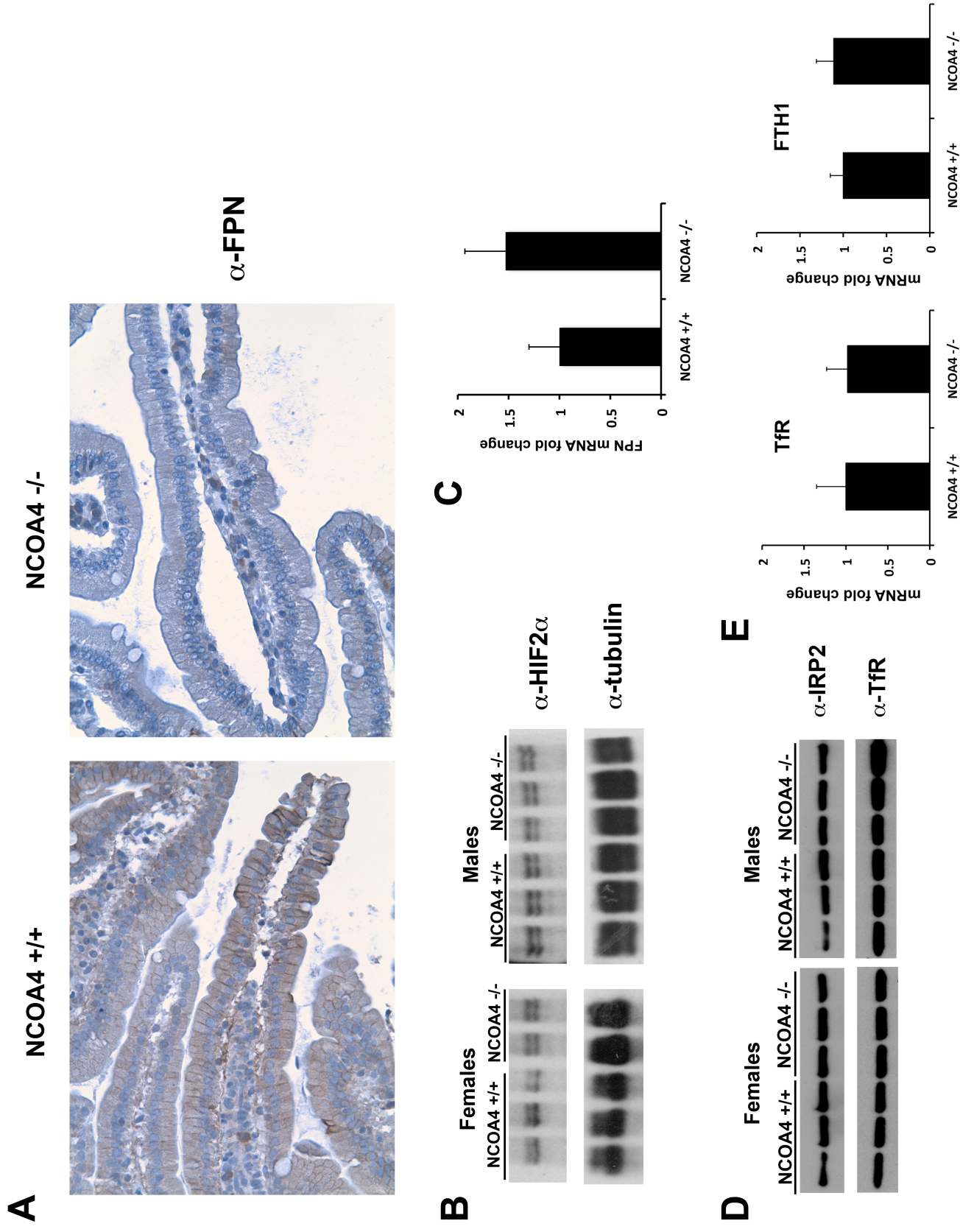


Figure S4

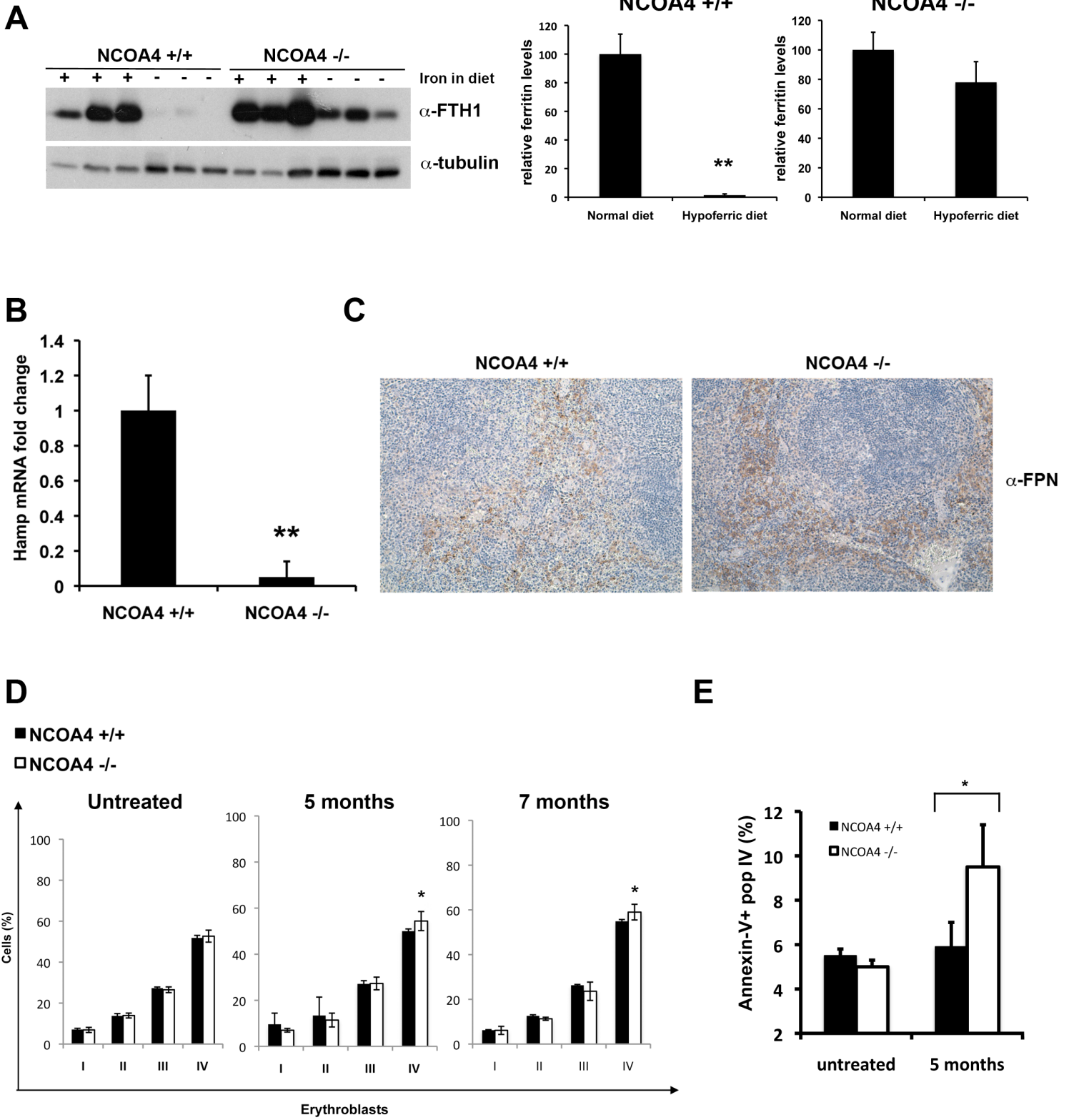


Figure S5

